Geoscience Laser Altimeter System (GLAS)

Algorithm Theoretical Basis Document
Version 3.0

Derivation of Range and Range Distributions From Laser Pulse Waveform Analysis for Surface Elevations, Roughness, Slope, and Vegetation Heights

Prepared by:

Anita C. Brenner[3], H. Jay Zwally[1], Charles R. Bentley[2], Bea M. Csathó[4], David J. Harding[1], Michelle A. Hofton[7], Jean-Bernard Minster[5], LeeAnne Roberts[3], Jack L. Saba[3], Robert H. Thomas[6], Donghui Yi[3]

[1]NASA Goddard Space Flight Center
[2]University of Wisconsin
[3]Raytheon ITSS/NASA Goddard Space Flight Center
[4]Ohio State University
[5]University of California at San Diego
[6]EG&G/Wallops Flight Facility
[7]University of Maryland at College Park

July 2000

i. Changes from version 1.0 to 1.1

- sec 3.1.2.1 Figure 1 replaced for clarity
- Section 3.1.2.2.5 last sentence replace △ E with RMS wave height
- Section 4.1.1 – table 4.1 changes: ngt_noise added, ref_range removed, filterwdmin & filterwdmax moved from "Numerical Program Parameters" to "Instrument Parameters"
- Section 4.1.3.2

OLD:

Assuming gate 1 is farthest from the satellite, this is the time t such that Wf (t) < Noise_ob + Nsig * σ_noise_ob < Wf (t+1). Given this t,

NEW:

Assuming gate 1 is farthest from the satellite, this is the time t(i) such that
Wf(t(i')) < Noise_ob + Nsig * σ_noise_ob for all i'<=i
Wf(t(i+1)) > Noise_ob + Nsig * σ_noise_ob
where i is the gate number.

- Equation changed in section 4.1.3.2 from "WF_range_cor_std = t * ΔT_hires * c" to "WF_range_cor_std = t * c/2"
- Text changed in 4.1.3.4 from "the time it takes to travel to and from the ground using Range_std" to "the time it takes to travel to the ground using Range_std"
- Equation changed in section 4.1.3.4 from "Time_gb(i)= GPSshotTime (i) * Range_std * 2/c" to "Time_gb(i)= GPSshotTime (i) + Range_std /c"
- Section 4.1.3.7

IF Psattm > Psat_spec and Psattm < Psat_stop THEN

replaced with

Psattm ≥Psat_spec and Psattm < Psat_stop THEN

IF Psattm > Psat_stop processing, SET Flag_sat=2

replaced with

IF Psattm ≥Psat_stop processing, SET Flag_sat=2

IF Psattm > 0 and Psattm < Psat_stop, SET Flag_sat=1

Replaced with

IF Psattm > 0 and Psattm < Psat_spec, SET Flag_sat=1

- Section 4.1.3.8 Noise calculation changed
- Section 4.2 replaced
- Section 4.3.3.2 Figure 6 changed for clarity
- Section 4.3.3.2 Figure 8 reference changed to Figure 7. Figure 7 shrinked so caption fits on same page
- Section 4.3.4.2 moved 3rd bullet to after definitions for 2nd bullet
- Section 4.3.4.3 modified words of 2nd bullet

- Chapter 5 tables labeled with correct numbers and more meaningful titles, table 5.5 removed since same as 5.3
- Table 5.1 items 2, 3, 11, and 12, changed descriptions and units
- Chapter 5 sea ice and ocean output parameters put into tables instead of lists

Added paragraph above table 5-7"'Ocean' data will be as determined from the global DEM, to include all regions larger than, say 1000 sq km that are at sea level. Thus, 'ocean' tracking will be implemented over large lakes and over sea ice, in addition to the special tracking appropriate to these areas."

ii. Changes from version 1.1 to 2.0

Sec 1

- added Figure 1

Sec 2

- Added discussion of how instrument algorithm design (sec 2.7) meets the science requirements

Sec 3

- Added statement that Gaussian return is assumed for elevation algorithms
- Added section 3.1.2.3 on skewness and kurtosis

Sec 4

- Minor changes added to make the algorithms work in an operational environment
- Added figures from ATBD for clarity
- Standard range changed to preliminary range
- Threshold retracker added
- Quantitative results presented showing elevation, roughness, and slope errors expected over ice sheets

Sec 5

- Added geolocation information to level 1a waveform product
- Added discussion on product granule size distribution and archiving
- Added figures from oral ATBD presentation for clarity

iii. Changes from version 2.0 to 3.0

- In section 2.1, paragraph three, changed the last sentance from "There are no ice shelves around Greenland" to "There are few ice shelves in Greenland".
- In section 2.6, paragraph five (A small footprint ...), replaced entire paragraph as per Robert Thomas.
- In section 2.7, in the last paragraph changed "used solely to determine where the start of the raw digitized data" to "used solely to determine where the start of the received waveform digitized data", and changed "The data to be sent to the ground are obtained directly from the raw digitizer waveform" to "The data to be sent to the ground are obtained directly from the received digitizer waveform".
- In section 3.1.2.2.5, replaced old paragraphs 2 through 5 with new paragraphs 2 through 4 as per Robert Thomas.
- In section 3.2.2, last paragraph, remove items 1 & 2 regarding Var_mult & Var_check.
- In section 4.0, Outline Of Procedure, changed "Characterize raw" to "Characterize received".
- In section 4.1.1, removed Var_mult & Var_check from Table 4-1 and added minAmpPcnt, sigmaMinInit, minIter, minGatesNs, minNoise, and min4sat.
- In section 4.1.1.1, Table 4-2, removed Psattm, and changed "The waveform in raw units" to "The received waveform".
- In section 4.1.3.1, changed the formula for the normalized time array.
- In section 4.1.3.10, Loop Begin, second sentance, changed "the smooth value will equal the raw value" to "the smooth value will equal the received value".
- In section 4.3.2.1, after Figure 8, fourth sentance, changed "centroid of the raw waveform" to "centroid of the received waveform".
- In section 4.3.2.1, after Figure 9, first sentance, changed "centroid of the raw return" to "centroid of the received return".
- In section 4.3.3.1, third bullet, first sub-bullet, changed "centroid of the raw waveform" to "centroid of the received waveform".
- In section 4.3.3.1, third bullet, third sub-bullet, changed "fit to the raw waveform" to "fit to the received waveform".
- In section 4.3.3.1, fourth bullet, second sub-bullet, changed "fit to the raw waveform" to "fit to the received waveform".
- In section 4.3.3.1, fourth bullet, fourth sub-bullet, changed "centroid of the smoothed waveform" to "centroid of the received waveform".
- In section 4.3.3.1, fourth bullet, added the following sub-bullets and text:
  - The number of peaks in the gaussian fit
  - The maximum smoothed amplitude
  - The reflectance
  - A forward-scattering parameter TBD

  For the same 100km strips (adjustable), the number of problem flags will be calculated and displayed, and the map will be marked if the surface ID (land, ocean, ice sheet, sea ice) has changed.

- In section 4.3.3.2, changed "T_c = time delay of the centroid of the raw" to "T_c = time delay of the centroid of the received".
- In section 4.3.8, replaced Psattm with Psat, and added algorithm for computing saturation.
- Replaced Figure 5 with new Figures 5 and 6. Changed reference numbers for figures 6 through 17 to 7 through 18.

- In section 5.1, table 5-1, items 16, 17, 27, and 28, changed "raw" to "received".
- In section 5.1, table 5-1, item 22, changed "as offset from first telemetered gate" to "as offset from last telemetered gate".
- In section 5.1, table 5-1, items 35 and 36, changed "raw" to "transmitted".
- In section 5.2.3, changed "The equation to scale the received energy to account for the range is TBD." to "The equation for the surface reflectivity is:", added formulas 37, and 38 for reflectance from instrument team, and added formulas 39, 40, and 41, and a procedure for determining transmitted and received energy.
- In the first paragraph in section 5.5, changed "These algorithms will be applied both to the full set of stored Gaussian fits and also to the Gaussian fit to the last (lowest) peak" to "These algorithms will be applied to the Gaussian fit to the last (lowest) peak".
- In section 5.2.5, the source for the 1 km resolution land DEM to be used for ICEsat data processing is Global 30 Arc-Second Elevation Data Set (GTOPO30).
- In section 5.5, removed "Surface Roughness from Ice sheet algorithms using all fits" and " Surface slope from ice sheet algorithms using all fit " from Table 5-6.
- In section 5.2.6, Table 5-2, changed "centroid of raw" to "centroid of received".
- In Table 5-2, & Table 5-4, changed "Reflectance" to "Reflectance * round trip atmospheric transmission".
- In section 5.3, second paragraph, ninth sentance, changed "of the raw waveform" to "of the received waveform".
- In section 5.3, table 5-4, changed "Standard deviation of raw" to "Standard deviation of received", "Kurtosis of the raw" to "Kurtosis of the received", "Skewness of the raw" to "Skewness of the received", and "Range increment from reference range to centroid of raw waveform" to "Range increment from reference range to centroid of received waveform".
- In section 5.4, table 5-5, changed "Average elevation of all surfaces in the footprint from the centroid of the raw" to "Average elevation of all surfaces in the footprint from the centroid of the received", "Standard deviation of raw" to "Standard deviation of received", "Skewness of the raw return" to "Skewness of the received waveform", and "Range increment from reference range to centroid of raw" to "Range increment from reference range to centroid of received".
- 5.4.1, item a, changed "Sea-ice mask, possibly based on daily sea-ice extent charts from the National Ice Center" to "Sea-ice mask, defined from the GSFC SMMR-SSM/I ice concentration data".
- In section 5.5, first paragraph, second sentance, changed "the centroid of the smoothed" to "the centroid of the received".
- In section 5.5, table 5-6, changed "Standard deviation of raw waveform using all fits" to "Standard deviation of received waveform using all fits", "Standard deviation of raw waveform using stored fits" to "Standard deviation of received waveform using stored fits", and "Skewness of the smoothed waveform" to "Skewness of the received waveform from signal begin to signal end".
- In section 5.6, table 5-7, changed "Standard deviation of raw" to "Standard deviation of received", and "Range increment from reference range to centroid of the raw" to "Range increment from reference range to centroid of the received", "Skewness of the smoothed return" to "Skewness of the received waveform from signal begin to signal end", and "Ocean surface elevation calculated using the centroid of the last peak in the waveform" to "Ocean surface elevation calculated using the centroid of the waveform".
- In section 6.1.3, fifth paragraph, item 4), changed "centroid of the raw" to "centroid of the received".
- Added references Krabill et al., (1995) and Krabill et al., (2000).
- Corrected reference Zwally et al., (1983) to include R.H. Thomas.

Table of Contents

TABLE OF FIGURES

LIST OF TABLES

1.0 INTRODUCTION

The primary purpose of the GLAS instrument on the ICESat mission is to detect ice elevation changes that are indicative of changes in ice volume (mass balance) over time. GLAS will do this by precision profiling of ice surface elevations over the Greenland and Antarctic ice sheets. Other objectives include measurements of sea ice, ocean, and land surface elevations; ice, water, and land surface roughness; multiple near-surface canopy heights over land; and cloud and aerosol layer heights.

The GLAS instrument uses a laser altimeter to measure the range to the surface. Ranges are determined from the measured time between transmission of the laser pulse and detection of the photons reflected from the surface and received by the instrument. The laser footprint diameter on the surface is nominally 70 m, and the width of the transmitted pulse is 4 ns, equivalent to 60 cm in surface elevation. The returned laser pulse is broadened by the distribution of surface heights within the footprint as depicted in Figure 1. The surface height distribution is characterized by a mean surface slope and a surface roughness

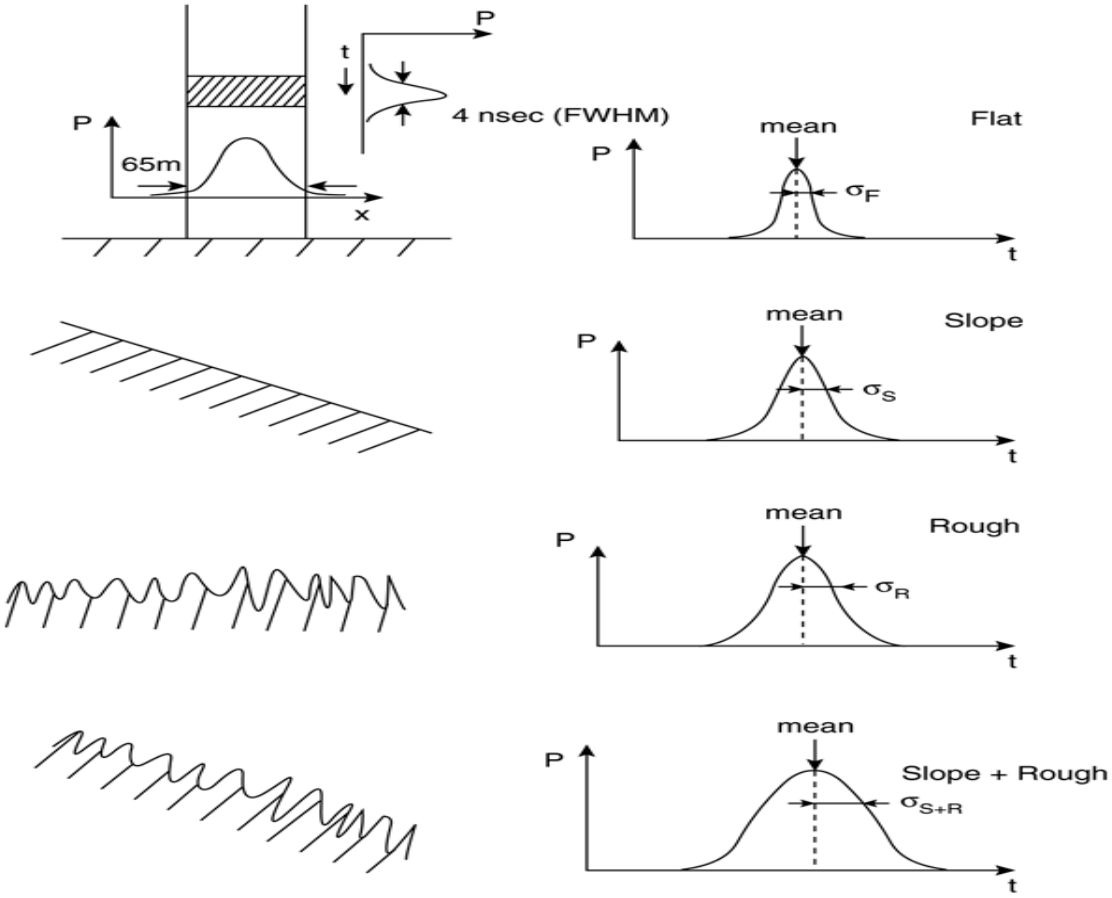

Figure 1 - Characteristics of returned laser pulse as a function of surface type. Presence of surface slope and roughness both broaden the pulse.

within the footprint. The detected pulse corresponding to the reflections from the surface is selected by an instrument algorithm and digitized in 1 ns (15 cm) range bins. From a total of 1000 selected range bins, a smaller number, 544 over ice sheets and land and 200 over oceans and sea ice regions, is selected

for transmission. The corresponding range widths of the transmitted bin are 81.5 m over ice sheets and 30 m over oceans and sea ice.

This document describes the analysis of the waveform of the laser pulse returned from the ground. The derived parameters are

- the average range (equivalent to the average surface elevation) within the laser footprint
- the ranges (elevations) to multiple reflecting surfaces
- the pulse width and other waveform shape parameters related to surface slope and roughness

Other GLAS ATBDs describe the orbit and attitude calculations, corrections for atmospheric path-length delays, and corrections for changes in the surface elevations due to tidal effects; these other data are needed to convert ranges into absolute surface elevations with respect to the geoid.

2.0 OVERVIEW AND BACKGROUND INFORMATION

GLAS is the Geoscience Laser Altimeter System consisting of both lidar and altimetry subsystems that will fly on the dedicated platform comprising the mission referred to as ICESat, the Ice, Cloud, and Land Elevation Satellite. The following subsections talk to the properties of ice sheet, sea ice, land, and ocean, and what quantitative measurements will help us understand global climate warming and the interactions with these ecosystems and our environment.

2.1. Ice Sheet

There are only two major ice sheets in the world, one on Antarctica and one on Greenland. A good general description of the Antarctic ice sheet can be found in a book by Fifield (1987), from which the following paragraph is adapted. The Antarctic ice sheet is composed of two unequal parts. The larger portion (10.35 million km^2) lies in East Antarctica, where it reaches a maximum central elevation of just over 4000 m. This part of the ice sheet is mostly terrestrial, that is, it rests on a bed that would be mostly above sea level if the ice were removed and isostatic rebound allowed to take place. The massive Transantarctic Mountain chain, which stretches from Atlantic to Pacific across the continent, separates East Antarctica from West Antarctica (the two portions lie principally in the Eastern Hemisphere and the Western Hemisphere, respectively). The West Antarctic ice sheet itself comprises three very different provinces: the "inland ice", the ice shelves, and the Antarctic Peninsula. The inland ice, which is the main part of the ice sheet, 2 million km^2 in area, is mostly marine (i.e. it rests on a bed that would be sea floor in the absence of the ice) and attains a surface height of 2300 m. Abutting it on the Atlantic and Pacific sides are two large floating ice shelves, each about 0.5 million km^2 in area. The Antarctic Peninsula (also about 0.5 million km^2), which stretches far northward from the main body of Antarctica toward South America, is an area of extensive mountainous terrain and complex ice cover, with several merging small ice caps, ice shelves, and outlet glaciers, and many ice-covered offshore islands.

The Antarctic ice sheet is in places over 4000 m thick; it contains 91% of the world's ice and 70% of the world's store of fresh water. Much of Antarctica is technically a desert - each year more than half of its surface receives in snowfall less than the equivalent of 100 mm of water. Essentially no melting of the snow occurs (except close to the more northerly margins) even in summer and each year a new layer is added. As the snow layers are added, deeper layers become compressed, eventually being transformed into ice. Gravity forces the ice to flow downwards and outwards towards the coast, where it is eventually lost to the ocean, principally by calving of icebergs.

The Greenland ice sheet (1.73 million km^2) is a single, bowl-shaped unit whose bed in the interior of Greenland lies more or less at sea level. The ice flows outward through the mountains that ring the island in a series of outlet glaciers, most of which reach the ocean either directly, or, more often, through fjords

that connect to the ocean. Snowfall rates in the interior and melt rates around the periphery are greater than in Antarctica. As it is eight times smaller than the East Antarctic ice sheet it has approximately an eight-fold larger perimeter:area ratio. Because of this and the relatively high melt rates surface melting is a much more important component of the overall ice-mass balance in Greenland than in Antarctica. There are few ice shelves in Greenland.

Slope characteristics: The speed of outward ice flow from an ice sheet is sufficient large to balance the incoming snowfall (when averaged over many centuries). In this way, ice sheets are able to maintain approximately parabolic profiles. The central regions are consequently very flat, with gradients on the order of 1:1000. Toward the ice margin, surface slopes and flow speeds are higher, the ice is thinner, and stresses from flow over the irregular sub-glacial bed makes the ice surface more undulating. Within 200-300 km of the coast, the ice may become channeled, either through peripheral mountains where outlet glaciers develop, or through ice streams, fast-flowing zones within the ice sheet. Here the slopes are highly variable, from as much as 1:10 where the ice is flowing slowly to as little as 1:1000 on the fast-flowing, low-gradient ice streams. The coastal regions, with their widely variable slopes, are of particular importance in the context of global change, because it is here that any reaction of the ice sheets to changes in climate will first appear. More than half of Antarctica has gradients less than 1:300 and 90% has gradients less than 1.5%. Only 3% of the ice sheet, in the marginal areas, exhibits gradients larger than 3% (Drewry et al, 1985). Greenland has a similar distribution of slopes, except that the ratio of the marginal areas to the total is several times larger.

Most of the ice discharging from the Antarctic ice sheet flows into the sea. In many places it floats and continues to move outward in the form of ice tongues and coalescing ice shelves, which spread out under their own weight. The largest ice shelves are hundreds of kilometers across and exhibit changes in ice thickness on the order of 1 m per kilometer. Since the ice shelves float in hydrostatic equilibrium, this produces surface slopes on the order of 1: 10,000.

Roughness characteristics: At first glance the surfaces of the ice sheets appear smooth, but in reality they are roughened in three fundamentally different ways. On the smallest scale there is the roughness caused by the wind and variations in the rate of snow accumulation, which comprises irregular features called "sastrugi" and "snow dunes" (Kotlyakov, 1966; Doumani, 1967). Sastrugi are erosional or erosional/depositional features that vary widely in size, both vertically and horizontally, depending on the wind characteristics and history in a particular region. In many areas the irregularities of the surface are 0.1 m or less in height, with typical horizontal wavelengths on the order of several meters. Over parts of the interior of Antarctica, however, the sastrugi can reach heights as great as a meter (e.g. Endo and Fujiwara, 1973); horizontal wavelengths are larger, although not necessarily proportionally larger. Snow dunes are accumulational features that are somewhat larger than sastrugi - they can be up to several meters in amplitude and tens of meters in wavelength. (N. B. These physical features are larger than the meteorologically defined "surface roughness parameter," which is the height, above the mean surface, at which the wind speed is zero and it typically has a value of 0.01 m so over a snow surface with sastrugi (Paterson, 1994, p. 62-63), because of the streamlined shapes of the sastrugi and dunes.)

Roughness due to sastrugi is anisotropic; sastrugi ridges are elongated in the direction of the wind, so the roughness characteristics are different along, and normal to, that direction.

An absence of surface roughness can also be an important characteristic of the ice-sheet surface. In particular, a smooth, glazed surface probably represents a region that has been free of snow accumulation for several years or more (Watanabe, 1978).

The second type of roughness has much longer wavelengths and has two different causes. First, there are the undulations of the surface that result from the flow of the ice over topographic irregularities in the bed. Although the flow characteristics of the ice are such that the vertical scale of the relief of the surface is much less than that of the bed, surface relief nevertheless exists and in many places is pronounced. Amplitudes of this relief are commonly a few meters to tens of meters, with horizontal wavelengths of

hundreds of meters to many kilometers. The thickness of the ice sheet modulates the surface relief in two ways - the thicker the ice, the smaller the amplitude of the surface relief and the greater its dominant horizontal wavelengths. The ice sheet acts like a band pass filter - subglacial relief of wavelengths short compared to the ice thickness is damped by the strength of the ice sheet, whereas very long wavelengths are attenuated by the plastic flow of the ice. Second are the megadunes, identifiable on AVHRR and SAR images, which are comparable in size to the flow-produced undulations but more regularly sinusoidal in form. Megadunes, which are believed to br produced by atmospheric standing waves, cover about 20% of the Antarctic ice sheet (K. C. Jezek, pers. Comm., 1999). They have not been recognized in Greenland

It is the long-wavelength roughness which grows more pronounced in the coastal regions where the ice is thinner and moving faster, that causes one of the most serious problems for radar altimetry, with its wide beam. The surface undulations are such that often the nearest point on the surface to the satellite carrying the altimeter is displaced substantially from the nadir point on the surface, or even from the nearest point on the mean sloping surface. Furthermore, the radar altimeter commonly records overlapping returns from two or more topographic high points. Under most circumstances the surface relief is far too complex, and the sampling from the radar altimeter too sparse, for it to be possible to deconvolve the radar returns to extract the real surface topography.

The third type of roughness stems from cracks in the surface - crevasses. These develop anywhere that the stresses in the ice from variations in flow exceed the breaking strength of the ice in tension. They are caused by lateral variations in flow speed and/or direction as the ice flows over basal topography, around bends in a subglacial channel, or through regions of rapid acceleration (longitudinal or transverse). Crevasses vary widely in scale, from millimeters to tens of meters across and from tens of meters to kilometers long. Spacings between crevasses are characteristically on the order of one or two hundred meters. Like the undulations, crevassing has a strong tendency to be more pronounced in locations nearer to the coast. In extreme cases, (e.g. the Jakobshavn ice tongue in Greenland) the crevassing is so severe that the surface becomes a jumbled series of pinnacles - seemingly more crevasse than ice.

Even a moderately crevassed surface will destroy the coherence of a back-scattered pulse from a satellite radar altimeter if the crevasses are open, because even a single crevasse can provide a multitude of reflecting (or diffracting) points. Furthermore, much of the strength of the signal is lost by being scattered out of the return beam.

Surface and airborne observations: In view of the extensive oversnow traverses that have been conducted in Antarctica and Greenland it is perhaps surprising that so little quantitative information has been published on surface roughness. Comments often appear in traverse reports, but they are typically qualitative and subjective, relating principally to the difficulty caused to travel by large and hard sastrugi.

A few studies of small-scale roughness from surface measurements do exist, principally from work of the Japanese Antarctic Research Expedition. The most comprehensive is that of Watanabe (1978) in central Queen Maud Land, Antarctica; that work was extended eastward to Enderby Land by Furukawa et al, 1992. The emphasis of these analyses has been on the categorization of the wind systems, particularly of the katabatic winds that dominate the East Antarctic slope region and control the orientation of the sastrugi.

Measurement of the undulations related to the subglacial topography were limited to two-dimensional profiles when the only source was the surface traverses. Analyses and theoretical studies led to various quantitative relationships between surface and basal topography (Robin, 1967; Budd, 1970; Budd and Carter, 1971; Hutter, 1981; Whillans and Johnsen, 1983; Reeh et al, 1985). When the results of extensive airborne radio-echo sounding became available, McIntyre (1986) showed the importance of extending the study into three dimensions. He found that wavelengths of two to ten times the ice thickness tend to predominate and that the energy of the surface-relief spectra increases markedly towards the coast.

Measurement objectives: There are two principal reasons for measuring the small-scale roughness (the first type). In the first place, the interaction between the rough surface and the wind moving over it is an important aspect of boundary-layer meteorology. Furthermore, the size and time-history of the surface roughness of the first type discussed above is a measure of the magnitude and history of strong winds. Secondly, the roughness is an important limiter on the accuracy of the surface-height measurements. Roughness on this scale will be reflected in the broadening of the pulse and will be indistinguishable, by that measure alone, from a mean surface slope within the footprint. For research purposes the roughness will have to be separated from the slope after the fact, when the surface elevations (and hence slopes) have been mapped.

The second type of roughness is important for the information it will reveal about ice dynamics and the subglacial topography. Those longer-scale irregularities of the surface will be revealed by the main surface-elevation mission.

It is unlikely that any quantitative measurement of crevasse characteristics (the third roughness type) will result from the GLAS measurements. Nevertheless, the occurrence of multiple returns from the ice sheet will provide a warning of the presence of crevasses, which affect the accuracy of the basic height measurements.

Radar altimetry: Many of the characteristics of satellite laser altimetry over ice sheets carry over from radar altimetry, which has a 20-year history. The basic measurement is the same in principle - the determination of the time of flight of a electromagnetic pulse from the satellite to the surface and back. For both types of altimeter the shape of the return pulse is modified by irregularities in the ice-sheet surface. There are, however important differences that arise from the different wavelengths and beam widths and that affect both the height and the surface roughness calculations. Before discussing those, however, we will review briefly the effect of surface slope and roughness on the radar pulse.

Because of the wide radar beam, the surface slope has a fundamental effect on the radar return - the return will come, not from nadir, but from the nearest point on the surface that lies within the beam. There is no immediate information in the return on the location of that point - it can only be determined using knowledge of the surface topography generated from the measurements themselves. Several schemes have been devised for doing this that differ in where the corrected height point is taken to be relative to the sub-satellite point (Brenner et al, 1983, Rémy et al, 1989; Bamber, 1994). All schemes suffer from the lack of detailed slope information in the direction normal to the sub-satellite track on the surface. This problem will be alleviated but not eliminated as digital elevation models of the surface are improved (Bamber and Huybrechts, in press).

The roughness of the surface will affect the shape of the back-scattered pulse - the greater the roughness (of the first type cited above) the broader the received pulse will be, other things being equal. The problem with using this characteristic to evaluate surface roughness is that the dominant effect on the radar pulse shape is often the undulations of the surface (roughness of type 2, above) (e.g. Martin et al, 1983). McIntyre (1986) showed that the amplitude of undulations at wavelengths less than 10 km is significant, even in the central part of the ice sheet. Distortion of the returned pulse can be exacerbated by crevassing (roughness of type 3).

Another complicating factor is that a significant portion of the incident signal may penetrate the firn to a depth of some meters before being scattered back (e.g. Partington et al, 1989). Nevertheless, by averaging a large number of wave forms and taking penetration into account, Partington et al, 1989 were able to calculate average roughness values on the plateau of Wilkes Land, Antarctica - they found the rms roughness to be about 1 m. This is significantly larger than the estimates from surface measurements, which suggests that the effects of volume scattering and/or type 2 surface undulations have not been taken fully into account. Davis and Zwally (1993) and Yi and Bentley (1994) made similar calculations from similar models, also for the East Antarctic plateau. Davis and Zwally found roughnesses ranging from

0.05 m to 0.15 m, substantially less than found by Partington et al, 1989, whereas Yi and Bentley (1994) calculated values in the 0.5 to 1 m range, closer to those of Partington et al, 1989.

Another approach is to use the total returned power, averaged over a large number of returns, as a measure of the mean surface roughness. In this way Rémy et al, 1990 calculated variations in roughness that agreed well with the expected katabatic wind variations on the East Antarctic plateau. This method, however, does not yield any quantitative estimate of the absolute roughness.

Other satellite studies. Variations in surface roughness have also been estimated from passive microwave data. Seko et al, 1991 related small differences in brightness temperature to band-shaped undulations of the surface with amplitudes of a few tens of meters and spacings of tens of kilometers. Rémy and Minster (1991) employed the fact that the difference between the brightness temperatures (or emissivities) for horizontally and vertically polarized microwaves radiated from the surface diminishes as the surface roughness increases. These differences showed a remarkably good correlation with the variations in returned power over an extensive portion of East Antarctica. Further support for the association of roughness with katabatic wind speed was found from an analysis of SEASAT scatterometer data over the same region (Rémy et al, 1992; Ledroit et al, 1992).

Comparison with laser altimetry: There are two crucial ways in which the laser altimeter differs from the radar altimeter - it has a much smaller footprint and it operates at a much higher electromagnetic frequency. The small footprint means that returns will come from only one spot on the surface at a time and that the position of that spot will be known. The high frequency means that the signal will not penetrate deeply below the surface. These characteristics simplify greatly the determination of the surface geometry. On the other hand, clouds and aerosols in the atmosphere affect the laser beam, so

- Heavy clouds (optical depth >2 or so) will completely block ground returns
- Thinner clouds and aerosols cause forward scattering which distorts the waveform, thereby shifting the centroid of the return pulse (and of fitted Gaussians) to later times.

2.2. Sea Ice

The polar oceans are, at least seasonally, covered by a thin, uneven sheet of sea ice. Although its thickness is small (a few centimeters to a few meters), sea ice has a profound influence on the physical, chemical, and biological characteristics of the oceans and the global climate system (e.g. Comiso, 1995). Because of the huge area, hostile weather conditions and long period of darkness, satellite remote sensing systems have been the major tools for mapping and monitoring the sea ice, with emphasis on microwave sensors, both active and passive (e.g. Carsey, 1992; Comiso, 1995; Perovich, 1996).

Sea ice is a complex material consisting of an ice matrix with inclusions of air, brine, solid salt and contaminants. It varies, spatially and temporally in thickness, composition, snow cover, wetness, and surface roughness. Sea ice can be classified by age (typically new ice, first-year ice, and multi-year ice), by structure (e.g. frazil, grease ice, nilas, pancake, columnar etc), or by the degree of deformation. During the winter, the surface is generally covered by snow, which in summer may melt to form slush and melt ponds. Particularly in the Antarctic, where the ice is thin, heavy snow loads can depress the ice sufficiently to permit flooding of seawater above the ice/snow interface.

Sea ice affects both the overlying atmosphere and the underlying oceans in several ways. It is a strong insulator, limiting heat exchange between ocean and atmosphere, it modulates the exchange of momentum between atmosphere and ocean, and with its high albedo it strongly affects the absorption of radiant energy by the Earth. During formation, sea ice rejects salt, and it produces fresh water when melting, thus affecting the salinity structure of the ocean with important ramifications for deep convection, bottom-water formation, and blooms of ocean biological productivity associated with the ice edge in spring. In addition to these characteristics that influence weather and climate in ways that are still

poorly understood, sea ice obstructs shipping, modifies submarine acoustics, and provides an environment essential to the survival of a wide variety of polar animals.

Sea-Ice Surface Characteristics: The most notable sea-ice deformation features are ridges, rubble fields, ice rafts, and open-water leads. Ridges can be long quasi-linear features extending for several kilometers, but they generally are sinusoidal and extend for several hundred meters. Repeated ridging causes rubble fields. Ridges usually are a meter to a few meters high and their appearance depends on their age. First-year ridges are composed of piles of very angular ice blocks, while multi-year ridges are typically well rounded, hummocky features with few, if any, voids.

On a somewhat smaller scale are the broken and rafted ice fields. Broken ice fields are formed from refrozen ice blocks and their characteristic vertical roughness ranges from a few centimeters to a meter. Rafting occurs when convergence causes one sheet of ice to override another, causing linear or sinusoidal features sometimes extending several kilometers, with vertical relief of less than a meter. Often, however, finger rafts occur, which have a distinctive square wave appearance. Wind-induced snow dunes and snowdrifts also frequently occur on snow-covered sea ice. These typically have vertical dimensions of a few cm to tens of cm.

On a very small scale, roughness is determined by the crystal structure of the surface snow or ice layer. Tucker et al, 1992 summarize the standard deviation and correlation length values published in the literature. The surface roughness usually ranges from 0.05 to 2 cm over a correlation length of 0.5 to 20 cm.

Perovich (1996) provides the most recent and comprehensive summary of sea ice optical properties. Albedo values quoted in this section are from Grenfell and Perovich, 1984. The spectral albedo of snow and sea ice is characteristically highest at visible wavelengths, decreasing strongly in the infrared because of increasing absorption by ice and water. Variations are due primarily to differences in the air bubble density, crystal structure, and fresh water content of the upper layer of the ice.

For sea ice, which is covered by fresh, cold snow, albedo is generally high. For sea ice covered by cold snow near-infrared (NIR) albedo can be as high as 0.7[1]. The aging of snow results in an albedo decrease at all wavelengths, because of the increase of grain size and rounding of the grains. This decrease is especially pronounced in the infrared (albedo for melting snow = 0.5), where absorption by ice and water is very large and the upward scattered radiation is very sensitive to the scattering properties of individual grains at the surface.

Bare sea ice has lower albedo values and exhibits more pronounced specular behavior than that of ice covered by snow. Drained white sea ice, which is located above the local freeboard level, has only slightly smaller albedos (about 0.4) than melting snow. Blue ice occurs when the surface becomes saturated with meltwater, which fills in near-surface irregularities so that backscattering is reduced. When blue ice develops into melt ponds, it can reduce the infrared albedo down to the specular reflection limit of 0.05, and it remains constant for the ponds until they refreeze or drain completely. The absorption coefficient of sea ice is very close to that of seawater, therefore the light penetration is negligible at NIR wavelengths.

Multiyear ice has survived a summer melt season, with the attendant surface melting and brine drainage to form a well-developed surface-scattering layer with many air bubbles. Consequently, albedos are typically larger then first-year ice values (Perovich, 1996).

Most sea ice can be regarded as a nearly horizontal, rough surface. The roughness is an indication of the history of the ice, and strongly influences its drag coefficient and hence its response to winds. The surface elevation of flat regions is a close approximation to local sea-surface elevation, but slightly biased upwards, depending on the ice thickness. Sea-ice covered ocean also contains icebergs, with surface

[1] All albedo values in this section are at the wavelength of the GLAS system, i.e. 1.064 microns

elevations significantly higher than that of the sea ice. The algorithms described in this document will be applied to GLAS data to provide estimates of sea-ice elevation and roughness, and of iceberg elevations.

2.3. Land

The Earth's land surface is a complex mosaic of geomorphic units and cover types resulting in large variations in elevation, slope, roughness, vegetation height and reflectance, often with the variations occurring over very small spatial scales. The spatial variations of these land surface properties are important in a host of scientific applications encompassing all Earth science disciplines. These properties are the product of a diverse set of lithospheric, cryospheric, hydrospheric, ecologic, and atmospheric processes acting on multiple time scales whose integrated effects generate the landscape seen today. Documentation of these landscape properties is a first step in understanding the interplay between the formative processes. Characterization of the landscape is also necessary to establish boundary conditions for models which are sensitive to these properties, such as predictive models of atmospheric change that depend on land-atmosphere interactions. Adequate knowledge of these characteristics is also critical to proper utilization of the land as a resource. Current descriptions of these land properties are in many respects deficient. The best publicly available global representation of the Earth's topography is a Digital Elevation Model (DEM) with a spatial resolution of 1 km, too coarse for the needs of most land process studies. This product is also an amalgam of many disparate topographic sources with inconsistent, and often poorly known, methods of production and a diversity of horizontal and vertical datums. Furthermore, on a global basis, there is no product presently available that characterizes the variation of the Earth's surface roughness and vegetation height at the short spatial scales necessary for many process studies and models. ICESat's contribution will be to provide a global sample of land topography and vegetation height data of value in their own right for characterization of landscape properties but also of great value as a reference for calibration and validation of topographic and vegetation products generated by other means. In particular, high-resolution, land topography DEMs and, to some extent, vegetation height images derived from spaceborne optical stereo photogrammetry and interferometric synthetic aperture radar techniques are becoming more readily available. The ICESat products, inherently defined in a consistent, Earth-centered reference frame will establish globally distributed geodetic control for these products.

Because of the complex variations in land surface properties at short spatial scales, the interpretation of GLAS land waveforms will be less certain than is the case for the simpler cases of ice sheets, sea ice, and ocean. Within any one GLAS laser footprint, multiple targets distributed in height can contribute to the received backscatter signal. For the land, sloped and/or rough ground, vegetation, and cultural features (e.g., buildings, vehicles, etc.) may all be contributing to a waveform. The purpose of this document with respect to land waveforms is to define methods for processing and analysis that account for the potential complexities of the surface-height distribution within land footprints.

2.4. Ocean

ICESat will spend most of its lifetime over the ocean acquiring a vast amount of information on sea-surface characteristics. The shape of the GLAS return-pulse waveform will be determined primarily by the surface-height distribution within the footprint, which is small enough to be affected by individual large waves.

Over distances of cm to a few hundred meters, the sea surface is roughened by waves and ocean swell, but over distances of many km, the sea surface is almost flat and horizontal. Nevertheless, surface slopes and long-wavelength undulations are present, caused by variations in Earth's gravity field, associated for instance with sea mounts, ocean currents, and variations in atmospheric pressure and seawater density. Satellite radar altimeters have shown remarkable success in measuring sea-surface elevation and significant waveheight, and will continue to be the prime tool for this purpose. Because of its large effective footprint, a satellite radar altimeter averages the effect of the small-scale roughness in the

information contained within the composite, 0.05 -0.1 second return pulse from which estimates of surface elevation and roughness are inferred. Consequently, the resulting sea-surface elevations can be used to study the longer-wavelength variability, and estimates of surface roughness are a statistical indication of the wave height. Errors are primarily associated with orbit uncertainty, atmospheric effects, and noise in the instrument system. The noise effects require averaging of several return pulses (at least 1 second's worth) for highest accuracy, which limits along-track spatial resolution. There may also be a range-measurement bias, associated with asymmetry in the shape of ocean waves, which increases with increasing wave height.

2.5. Experiment Objectives

The objectives of GLAS surface elevation measurements are stated in detail in the *Geoscience Laser Altimeter System (GLAS) Science Requirements* document available online at http://www.csr.utexas.edu/glas/Science_Objectives/. In summary, they are:

- Measure elevation changes of the Greenland and Antarctic ice sheets for the purpose of assessing:
    a. mass balance,
    b. seasonal and interannual elevation variability,
    c. elevation trends, and
    d. contribution to sea level rise
- Determine precise elevation topography and surface roughness of ice sheets and sea ice.
- Conduct global topographic measurements to contribute to topographic maps and digital elevation models as well as detect land elevation changes in excess of 1 meter per year in certain selected regions.

In order to achieve these objectives, accurate and consistent interpretation of the waveforms is necessary. Toward that end, the goals of the waveform surface elevation algorithm development are:

1. Define and determine the surface elevation from the laser waveforms
2. Identify and interpret multiple returns
3. Determine surface roughness and slope based on waveform characteristics.

2.6. Historical Perspective

The idea of using an altimeter in a space orbit to measure the earth's surface was first shown as feasible when a radar altimeter was flown on Skylab in 1974. In 1975 GEOS-3 became operational with a radar altimeter that was designed to measure the ocean surfaces. GEOS-3 covered latitudes of +/- 65 deg which included the southern tip of the Greenland ice sheet. Brooks et al, 1978 showed the feasibility of using these radar altimeter measurements to get topographic measurements over Greenland. Two other U.S. missions, SEASAT in 1978 and GEOSAT (1985-89), flew radar altimeters also designed to measure ocean surfaces. These covered latitudes to +/- 72 deg and could only maintain track over slopes less than 1 deg giving coverage of 40% of Greenland and 24% of Antarctica. NASA developed algorithms (Martin et al, 1983) to post-process the return pulse energy waveform to calculate surface elevations of the ice sheets, and topographic maps were produced (Zwally et al, 1983). Methods were also developed to calculate elevation changes using information from crossing arcs from measurements at different times (Zwally et al, 1989).

The launching of the ERS-1 radar altimeter and its successor ERS-2 have given us continuous ice sheet measurements since 1991 that extended coverage up to +/- 81 deg. These newer altimeters were also

designed with a special ice mode capability to extend coverage of tracking into the more sloping regions of the ice sheets and land. Elevation change estimates have been calculated from the radar measurements giving change histories from 1978 to present day (Wingham et al, 1998, Davis et al,1998). However, due to limitations of radar altimetry these have large error bounds. Radar altimeter data have also been applied to measurement of land elevations in a few cases. (Frey and Brenner 1990, Brenner et al, 1990, Koblinsky et al, 1993, Bamber and Muller 1998).

There are several limitations in measuring ice sheet and land elevations using radar altimetry:

1. The footprint is very large 10-20 km in diameter, increasing with the surface slope.
2. The measurement is a mean elevation over the footprint surface for flat surfaces with small undulations.
3. Over sloping surfaces, the measurement is to the higher elevations which are not necessarily at the sub-satellite location, and topographic knowledge is inadequate to properly geolocate the measurement.
4. Tracking can only be maintained over small slopes, ~ 1 deg

A spaceborne laser altimeter can overcome many of these limitations. The footprint for GLAS is ~70m so that the effect of sloping surfaces is reduced greatly. GLAS should easily be able to track surfaces on slopes up to 3 deg, which includes the majority of the continental ice sheets. The main problem with the small footprint is the accuracy to which the off-nadir angle must be known in order to precisely geolocate it. This is being addressed with the star cameras and the laser spot imaging.

A small footprint (1m), scanning laser altimeter, the Airborne Topographic Mapper (ATM) has been flown successfully over the past 10 years on aircraft over the Greenland ice sheet (Thomas et al, 1994,) with the objective of measuring the rate of change of surface elevations towards assessing ice-sheet mass balance. As with all laser altimeters, major limitations are the accuracy of the aircraft position in inertial space and atmospheric interference in the form of clouds or ice fog. Nevertheless, 10-cm accuracy is achieved over flight lines of several hundred km (Krabill et al., 1995), yielding data that have been used to infer rates of ice thickening and thinning over much of the ice sheet (Krabill et al., 2000). The scanning ability of the ATM provides highly-detailed surface topography within the 140-300m surveyed swath, which can be used to help simulate GLAS waveforms and, after launch, to validate GLAS-derived surface elevations and roughness.

The predecessor of GLAS, the Mars Orbiting Laser Altimeter, MOLA, uses algorithms similar to those that GLAS will use and has shown the feasibility of using a spaceborne laser to map a planet surface (Zuber et al, 1998). The accuracy of MOLA is limited by its tracking algorithm (post-processing is not feasible since there are no waveforms telemetered) and the orbit accuracy which is driven by the precision of the gravity models available to date. Orbit determination with the advent of GPS, more accurate force models, and sophisticated computer techniques can give us the position of the earth-orbiting ICESat satellite to an accuracy of 5 cm in inertial space. This, combined with the very accurate attitude knowledge, altimeter measurements, and models to account for the atmospheric delays and earth dynamic effects, will allow us, in ideal conditions, to measure the ice sheets to within 10 cm. The Shuttle Laser Altimeter (SLA) experiment provides space-based heritage for the ICESat mission. SLA is a pathfinder experiment devoted to: (1) evaluating engineering and algorithm techniques for high-resolution, orbital laser altimeter observations of terrestrial surfaces, and (2) providing pathfinder scientific datasets of value in addressing global Earth System science issues (Garvin, et al, 1998). The first and second flights of SLA characterized ocean, land, and cloud top elevation and vertical roughness in 100 meter diameter laser footprints spaced every 700 meters along a nadir profile. SLA is a hybrid instrument combining ranging electronics modified from the MOLA design (Zuber, et al, 1992), with a high-speed digitizer used to record the backscatter return amplitude as a function of time (i.e., waveform). Processing methodologies developed from the Shuttle Laser Altimetry, SLA, missions (Garvin et al, 1998) and radar

altimetry (Zwally et al, 1994) have laid a good background from which to produce operational algorithms to process the GLAS measurements and allow us to meet our science requirements.

Airborne laser altimeter heritage also provides experience in utilizing lidar waveforms for characterizing surface elevation and vegetation canopy height. Several implementations of airborne surface lidars have adapted bathymetric water depth sounding lidars in order to assess their ability to measure forest canopy height using green wavelength backscatter waveforms (Aldred and Bonnor 1985, Nilsson 1996). A near-infrared, ND:YAG lidar system developed at Goddard Space Flight Center was specifically optimized to measure canopy vertical structure and the elevation of the underlying ground (Bufton et al, 1991, Blair et al, 1994). A scanning version of this system, the Scanning Lidar Imager of Canopies by Echo Recovery (SLICER), has been used to measure canopy structure of Eastern U.S. deciduous forests (Lefsky 1997, Lefsky et al, 1999) and Pacific Northwest fir stands (Harding et al, 1994, Harding 1998, Lefsky et al, 1998, Means et al, 1999). The SLICER waveform measurements of canopy height and structure show strong correlations with ecologically important forest stand attributes such as above ground biomass and stem basal area. The waveform data used to date to characterize canopy structure and ground topography beneath canopies were acquired using laser footprints on the order 10 m in diameter. Airborne lidar waveform measurements with footprints in a variety of sizes and configurations have been used to monitor topographic change at Long Valley Caldera, California (Hofton et al, in press). The Goddard airborne lidar system has also been used in a large-footprint profiling mode (Bigfoot) to collect data over the Greenland ice sheet and vegetated terrains of North America that emulate the waveform data to be acquired by ICESat.

2.7. Instrument Characteristics

The GLAS instrument uses an Nd:YAG laser with 1064 and 532 nm output. The elevation measurements are determined from the round-trip pulse time of the infrared pulse, while cloud and aerosol data are extracted from the green pulse. The instrument is nadir-viewing with a pointing accuracy of 20 arc seconds. The post-processed pointing knowledge is expected to be 1.5 arc seconds. At a nominal altitude of 600 km, the 375 microradian field-of-view telescope has a spot-size of 70 $\pm$ 10 m in diameter. The pulse frequency is 40 Hz, which results in spots that are separated by 175 meters center-to-center on the ground. The requirement for knowledge of post-processed position is better than 5 cm in the radial direction, and better than 20 cm horizontally.

The platform is to be placed in a 183 day ground track repeat cycle (except in the initial 90-day verification phase) which yields 15 km spacing between repeat tracks at the equator, and 2.5 km spacing at 80 degrees latitude. This will allow for adequate measurements to be able to calculate the required accuracy of mean elevation changes after averaging over 100 km^2.

The GLAS instrument algorithms are described in detail in McGarry et al. The following excerpts give enough information so that the reader can understand the algorithms described in this ATBD. The laser altimeter on ICESat will collect about 4,500,000 1-ns samples for each transmitted laser pulse. It will not be possible to telemeter this entire data stream to Earth, so on-board processing of the GLAS waveforms will be essential to retrieve the desired data. 544 samples will be telemetered over ice sheet and land surfaces and 200 samples over sea ice and ocean surfaces. The GLAS on-board altimetry algorithm was developed to maximize the chance that the telemetered data will include the ground return. This meets the science requirement of being able to maintain measurement over 3 deg slopes and gives a large enough range window (81.6m over land and land ice and 30 m over sea ice and ocean) to measure all levels of expected roughness.

The algorithm does not include an acquisition or tracking phase, but relies on a simpler scheme using a Digital Elevation Model (DEM) to select the region of the echo waveform to be searched for the ground return.

The altimeter algorithm bounds the search area of the digitized waveform using apriori information stored in an onboard Digital Elevation Model (DEM). The DEM is interrogated once per second to determine min and max values of the range window and the type of surface (ocean, sea ice, land, or ice sheet), which will determine the number of elements in the returned waveform and the vertical range it covers.

The digitized waveform information within this DEM bounded region (called the Range Window) is filtered through 6 matched filters (in the hardware electronics) to maximize the probability of finding echoes from sloped or rough terrain and minimize the probability of selecting cloud returns. A separate threshold is determined for each of the filtered waveforms to distinguish the signal level from that of the noise. The thresholds are set as a function of the noise using a 1 km region of the digitized waveform beyond the end of the Range Window where we are sure that no laser light is reflected back to affect the calculation.

Because the echo from the ground is expected to be the last local maximum in the Range Window, the algorithm searches for the surface echo backward in time from the end of the Range Window towards the start. The pulse defined by the first threshold crossing (from below the threshold to above) to the next corresponding threshold crossing (from above the threshold to below) is selected for each filter (providing that such a pulse exists for each filter). A weighting factor which is a function of pulse attributes is used to determine which filtered output is most likely to contain the surface echo.

Once the filter has been selected, it is used solely to determine where the start of the received waveform digitized data sampling will be. The data to be sent to the ground are obtained directly from the received digitizer waveform. 1000 1 ns samples are stored on-board from which to select the telemetered return. The samples can be sent at full resolution or compressed to enlarge the measured range span to cover tall trees and large topographic relief. Two different compression ratios can be used, one for the beginning and one for the end of the waveform. The sample at which the compression ratio changes is also input. The compression ratio allows one to increase the range window over land if requested in order to assure that all canopy heights are included. Nominally the 81.6m range window should be adequate, but for special requirements the compression option will be turned on.

3.0 ALGORITHM THEORY

This section presents the physics behind the problem and how to parameterize the altimeter return pulse to obtain physical results.

3.1. Physics of Problem

3.1.1. Introduction

The GLAS system will use a pulsed laser to measure the precise range from the satellite to the terrain and to provide clues of the surface elevation distribution within the laser footprint. Average reflectivity of the surface at the monochromatic laser wavelength will also be obtained from the ratio of the transmitted and received energy.

This chapter summarizes the background on the waveform and timing of the backscattered laser signal. Assuming that the effect of forward scattering by clouds and aerosols is negligible the shape of the received signal is determined by the range distribution inside the laser footprint modulated by the local reflectivity and the incident beam pattern. Gardner (1982, 1992) and Tsai and Gardner (1982) have developed detailed analytical expressions (see Section 3.1.2.1) to describe the received pulse for simple ground target geometry. These expressions have been used to evaluate the performance of satellite laser altimeter systems (Gardner, 1992 and Harding et al, 1994) and to develop algorithms for GLAS data

processing (Csathó and Thomas, 1995). For complex terrain the received waveform can be computed by using the Goddard Laser Altimetry Simulator Software (Abshire et al, 1994).

3.1.1.1. Ice Sheet Elevation.

The satellite laser altimeter makes three basic measurements: the range between the satellite and the surface footprint, the shape of the return waveform after reflection from the earth surface, and the laser power returned from the surface. The ice sheet elevation for GLAS is measured as the mean surface height of the laser footprint, which is the difference between the satellite height and the range between the satellite and the surface. The satellite height is determined from the orbit and is independent of the laser measurement. The range is measured by calculating the laser pulse travel time to the surface, correcting for atmospheric and instrument and accounting for the heights of the ocean, solid, load, and polar tides. The shape of the return waveform is affected by the transmitted pulse, the surface height distribution within the footprint, atmosphere scattering and the receiver. If the transmitted pulse is close to a Gaussian, the surface is a mean slope plus random height variations, and there is no atmospheric forward scattering, the return pulse shape will be very close to a Gaussian. Our test results show that fitting a Gaussian pulse to the waveform and then using the centroid of the Gaussian will help to diminish the effects of non-ideal conditions including irregular surfaces and forward scattering when the fitting using only the gates near the pulse center.

3.1.1.2. Ice Sheet Roughness And Slope.

Our approach is based on the assumption that there is a spectral minimum in surface roughness that lies in the range of a few hundred meters and separates the wind-generated roughness at shorter wavelengths from the undulation generated by basal topography at longer wavelengths. That being the case, we can consider the surface within the footprint as characterized by a mean slope, which is a short segment of the long-wavelength undulations; superimposed on that slope is a large number of wind-generated bumps of short wavelength. Correspondingly, we make two calculations, based on the alternate assumptions of a smooth, linearly sloping surface and a rough flat surface. After more quantitative knowledge is gained of the slope from GLAS, we may be able to calculate the roughness using this.

We assume that the surface is a diffuse (Lambertian) reflector, that is the emerging radiance is constant for all directions in a hemispherical solid angle. The surface reflectivity is also assumed to be uniform within the 70 m footprint.

Effect of roughness: We assume that small-scale roughness has a Gaussian distribution, which also implies that there are a sufficient number of bumps within the footprint to justify a statistical approach. Although there is no reason to suppose that this distribution of heights is realistic for the snow dunes and sastrugi that roughen the surface, since they tend to have a regularity of form and size within a small area (Doumani, 1967), there is no quantitative basis for any other assumption. It will require ground-truth experiments to provide a quantitative correlation between surface conditions and the roughness calculated from the GLAS algorithm.

Effect of slope: For the purposes of algorithm development we assume a linear slope. Since the dominant wavelengths of surface undulations are generally over 10 km (McIntyre, 1986), this should be a good approximation across the 70 m footprint.

Combined effect: There is no realistic way to ascertain from the shape of a single returned pulse to what extent the pulse-broadening has been caused by the roughness and to what extent by the mean slope, even though the pulse shapes are slightly different in the idealized, theoretical cases, because the distortion caused by deviations from our idealized assumptions will surely be large compared to that slight difference. We therefore make no attempt to separate the two effects; our data product will be two numbers stemming from alternate analyses of the same pulse. One will give $\mathrm{Var}(\Delta x)$, calculated on the assumption of roughness alone, and the other will give the mean slope, calculated on the assumption of a

tilted, planar surface. Which is more nearly appropriate in a given situation is a matter that can only be determined by reference to ancillary information about the nature of the region observed.

3.1.1.3. Sea Ice Elevation And Roughness

Within each 70-meter GLAS footprint, incident near infrared (NIR) laser energy will be reflected to the receiving telescope with a time delay determined primarily by surface elevation and surface roughness (for the moment, we neglect the effect of forward scattering by clouds and aerosols), and intensity determined primarily by reflectivity of the surface and the energy beam pattern incident upon the surface. The average time delay of the return energy gives the average range to surfaces within the footprint, and the temporal variation of return-pulse intensity is a measure of the range distribution within the footprint modulated by local reflectivity and the incident beam pattern. The shape of the return pulse is smoothed by the detection system, limiting the information that can be retrieved. Moreover, forward scattering of laser energy in transit through the atmosphere will increase return-pulse spreading beyond that caused by surface roughness. Consequently, little is to be gained by overly sophisticated algorithms, and our objective is to extract the least ambiguous sets of information, and to identify them as objectively as possible.

The major sea-ice parameters determined from GLAS waveforms include elevation, surface slope and roughness, and surface reflectivity. Surface roughness is a statistical description of the surface, representing its deviation from a smooth reference surface (Ogilvy, 1991). The standard deviation of surface elevations from their mean is a good way to characterize the surface roughness of horizontal surfaces. The reflectance (ratio of reflected energy flux to the incident flux) measured by GLAS can be related to the spectral albedo of the surface (ratio of total upwelling irradiance and the total downwelling irradiance).

3.1.1.4. Land Elevation, Surface Slope and Roughness, and Vegetation Height

Interpretation of land properties from GLAS return pulse waveforms is complicated by the diverse nature of land constituents and the small spatial scale over which these constituents can vary. The possibility of steep surface slopes, large roughness and the potential presence of vegetation and/or cultural features (e.g., buildings, vehicles, structures) within a laser footprint leads to ambiguity in waveform analysis. For the purpose of this document, land slope is considered to be the mean planar slope of the surface across the laser footprint and land roughness is random height deviations of the surface from that mean plane. Land surface relief is the minimum to maximum elevation within the footprint caused by slope and roughness. The land surface is considered to be the surface absent any overlying vegetation (living or dead) or cultural features. The land surface may be composed of solid Earth components (e.g., rock, sand, soil), water (e.g., inland lakes, rivers, inundated areas), snow, or ice.

For footprints lacking vegetation or cultural features, the interpretation of the land surface elevation is like that for ice sheets, sea ice, and oceans. The time history of backscatter energy is a measure of the vertical distribution of intercepted surface area (projected in the direction of the laser vector) weighted by the reflectance of the surfaces at the monochromatic laser wavelength and the spatial distribution of laser energy across the footprint. The recorded waveform is the product of this measure convolved with the temporal character of the transmit pulse, the receiver electronics, and atmospheric scattering. These convolved effects are ideally removed by waveform processing yielding a reflectance- and illumination-weighted surface height distribution. The centroid of that distribution is taken to be the measure of the footprint elevation. As is the case for ice sheets, lacking independent information the slope versus roughness contributions to the surface height distribution can not be distinguished within the ICESat footprint. End-member, model measures of slope and roughness can be derived assuming no roughness and slope contribution to the pulse spreading, respectively.

For footprints containing vegetation and/or cultural features, the surface height distribution created by slope and/or roughness will be combined with the height distribution of canopy components (living or

dead foliage and woody tissue) and cultural features. In areas of low to moderate slope and roughness, experience with small footprint (on the order 10 meter diameter) airborne lidar data have shown that vegetated or urbanized landscapes typically yield multi-modal waveform returns. Each mode, or peak, of the waveform corresponds to footprint constituents differentiated in height. Where sufficient laser energy penetrates the canopy and reaches the underlying ground, a last peak corresponding to the ground surface is acquired in the waveform. Higher peaks correspond to discrete vegetation layers and/or the tops of cultural features. The initial return corresponds to the upper-most detected canopy surface or highest cultural feature. Maximum vegetation or building height within the footprint is readily derived from the time delay between the initial and last returns, where maximum refers to the height at which there is return energy sufficient to be detected (dependent on intercepted area, reflectance and laser spatial energy).

The ability to differentiate the height of discrete components within the footprint decreases as the surface relief, due to slope and roughness, increases and as the footprint size increases. With increasing relief the height distribution of the surface becomes mixed with the height distribution of vegetation or cultural features. This effect is compounded by increasing footprint size. For 70 m ICESat footprints, moderately sloping and/or rough terrain can have surface relief commensurate with the height of overlying vegetation or cultural features, causing these contributions to be unresolvable in the waveform. Furthermore, the canopy height distribution becomes less resolved at larger footprint scales as multiple vegetation layers at various heights become spatially averaged. Finally, the meaning of maximum vegetation height, which pertains to the highest vegetation above the ground at a specific location, becomes ambiguous for large footprints where ground relief can be of the same magnitude as vegetation height. Experience with 100 m diameter SLA footprints and 70 m diameter airborne lidar footprints demonstrates that multi-modal returns are common but it is difficult, without independent knowledge of land cover and surface relief, to confidently assign returns within the waveform to specific terrain components.

As is the case with atmospheric forward scattering, multiple scattering from canopy components will cause increased path length and thus delayed return energy in waveforms from footprints containing vegetation. Multiple scattering of optical energy in canopies is a complex process dependent on wavelength, the amount of transmission through foliage, and the three-dimensional distribution of canopy components. The published literature to date evaluating airborne lidar and SLA canopy waveforms has not incorporated models of multiple scattering, considering the effect on canopy height derivation to be small. Consideration of canopy multiple scattering is beyond the scope of operational ICESat waveform processing, and is more appropriately treated as a research issue.

3.1.1.5. Ocean Elevation And Roughness

Each clear-weather GLAS return pulse will provide estimates of average surface elevation and of surface-height distribution within the corresponding 70-meter footprint, at a rate of 40/second. However, these footprints will, in general, cover less than one of the longer ocean waves, and it will be necessary to include information from many consecutive footprints to infer sea-surface elevation and wave height. Surface elevation will be obtained by averaging the elevation of these many footprints, and the maximum wave height will be given by the highest and lowest surface elevations inferred from the all the pulse widths for wavelengths less than twice the footprint diameter. The length of orbit track over which this "averaging" must be done will depend on the sea state, and it should be possible to calculate this length from the sea-state information that GLAS will provide.

3.1.2. Analysis Of Waveforms Obtained By Pulsed Laser Altimeters

Pulsed laser altimeters estimate the range to the terrain surface by measuring the round trip time-of-flight of a laser signal. The received signal is spread in time, in part due to the variation of range between the laser firing point and the surface features. For statistically uniform, diffuse surfaces with uniform reflectivity the expected signal at the receiver output can be expressed as the convolution of the surface

profile probability density with the flat diffuse target response (Gardner, 1982). For returns from the ocean surface the shape of the backscattered signal is closely related to the height probability density of the specular points within the footprint (Tsai and Gardner, 1982). The following description of the analytic expressions is adapted from (Gardner, 1992).

3.1.2.1. Analytic Expressions For Flat Or Uniformly Sloping, Terrain

The geometry of the model is illustrated in Figure 2. The coordinate system is defined by the optical axis of the altimeter and the line from the altimeter (A) to the center of the Earth, which determines the direction of the z-axis. The x-axis lies in the plane defined by z and the optical axis and it is perpendicular to z, and y completes the right hand system. The origin of the coordinate system is at the intersection of the optical axis and the terrain surface (F).

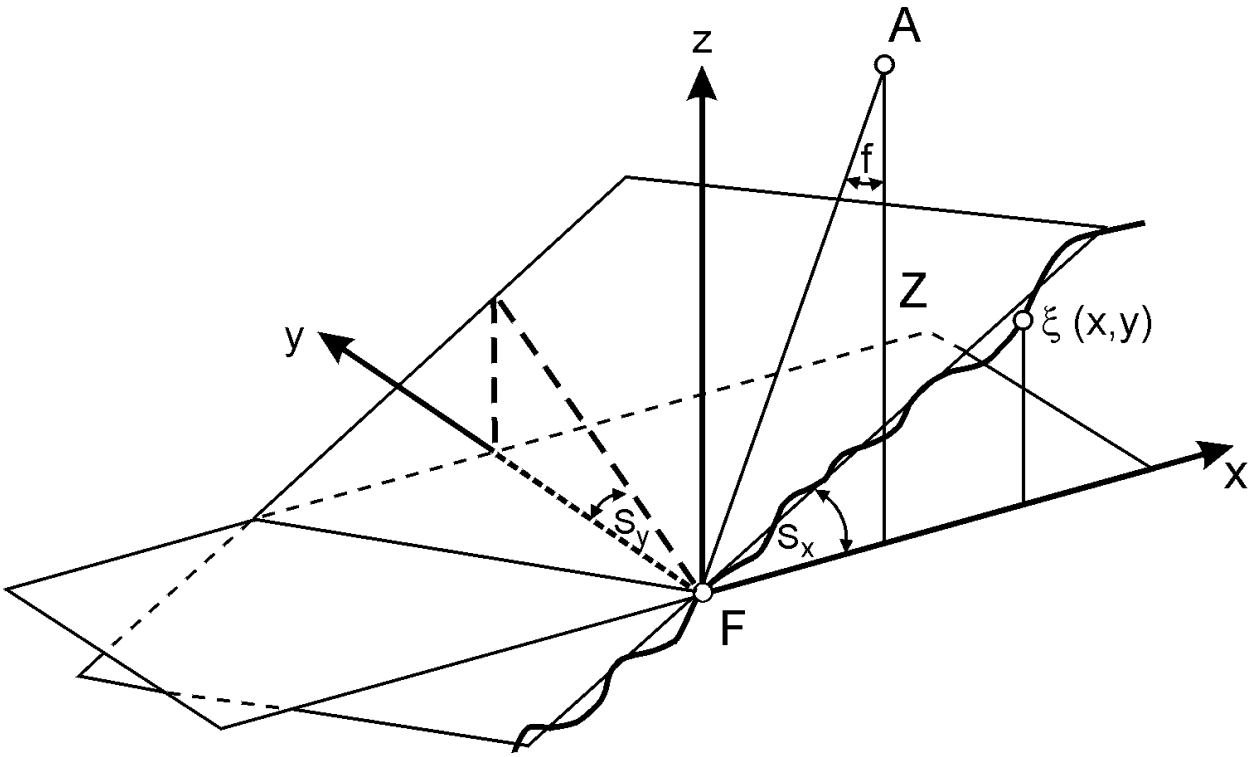

Figure 2- Generalized geometry of the terrain

The surface profile within the laser footprint is modeled as

$$\xi(\vec{r}) = \xi_0 + \vec{S} \bullet \vec{r} + \Delta\xi(\vec{r}) \qquad [1]$$

where $\vec{r} = (x, y)$ is the horizontal position vector on the ground, ξ_0 is a constant offset, $\vec{S} = (S_x, S_y)$ is the mean surface slope within the footprint, and $\Delta\xi(\vec{r})$ is the random microstructure of the surface.

3.1.2.1.1. Diffuse Terrain Types (Land, Snow)

Gardner (1982, 1992) has analyzed the performance of pulsed laser altimeters for sloping, Lambertian (diffuse) terrain with quasi-random surface roughness and uniform reflectivity. He neglected the effect of the forward scattering by clouds and aerosols. By assuming a Gaussian laser beam cross-section he obtained the following analytical expressions for the mean pulse delay and for the RMS pulse width.

The expected mean pulse delay is composed from the propagation delay along the center from the laser beam, the additional delay resulting from the phase front curvature of the diverging laser beam, and the biases caused by the pointing jitter, that is

$$E(T_P) = \frac{2z(1+\tan^2 q_T)}{c\cos f} \left[1+\left(1+2\tan^2(f+S_x)\right)\frac{Var(\Delta f_x)}{2}+\cos^2 f\left(1+\frac{2\tan^2 S_y\cos^2 S_x}{\cos^2(f+S_x)}\right)\frac{Var(\Delta f_y)}{2}\right] \quad [2]$$

where T_P is the propagation delay measured by the pulse centroid time, c is the effective velocity of light (m/s), f is the off-nadir pointing angle of laser beam, S_x is the surface slope in (xz) plane, S_y is the surface slope in (yz) plane, z is the altimeter height above the terrain (m), q_T is the halfwidth divergence angle of the laser beam measured at the $1/\sqrt{e}$ point (rad), Δf_x is the pointing error parallel to the pointing direction, and Δf_y is the pointing error perpendicular to the pointing direction.

The mean-square pulse width is the sum of the effects of the system, surface roughness, beam curvature, off-nadir angle, and surface slope, that is

$$E(s_P^2) = (s_l^2+s_h^2)+\frac{4Var(\Delta\xi)\cos^2 S_x}{c^2\cos^2(f+S_x)}+ +\frac{4z^2\tan^2 q_T}{c^2\cos^2 f}\left[\tan^2 q_T+\tan^2(f+S_x)+\frac{\tan^2 S_y\cos^2 S_x}{\cos^2(f+S_x)}\right] \quad [3]$$

where s_P is the RMS received pulse width (s), s_l is the RMS transmitted pulse width (s), s_h is the RMS width of receiver impulse response (s), $\Delta\xi$ is the surface roughness (m).

3.1.2.1.2. Ocean Surface

The ocean surface is a specular (non-diffuse) reflector. Tsai and Gardner (1982) have derived expressions to compute the mean pulse delay and the RMS pulse width over specular surfaces. To simplify the analysis they assumed Gaussian transmitted laser pulse shape and laser cross section. If the altimeter points at nadir ($f=0, \Delta f_x=0, \Delta f_y=0$), and Gaussian ocean surface statistics are assumed, the statistics of the returned pulse can easily estimated. Although for large beam divergence angles (larger than 10^{-2} rad) the received waveform is highly asymmetrical, for the small divergence angles used on satellite laser altimeters the waveform is nearly Gaussian. For small beam divergence angles the expected pulse delay is:

$$E(T_P) = \frac{2z}{c}+\frac{2z}{c}(\tan^{-2} q_T+2S^{-2})^{-1} \quad [4]$$

where S = magnitude of $\vec{S}$.

Equation 4 differs from the reflection from the diffuse surface (equation 2) only by the presence of the S^{-2} term. Upon reflection from the ocean surface, the laser cross section is modified by the distribution of the surface slopes and the S^{-2} term accounts for this modification. This additional delay will introduce a small error into the ocean surface elevation. More research needs to be undertaken to determine the size of this error and its effect.

The RMS width of the received pulse is:

$$E(s_P^2) = (s_l^2 + s_h^2) + \frac{4}{c^2}\Delta\xi^2 + \frac{4z^2}{c^2}(\tan^{-2} q_T + 2S^{-2})^{-2} \qquad [5]$$

If the beam divergence is of the order of 10^{-3} rad or smaller, the last term will be approximately $(4z^2/c^2)\tan^4 q_T$. Then the surface roughness can be computed from the RMS pulse width of the return signal and known system parameters. Tsai and Gardner also derived expression for non-Gaussians ocean surface using the skewness coefficient to describe the non-Gaussian behavior. Due to the complex nature of the ocean returns the errors in the mean elevation and the significant wave height computed from individual returns can be quite large. To reduce the errors several waveforms should be averaged or "stacked" as it is recommended in 3.1.1.5.

3.1.2.2. Algorithms Derived From The Analytical Expressions

Algorithms can be derived from the analytical expressions to compute parameters describing the changes in surface elevation within the laser footprint (for example roughness, slope).

3.1.2.2.1. Ice Sheet Elevation

The assumption is being made that the return will closely resemble a Gaussian and therefore a Gaussian pulse will be used to fit the waveform. The centroid of the Gaussian pulse will be used to calculate the range to the mean surface. This range then must be corrected for atmospheric delays using algorithms defined in the GLAS atmospheric correction ATBD, and the effect of time-varying tides removed using algorithms in the GLAS tide ATBD. Using this corrected range, the satellite position above the ellipsoid, and the off-nadir pointing angle; the surface elevation can be calculated using the algorithms defined in the GLAS laser location and surface profile ATBD.

3.1.2.2.2. Ice Sheet Roughness/Slope

<u>Rough, flat surface</u>**:** For horizontal surfaces $\vec{S} = \vec{0}$ and equation 1 becomes

$$\xi = \Delta\xi + \xi_0 \qquad [6]$$

With $S_x = 0$ and $S_y = 0$ from equation 3 we get

$$E(s_P^2) = (s_l^2 + s_h^2) + \frac{4Var(\Delta\xi)}{c^2\cos^2 f} + \frac{4z^2\tan^2 q_T}{c^2\cos^2 f}(\tan^2 q_T + \tan^2 f) \qquad [7]$$

Satellite laser altimeters have a small off-nadir pointing angle and beam divergence. Therefore the third term in equation 7 can be neglected and we obtain

$$E(s_P^2) = (s_l^2 + s_h^2) + \frac{4Var(\Delta\xi)}{c^2} \qquad [8]$$

From equation 8 we finally have

$$sdev(\xi) = [Var(\Delta\xi)]^{1/2} = \frac{c}{2}\left(E(s_P^2) - s_l^2 - s_h^2\right)^{1/2} \quad [9]$$

By using this formula the RMS surface roughness of a horizontal surface can be estimated from the received pulse width and from the known system parameters of the GLAS altimeter.

Sloping, smooth surface:

Set $Var(\Delta\xi) = 0$, and $f = 0$, from equation (3), we have

$$E(s_P^2) = (s_l^2 + s_h^2) + \frac{4z^2 \tan^2 q_T}{c^2 \cos^2 f}\left(\tan^2 q_T + \tan^2 S_x + \tan^2 S_y\right) \quad [10]$$

Since,

$$\tan^2 S_x + \tan^2 S_y = \tan^2 S \quad [11]$$

and for GLAS q_T is on the order of 10^{-5} radians, we can ignore the $\tan^2 q_T$ term and write,

$$E(s_P^2) = (s_l^2 + s_h^2) + \frac{4z^2 \tan^2 q_T}{c^2} \tan^2 S \quad [12]$$

Then,

$$\tan S = \frac{c}{2z \tan q_T}\left(E(s_P^2) - (s_l^2 + s_h^2)\right)^{1/2} \quad [13]$$

Or,

$$S = \tan^{-1}\left[\frac{c}{2z \tan q_T}\left(E(s_P^2) - (s_l^2 + s_h^2)\right)^{1/2}\right] \quad [14]$$

3.1.2.2.3. Sea Ice Elevation And Roughness

Sea ice can be modeled by horizontal, randomly rough Lambertian (diffuse) surfaces, so equation 9 of the previous section applies.

In general, a sea-ice footprint will contain either a mixture of rough and smooth ice (or open water) or predominantly smooth ice (or open water). Less frequently, an entire footprint could be occupied by rough ice, or an iceberg, glacier, land ice, or land could occupy all or part of the footprint. In general, the average elevation of smooth or randomly rough ice (or open water) will be represented by the centroid of the latest, approximately Gaussian peak in the return pulse. Other surfaces in the footprint will have shorter ranges and their effect on return-pulse shape will be determined primarily by their surface height distribution. In some cases, such as when the smooth top of an iceberg fully occupies the footprint, the latest peak will not be smooth sea ice. However, this should be readily identifiable by its height above the geoid.

The key products to be derived for each GLAS "sea-ice" footprint will be:

a. Average elevation of sea ice or open water

b. Average elevation of features such as ice bergs that partly or entirely occupy a footprint

c. RMS sea-ice surface roughness

d. Average reflectance

The sea-ice elevations will help improve the geoid, and surface roughness strongly influences both heat and momentum exchanges between the atmosphere and the ice. The reflectance is indicative of sea-ice albedo, which also affects energy exchange. Recent work with satellite radar-altimeter data (Peacock et al, 1998) indicates the possibility of estimating sea-ice freeboard, a proxy indicator of thickness, by comparing elevations of open-water leads with those of the intervening ice. Data from GLAS could be better suited to this application because of their small footprint. Even if identification of open-water waveforms is difficult, it might be possible to identify leads by the abrupt change in elevation between lead and sea ice. This is a research area, and is beyond the scope of a sea-ice algorithm, but if successful it would represent a major enhancement to our ability to monitor sea ice.

3.1.2.2.4. Land Elevation, Surface Slope and Roughness, and Vegetation Height

Due to the potential complexity of land returns, the waveform processing methodology uses an approach that characterizes the return by fitting Gaussian distributions to each mode (i.e., peak) identified within the waveform. Each Gaussian distribution is described following the methodologies defined in 3.1.2.2.1 and 3.1.2.2.2 for ice sheets, with the centroid equivalent to the mean reflectance- and illumination-weighted elevation and the variance a measure of pulse spreading. Interpretation of those fitted distributions in terms of elevation, surface slope and roughness, and vegetation height then depends on the character of the return (uni-modal or multi-modal) and an assumption, or independent knowledge, of land cover type within the footprint. For uni-modal returns thought to be from footprints lacking vegetation or cultural features the interpretation is straightforward. The centroid is the mean surface elevation and the variance is due to the combined effects of surface slope and roughness that can be modeled as end-member cases as for ice sheets. Uni-modal returns thought to be from footprints containing vegetation or cultural features are more ambiguous since the contributing components can not be differentiated in height. The centroid in this case is the mean elevation of all intercepted components and its relationship to the surface elevation depends on the unknown density and spatial organization of overlying vegetation and cultural features. Similarly, the Gaussian variance is due to the height distribution of all intercepted components, not just surface slope and/or roughness. For multi-modal returns an assumption is made that the last peak in the waveform corresponds to the surface and that earlier peaks correspond to overlying vegetation and/or cultural features. The centroid and variance of the Gaussian distribution fit to the last peak are then used to define the mean surface elevation and the pulse spreading due to surface slope and/or roughness. The maximum height of overlying vegetation, or cultural features, is then taken to be the distance from the leading edge of the initial return in the waveform to the centroid of the last return.

The assumption that the last peak in multi-modal land returns corresponds to the surface is useful for operational processing of the waveforms, but it is recognized that the assumption is in error in a variety of circumstances:

- a multi-modal return can result if the surface within the footprint is composed of multiple discrete surfaces separated in elevation, as would be the case with surfaces offset by a scarp or cliff for example; the last peak in this circumstance corresponds to the lowest of the discrete multiple surfaces,
- dense vegetation everywhere across a footprint may prevent sufficient laser illumination from reaching the surface causing there to be no detectable surface return; the last peak in this circumstances corresponds to the lowest illuminated vegetation layer,
- the last peak may be a composite of low vegetation and the surface (e.g.. a low-lying under story or shrub layer), causing the same ambiguities as described above for composite uni-modal returns,

- a footprint could fall entirely on a large, complex cultural feature (e.g., large building with multi-level roof); the last peak in this circumstance corresponds to the lowest part of the cultural feature.

Such circumstances are likely to be rare. Assessment of the correspondence between last peaks and the surface is beyond the scope of operational ICESat waveform processing, and is more appropriately treated as a research issue.

The approach defined for land assumes that all the reflecting components within the footprint behave as Lambertian (diffuse) scatterers. Water surfaces, foliage, and some cultural features violate the assumption of Lambertian scattering. However, lacking complete knowledge of the proportion and distribution of components in the footprint, the effects of non-Lambertian scattering can not be established. The assumption of Lambertian scattering is a practical approximation of the potentially complex character of land footprints.

3.1.2.2.5. Ocean Elevation And Roughness

The proposed algorithm for ocean products will infer the average elevation (E) of a footprint, and the return-pulse width (above some threshold - initially the noise floor, but to be adjusted after launch) as the elevation spread (E_{max} - E_{min}) inside the footprint. In general, the 70-m footprint will cover very few waves, often one or less. Consequently, it will be necessary to average many values of E to obtain the mean sea-surface elevation over the corresponding length of orbit track. As an example: Assume that E varies by plus or minus H meters because of the waves. H=1 would probably correspond to either a high sea state or longer waves or swell with amplitude of about one meter. If the variability of E is random, then the average elevation of 100 consecutive footprint elevations has wave-induced errors, $\Delta E = 0.1$ meters, appropriate to 2.5 seconds of data, or about 16 km of orbit track. Although this capability is poorer than that of satellite radar altimeters, it may offer improved information over specific regions, such as coastal regions and at high latitudes, and for geodesy. Moreover, it may be useful in assessing radar-altimetry errors associated with wave shape. One concern is the possibility of waves of appropriate length being aliased with the footprint spacing to introduce a bias to the average value of E.

Average elevation of the footprint (E) will be obtained from the centroid of the best-fit Gaussian to the return waveform (Section 4.1.3.11). E_{max} and E_{min} will be inferred from the timing of the start and end thresholds of the return waveform, with the option of using similar information from the best-fit Gaussian if actual GLAS data reveal significant problems with forward scattering amplifying the tail of the return waveform. Section 4.1.3.4 provides details of threshold tracking.
The total area beneath the return waveform between the start and end thresholds (A) will be used to infer the reflectivity of the surface. Values of E, E_{max}, E_{min}, and A will be archived for each footprint location, and they will be strongly affected by local sea state. A mean elevation (E_m) over 1 full second will also be calculated as an average of all N values of E acquired during the second, and both E_m and N will be archived at the full glas data rate with a sliding one-second window. The value of N will indicate regions of patchy cloud cover. "Ocean" data will be as determined from the global DEM, to include ..... tracking appropriate to these areas.

Within the one-second window, the extreme values of E_{max} and E_{min} give the full range of wave amplitudes for short wavelengths. However, a better representation of waveheight, and one more comparable to that derived from radar-altimeter data, could be obtained from the width of a composite return pulse formed by stacking many adjacent waveforms. Consequently, after the launch of GLAS, the science team will investigate a level 3 OCEAN product derived from many (N+1) footprints to take account of the wave height. Average values of E will be determined for orbit segments of fixed length, say 10 km, with final selection based on experience with actual data. The averaging process will require temporary storage of N+1 waveforms: the current waveform plus those for the preceding and subsequent N/2 footprints. The waveforms will be "stacked" to yield a composite waveform appropriate to the 10-km segment of orbit track. This composite waveform will be used to provide an alternate estimate of average

elevation (from the centroid of its best-fit Gaussian) and an estimate of RMS wave height from equation 9 in Section 3.1.2.2.2. From the RMS wave height the Significant Wave Height (SWH) can be computed. The SWH is defined as the average of heights (from crest to trough) the highest one-third of the waves observed at a point. It is approximately equal to four times the RMS wave height (Tsai and Gardner, 1982). This would yield values of average E at the full rate of 40/sec, each with its own value of RMS wave height depending on sea state.

3.1.2.3. Skewness and Kurtosis

Skewness characterizes the degree of asymmetry of a distribution around its mean and kurtosis measures the relative peakedness and flatness of a distribution (Press et. al., 1992). Skewness and kurtosis values can indicate the shape of a waveform.

Skewness and kurtosis are defined by the following equations (Leon-Garcia,1989, p148 and Press et. al. 1992, p612)

$$skewness = \frac{1}{\sigma^3} \frac{\sum_{i=start}^{i=end} (i - mean)^3 w[i]}{\sum_{i=start}^{i=end} w[i]}$$

$$kurtosis = \frac{1}{\sigma^4} \frac{\sum_{i=start}^{i=end} (i - mean)^4 w[i]}{\sum_{i=start}^{i=end} w[i]} - 3$$

Where w[i] is the power of the ith gate of a waveform. Start and end are the start and end gate of the signal in a waveform. Mean and σ are the mean and standard deviation of the waveform,

$$mean = \frac{\sum_{i=start}^{i=end} i \ w[i]}{\sum_{i=start}^{i=end} w[i]}$$

And

$$\sigma^2 = \frac{\sum_{i=start}^{i=end} (i - mean)^2 w[i]}{\sum_{i=start}^{i=end} w[i]}$$

For a normal distribution, the skewness and kurtosis are equal to zero. Two different methods will be used to select which portion to be used to calculate the skewness and kurtosis. The first method is to choose the waveform between ± n sigma of the fitted Gaussian pulse width. If there is more than 1 peak, use -n sigma for the left most peak and +n sigma for the right most peak. The second method is to use a threshold to determine the data to be used. The threshold is determined by n times the standard deviation of the noise.

3.2. Mathematical Formulation

3.2.1. Development of Equations

Since the transmitted pulse is expected to be Gaussian, if the surface topography is Gaussian, the return should also be Gaussian. We can represent the return mathematically as a sum of Gaussians plus a bias. Over the oceans, sea ice, and most of the ice sheets, the return is expected to be a single Gaussian. Over land and more complicated ice sheet regions, there may be multiple distinct peaks within the footprint (such as a tree), that will show up as multiple peaks in the return. Therefore the modeled waveform is defined as

$$w(t) = \varepsilon + \sum_{m=1}^{N_p} A_m \exp\left[-\frac{(t - t_m)^2}{2\sigma_m^2} \right] \qquad [15]$$

where

N_p is the number of peaks found in the waveform

A_m is the amplitude of m^{th} peak

ε is the bias (noise level) of the waveform

t_m is the peak position

σ_m is the 1/e half-width (standard deviation) of the m^{th} peak

Nonlinear least squares will be used to compute the model parameters (the ε, A_m, t_m, and σ_m in Eq 15) by fitting the theoretical model to the observed waveform. This is a standard procedure detailed in many references (Bevington and Robinson, 1992, Menke 1989, Press et al, 1986, Zwally et al, 1990). The development here follows Menke 1989, modified to include weights and a priori error estimates on the parameters as in Zwally 1990.

The measured waveform, consisting of N samples, is

$$\mathbf{p} = [p_1, p_2 \ldots, p_N]^T \qquad [16]$$

The model waveform, written in discrete form, is

$$\mathbf{w} = [w_1, w_2, \ldots, w_N]^T \qquad [17]$$

The vector of the M model parameters (the ε, A_m, t_m, and σ_m in Eq 15) is

$$\mathbf{c} = [c_1, c_2, \ldots, c_M]^T \qquad [18]$$

where $M = 3N_p+1$.

The matrix of derivatives of the model waveform with respect to the parameters is

$$\frac{\partial w}{\partial c} = \begin{bmatrix} \frac{\partial w_1}{\partial c_1} & \frac{\partial w_1}{\partial c_2} & \cdots & \frac{\partial w_1}{\partial c_M} \\ \frac{\partial w_2}{\partial c_1} & \frac{\partial w_2}{\partial c_2} & \cdots & \frac{\partial w_2}{\partial c_M} \\ \vdots & \vdots & \ddots & \\ \frac{\partial w_N}{\partial c_1} & \frac{\partial w_N}{\partial c_2} & \cdots & \frac{\partial w_N}{\partial c_M} \end{bmatrix} \qquad [19]$$

Given an estimate of the M parameters, C^i, the first-order Taylor series expansion of w around w^i is

$$w_n^{i+1} = w_n^i + \sum_{m=1}^{M} \frac{\partial w_n^i}{\partial c_m} \delta_m \quad [20]$$

where superscript i refers to the i^{th} iteration and

$$\Delta_m = c_m^{i+1} - c_m^i \quad [21]$$

If we also define the difference between the measured and i^{th} estimate of the waveform,

$$\mathbf{B} = \mathbf{p} - \mathbf{w}^i \quad [22]$$

and the matrix **A** by

$$A_{nm} = \partial w_n^i / \partial c_m \quad [23]$$

then we can write

$$\mathbf{A\Delta} = \mathbf{B} \quad [24]$$

Since **A** may not be square, we cannot simply multiply both sides of this equation by $\mathbf{A}^{-1}$ to get **δ**. Instead, multiply both sides first by $\mathbf{A}^T$:

$$\mathbf{A}^T\mathbf{A}\,\mathbf{\Delta} = \mathbf{A}^T\mathbf{B} \quad [25]$$

and then by $[\mathbf{A}^T\mathbf{A}]^{-1}$, to get

$$\mathbf{\Delta} = [\mathbf{A}^T\mathbf{A}]^{-1}\mathbf{A}^T\mathbf{B}. \quad [26]$$

We can rewrite this equation as

$$\mathbf{\Delta} = [\mathbf{A}^T\mathbf{W}\mathbf{A}+\mathbf{V_0}]^{-1}\mathbf{A}^T\mathbf{W}\mathbf{B} \quad [27]$$

to incorporate weights and a priori values. Here the weight matrix is

$$\mathbf{W}_{ij} = wt_i\delta_{ij} \quad [28]$$

and the a priori matrix is

$$[\mathbf{V}_o]_{jk} = wt_{ck}\delta_{jk} \quad [29]$$

where wt_i is the weight for the i^{th} observation, wt_{ck} is the a priori weight for the k^{th} parameter c_k, and δ_{ij} is the Kronecker delta,

A new set of parameters can then be calculated from

$$\mathbf{c}^{i+1} = \mathbf{c}^i + \mathbf{\Delta} \quad [30]$$

The covariance matrix, $cov(s_{ij}^2)$ and the variance s^2 can be calculated from

$$\mathrm{cov}(\sigma_{ij}^2) = [\mathbf{A}^T\mathbf{W}\mathbf{A}+\mathbf{V_0}]^{-1} \quad [31]$$

and

$$s^2 = \frac{\sum_{n=1}^{N}(w_n - p_n)^2}{N - M}, \quad [32]$$

where M is the number of parameters.

The derivatives of the modeled waveform with respect to the parameters:

$$\frac{\partial w}{\partial \varepsilon} = 1$$

$$\frac{\partial w}{\partial A_m} = \exp\left[-\frac{(t - t_m)^2}{2\sigma^2}\right]$$

$$\frac{\partial w}{\partial t_m} = \frac{A_m (t - t_m)}{\sigma_m^2} \exp\left[-\frac{(t - t_m)^2}{2\sigma^2}\right] = \frac{A_m (t - t_m)}{\sigma_m^2} \frac{\partial w}{\partial A_m} \qquad [33]$$

3.2.2. Procedure

The symbols used in this section are defined in Table 4-1.

The fitting steps to be used are as follows:

1. Estimate the model parameters
2. Compute a new value for w using the first order Taylor expansion, Eq. 20
3. Compute a correction to the current estimate of the parameters, Eq 27
4. Update the parameter estimate, Eq 30
5. Repeat steps 2-4 until some exit criterion is satisfied
6. Compute the covariance matrix and variance, Eqs 31 and 32

The capability to use in the fitting procedure only that portion of the waveform within n * σ_m of the peak(s) needs to allowed for.

For each iteration step, the following constraints apply:

1. $\sigma_m > 0$ and $|\delta\sigma_m| < \delta\sigma_{m,max}$
2. $\delta t_m < \delta t_{m,max}$
3. $A_m > 0$ and $\delta A_m < \delta A_{m,max}$
4. $\varepsilon > 0$, $\delta\varepsilon < \delta\varepsilon_{max}$

Methods of incorporating these constraints into the code are being explored.

The maximum number of peaks (N_p) allowed is six.

The criteria for ending the fitting loop are

1. $|\delta\varepsilon_{mean}| < \delta\varepsilon_{check}$, $|\delta t_m| < \delta t_{m\_check}$, $|\delta\sigma_m| < \delta\sigma_{m\_check}$, and $|\delta A_m| < \delta A_{m\_check}$. The incremental change in each parameter is less than a given amount.
2. Number of iterations > MaxIter.

4.0 ALGORITHM IMPLEMENTATION

The waveform processing algorithms were adapted from methods developed for the analysis of waveforms acquired from

- the first and second flight of the Shuttle Laser Altimeter
- satellite radar altimeters
- aircraft laser altimeters over land and ice sheet surfaces.

The major goals of the algorithm are to

- characterize the surface reflectivity, roughness, variability, and slope
- calculate the surface elevation

The GLAS instrument will record signals from four types of surfaces – ice sheets, sea ice, land, and ocean. The science requirements differ for these different surfaces. The algorithms described here are the same for all surface types; the differences in the final results come from use of different sets of parameters to drive these algorithms. Two sets of parameters will be used, one that satisfies the ice sheets, sea ice, and ocean processing requirements and one that satisfies the land requirements. Under normal mode of operation the algorithms will be run twice, once with each set of parameters (unless they end up being identical). Therefore one can create a global data set using the level 1b elevation output that will use a consistent set of parameters. The processing software should also have the option of processing only ice sheet and sea ice data using just the appropriate parameter set.

There will be four regional level 2 elevation products; one each for ice sheet, sea ice, land and ocean. Four different surface masks will be used to define what data goes on each level 2 elevation product. It is possible that these masks will overlap and the data will be on more than one level 2 product. The definition of each of the parameters on the level 2 products, as defined in section 5.0, is dependent on the surface type.

Outline Of The Procedure

- Characterize the transmitted pulse and calculate time for beginning of range calculation
- Characterize the received waveform to determine if there is a signal and to determine the point on the waveform to be used to estimate the range and the preliminary footprint location on the Earth.
- Interrogate the database to determine the type(s) of surface at the footprint location.
- Smooth the waveform and determine initial estimates for the waveform parameters.
- Fit the waveform using the procedure developed in section 3.2 and described below.
- Calculate range to mean surface and surface elevation distribution
- Calculate atmospheric delay and tidal values
- Calculate a corrected range to the mean surface
- Correct time for travel time
- Calculate precise geolocation and mean surface elevation
- Calculate region specific parameters

The results of this waveform processing will then be used to calculate the global level 1b elevation product and the level 2 region-specific products defined in section 5.

4.1.1. Input Variables

Parameters input from ancillary file

Unless noted each parameter will have two values – one for ice sheet, sea ice and ocean processing, and one for land processing. Recognizing the potential complexity of land returns, land processing parameters will be designed to achieve waveform fitting that preserves all peaks inherently present in the waveform. In particular, criteria will be established that minimize removal of waveform peaks by smoothing, editing, or merging.

Table 4-1 *Parameters input from ancillary file*

Numerical Program Parameters	
Psat_stop	If waveform saturation is greater than this, the waveform will not be processed.
Psat_spec	If waveform saturation is greater than this but less than Psat_stop, the waveform will receive special processing.
nsig	The noise threshold is nsig * σ noise_ob
Ngt_noise	The number of gates used to calculate the noise value.
offsetb	the offset to subtract from the beginning of the waveform before the first threshold crossing if slctregn is set (ns)
offsete	the offset to add to the end of the waveform after the last threshold crossing if slctregn is set (ns)
maxiter	maximum number of iterations for fit
maxfit	max number of fits allowed
N_peak_min	A peak in the waveform is considered as possibly real if its peak amplitude is > N_peak_min *σ noise_ob + Noise_ob
Interval_min	Peaks that are closer together than Interval_min will be merged.
Thresh_lvl	The % of the maximum amplitude to use for defining the threshold retracker location.
δε	change in noise level in %; check for convergence in functional fit
δtm_check	change in location of peak of Gaussian in %; check for convergence in functional fit
δσm_check	change in width of Gaussian in %; check for convergence in functional fit
δAmp_check	amplitude of peak of Gaussian in %; check for convergence in functional fit
Stdev(σm)	The aprioi standard deviation of the σ_m parameter in functional fit
Stdev(tm)	The aprioi standard deviation of the peak position in functional fit
Stdev(Amp)	The aprioi standard deviation of the amplitude in the functional fit
Stdev(noise)	The aprioi standard deviation of the noise in functional fit
minAmpPcnt	Min amplitude as a percent of the max received amplitude
sigmaMinInit	Min value for peak sigma
minIter	Min number of iterations during functional fit

minGatesNs	Min gates to use to calculate noise if Ngt_noise gates are not available
minNoise	Min noise
min4sat	Min number of consequtive gates with the same amplitude to count as saturation
Program Switches	
Noisecal	1: calculate noise level and σ from waveform 0: use noise level and σ telemetered
Slctregn	1: select region of waveform from which to do evaluation 0: use all the gates telemetered in waveform evaluation
Instrument Parameters (1 each)	
filterwdmin	the minimum width of the filter used to smooth the waveform (ns)
filterwdmax	the maximum width of the filter used to smooth the waveform (ns)
ΔT_hires	time between gates for the highest resolution gate – nominally 1 ns

4.1.1.1. Parameters Input From The Data Stream

Table 4-2 *Parameters Input From The Data Stream*

Gain_trans	Gain on the transmitted pulse
Eff_trans	Optical to detector volt efficiency for transmitted pulse
Wf_trans(t)	Transmitted pulse waveform (32 gates)
Wf (t)	the received waveform (544 samples in land or ice sheet mode, 200 samples in ocean or sea ice mode)
Cr1	the compression ratio used on board for Wf(t) samples 1 to Ncr-1
Cr2	the compression ratio used on board for Wf(t) samples Ncr to the end
Ncr	the sample number at which the compression ratio changes
Gain_rec	the receiver gain
Eff_rec	Optical to detector volt efficiency for received pulse
Filter_ob	on board filter used to find signal
Sigbeg _ob	beginning of signal found by the on board algorithm
Sigend_ob	end of signal found by the on board algorithm
Noise_ob	background noise level as measured by the instrument
σnoise_ob	standard deviation of background noise level calculated by the on board algorithm
T_{ngates}	Digitizer address of last gate telemetered of the return pulse(farthest from spacecraft)
T_P	Digitizer address of the location of the peak of the transmitted pulse
GPSt(j)	GPS time for sub time j - one GPS time is received for every 10 sec

$Time_{FC}(I)$	Fire Cmd time for shot I linked to internal GLAS clock – time the digitizer is commanded to begin
GPSAck(j))	GPS time linked to internal GLAS clock at GPSt(j)
Ngates	number of gates telemetered – nominally 544 for land and ice sheet, 200 for ocean and sea ice

Variables from ancillary sources

- POD: precision orbit data
- PAD: precision attitude data
- Surface identifier grid

Figure 3 depicts the overall characterization of the transmitted and received pulse waveforms.

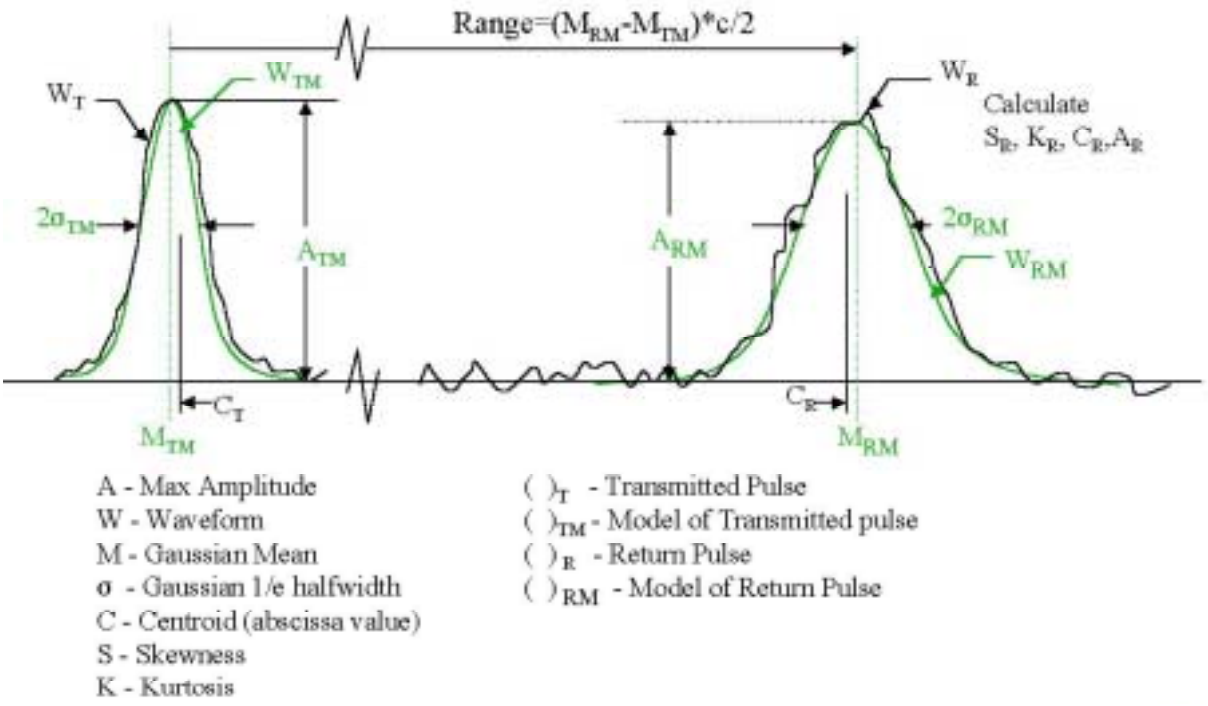

Figure 3 - Characterization of transmitted and received pulse waveforms

4.1.2. Transmit Pulse Characterization

The transmitted pulse is expected to be well represented by a single Gaussian (this will be checked when data become available) with a zero baseline. Characteristics of the actual transmitted pulse will be calculated along with the parameters from a single-peak Gaussian fit. All abscissa values are calculated relative to the laser fire command time. This is time that the digitizer is started.

- Transmitted Pulse
  - Centroid, $C_{T.}$
  - Skewness, S_T
  - Max Amplitude, A_T
  - Area under the pulse
- Gaussian Fit to transmitted pulse
  - Mean, $M_{TM,}$ in ns from the beg of the digitizer
  - Pulse 1/e halfwidth (σ_{TM}), (e=base of natural logs)
  - Amplitude of the peak, A_{TM}

The time from which the range will be calculated is the time corresponding to $M_{TM.,}$ T_{TM}

$T_{TM}=T_p+(M_{TM} - T_p)$

Note: The above equation assumes that T_{TM} and T_P which the instrument engineers refer to as addresses are really in ns from the beginning of the digitizer turn on, if they are not then they need to be converted to time in ns from the beginning of the digitizer turn on.

4.1.3. Received Pulse Characterization

This characterization will be done using two sets of input parameters, one for land and one for other regions.

4.1.3.1. Normalize The Abscissa – I.E., Convert From Gate Number To Time.

For gates 1 to Ncr-1:

t (n) = ΔT_hires * ((Cr1-1)/2 + Cr1 * (n-1)) where n = gate number.

For gates Ncr to Ngates:

t (n) = ΔT_hires * (Cr1 * (Ncr-1) + (Cr2-1)/2 + Cr2 * (n-Ncr))

Ncr = gate number where the second compression ratio was first used

Cr1 = first compression ratio

Cr2 = second compression ratio

ΔT_hires = resolution in ns of the highest resolution gate possible (nominally 1 ns)

note: at the end of this normalization, your time array is referenced to 0 at gate 1 of the digitized waveform before compression.

4.1.3.2. Determine the Reference Range, Range_ref

The reference range, Range_ref, is defined as the time difference in ns between the center of the transmitted pulse, T_{TM}, and the last gate of the received pulse telemetered (farthest from the spacecraft). Range_ref = T_{ngates}-T_{TM} Where T_{ngates} = time in ns from the beginning of the digitizer to the gate, ngates.

4.1.3.3. Determine the Preliminary Range (Range_pre)

The preliminary range is defined as the range value associated with the threshold crossing farthest in range from the spacecraft. First find the index, i, that corresponds to the first time, t(i) the waveform crosses a threshold value from the far end such that

$$Wf(t_i) > Noise\_ob + Nsig * \sigma\_noise\_ob$$

Then linearly interpolate between t(i) and t(i-1) to calculate the exact time in ns from the beginning of the waveform for this threshold crossing, t_{th}. Then calculate T_{TH}, the value in ns from the beginning of the digitizer of this threshold crossing,

$$T_{TH} = T_{ngates} - (t(ngates) - t_{th})$$

$$Range\_pre = T_{TH} - T_{TM}$$

Note - t is measured from the beginning of the received waveform, and T is measured from the start time of the digitizer. Figure 4 shows these definitions graphically.

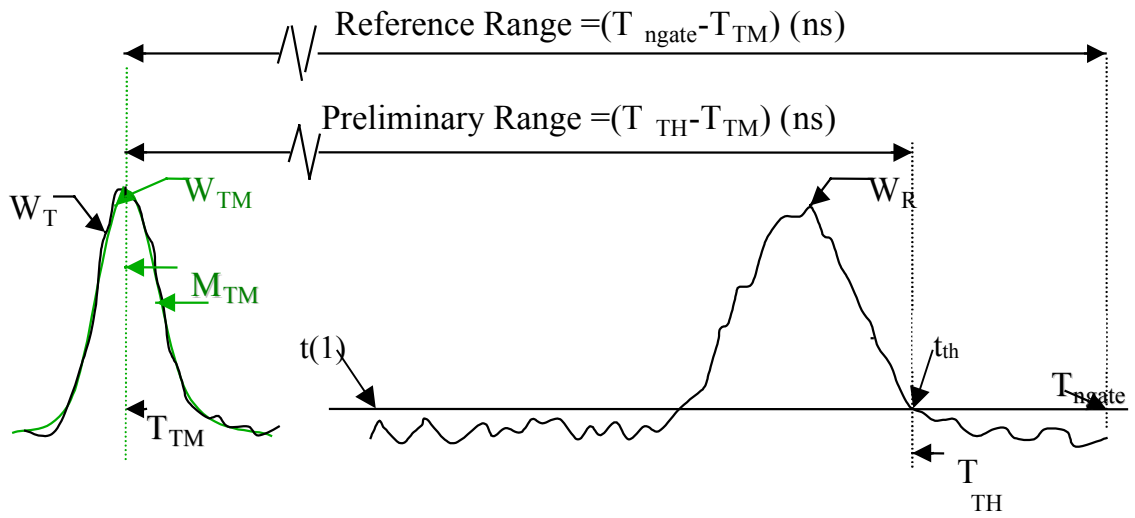

Figure 4 - Definition of Reference and Preliminary Ranges

4.1.3.4. Determine the Preliminary Range Correction

Range_pre_cor = Range_ref – Range_pre

4.1.3.5. Time Calculation

Each shot is uniquely time tagged using the fire command time (FireAck), the GPS time (GPSt), and GPS acknowledge time(GPSAck).

There is a unique FireAck time for each shot i telemetered with the associated waveform. The GPS time, GPSt, is sampled once every 10 seconds and at the GPS sample time the same clock that is linked to the FireAck time is latched to provide a GPSAck tag. So the basic time tag equation is for each shot:

GPSshotTime (i) = GPSt(j) + (FireAck(I) –GPSAck(j))

Where:

- GPSshotTime(i) is the GPS time for shot i.
- GPSt(j) is the GPS time for the smallest positive (FireAck(I) –GPSAck(j)). i.e. the last GPS time just before shot i.

The time at which we need to evaluate the orbit and attitude is referred to as the ground-bounce time, T_G, or the time at which the signal reached the ground. This is calculated by correcting GPSshotTime (i) for the time it takes to travel to the ground using Range_pre.

$$T_G(i) = \text{GPSshotTime}(i) + \text{Range\_pre}/2$$

The times on the data products as discussed in section 5.0 are UTC times. These are calculated from the GPS times by correcting for the leap seconds using a table to be supplied by the science team. The times on the data products, T_{out}, of GLA05, 06, and 12-15 are the ground bounce time in the UTC time frame.

$$T_{out} = T_G + \text{Tcor\_gps\_to\_utc}$$

Where Tcor_ gps_to_utc is the time correction from GPS to UTC

4.1.3.6. Geolocate The Footprint

Determine the geodetic latitude and longitude of the center of the laser footprint. The footprint location is a function of the spacecraft orbit and attitude and the range. The exact equations used to do the geolocation are found in the Precision Attitude Determination (PAD) Algorithm Theoretical Basis Document (ATBD), the Precision Orbit Determination (POD) ATBD, and the footprint location and surface profile ATBD.

The attitude data will be at the shot rate (40/sec). A unique index number will be on each attitude record that will correspond to the same index number on each of the GLAS standard products. The attitude data need to be merged using that index number. The POD file will give the sub-satellite (nadir) location of the laser in GPS time. The orbit needs to be interpolated from the POD file at T_G. Range_pre is then used in the geolocation algorithms to determine the location (Lat_pre_uncor and Long_pre_uncor), and the surface elevation (elev_pre_uncor). Range_pre is a preliminary range. It is not corrected for atmospheric delays and does not have the tides applied it is referred to as preliminary uncorrected geolocation output.

4.1.3.7. Determine Surface Identifier From Regional ID Grid

Find the region ID grid nodes surrounding the footprint geolocation.

If any of the nodes indicate land	THEN lland = 1
If any of the nodes indicate ocean	THEN locean = 1
If any of the nodes indicate seaice	THEN lseaice = 1
If any of the nodes indicate ice sheet	THEN licesheet = 1

4.1.3.8. Check Saturation

IF Psat ≥ Psat_spec and Psat < Psat_stop THEN

Special handling of saturated returns – TBD, SET Flag_sat=3

IF Psat ≥ Psat_stop processing, SET Flag_sat=2

IF Psat > 0 and Psat < Psat_spec, SET Flag_sat=1

IF Psat = 0, SET Flat_sat=0

Saturation occurs when the strength of the backscatter return exceeds the detection limit of the detector as established by the detector gain level. The shape of saturated signals are corrupted and must be treated as exceptions. For Psat ≥ Psat_stop the duration of saturation is excessive and no waveform processing is applied. For Psat > 0 and Psat < Psat_spec the duration of saturation is minimal and normal waveform processing is applied.

For Psat ≥ Psat_spec and Psat < Psat_stop the duration of saturation is moderate and some information on surface elevation can be approximated. For moderate saturation, the shape of the return pulse leading edge up to the onset of saturation is properly recorded, but the width of the pulse, the characteristic abrupt decrease in amplitude at the trailing edge, and subsequent detector 'ringing' (amplitude oscillations about the background level) are artifacts. Based on detector response in saturation, it is thought that the area under the saturated return is approximately equal to what the area would have been if the detector had a greater detection range and the signal were not saturated. This assumption of preserved area and the shape of the leading edge are used to fit a Gaussian distribution to the saturated return that models a non-saturated return, yielding an approximate measure of waveform parameters (width, amplitude, position) for the saturated peak. Functionally, waveform bin positions in saturation are weighted with a zero weighting in the Gaussian fitting process, and the area of the resulting Gaussian fit is constrained to be equal to the area under the saturated peak. Low-amplitude peaks following saturation are likely to be corrupted by detector ringing and should be deleted before applying the Gaussian fitting routines.

Psat is determined by dividing the number of saturated bins by the total number of bins in a waveform. A bin is saturated if it is part of a group of consecutive bins numbering at least min4sat, with amplitudes equal to the maximum amplitude of that waveform.

4.1.3.9. Calculate Noise Level

IF Noisecal is set THEN

Calculate mean value of the whole waveform Wf(t) (Wf_mean) Calculate the noise as the mean of Wf(t) for an input number of gates, ngt_noise, that are below Wf_mean starting at the end of the waveform farthest from the satellite. Calculate σ_noise as the standard deviation in Wf(t) for these same gates.

IF noisecal is not set THEN

σ_noise = σnoise_ob

Noise = Noise_ob

4.1.3.10. Smooth The Waveform And Check For A Viable Signal

Input: wf(t)

Filter_ob: the filter at which the instrument algorithm found the signal

Start at the width of the smallest on board filter, Filter_1 (4 ns) and redo this step incrementing the filter size through filter_ob until a signal region is found. If no signal region is found then stop processing the waveform and set flag_signal=1, otherwise set flag_signal=0.

Loop Begin

Smooth the waveform using a Gaussian filter with sigma equal to the sigma of the filter used on board. For samples where the time between contiguous abscissa values is greater than the filter width the smooth value will equal the received value. This can occur if different compression ratios were used for the waveform.

Determine the time of the beginning of signal, sig_beg = the first time t such that wfsm(t) > Noise + Nsig * σ_noise

and the time of the end of the signal sig_end = the last time t such that wfsm(t) > Noise + Nsig * σ_noise

IF (sig_beg-sig_end) > sig_width THEN set flag_signal=0. get out of loop

Loop End.

A block diagram showing the smoothing logic is shown in Figures 5 and 6.

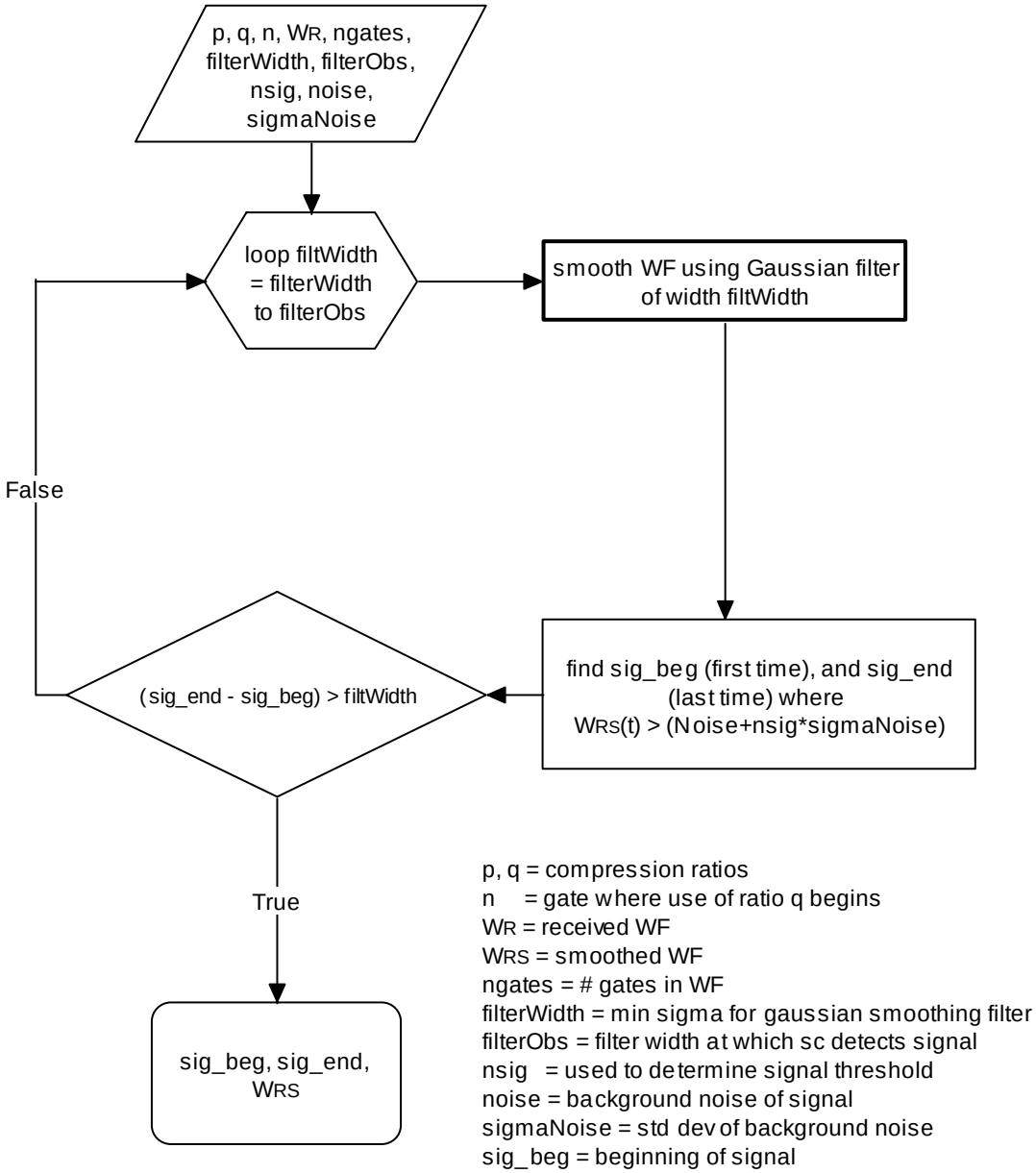

Figure 5 - Block Diagram of Waveform Smoothing Methodology

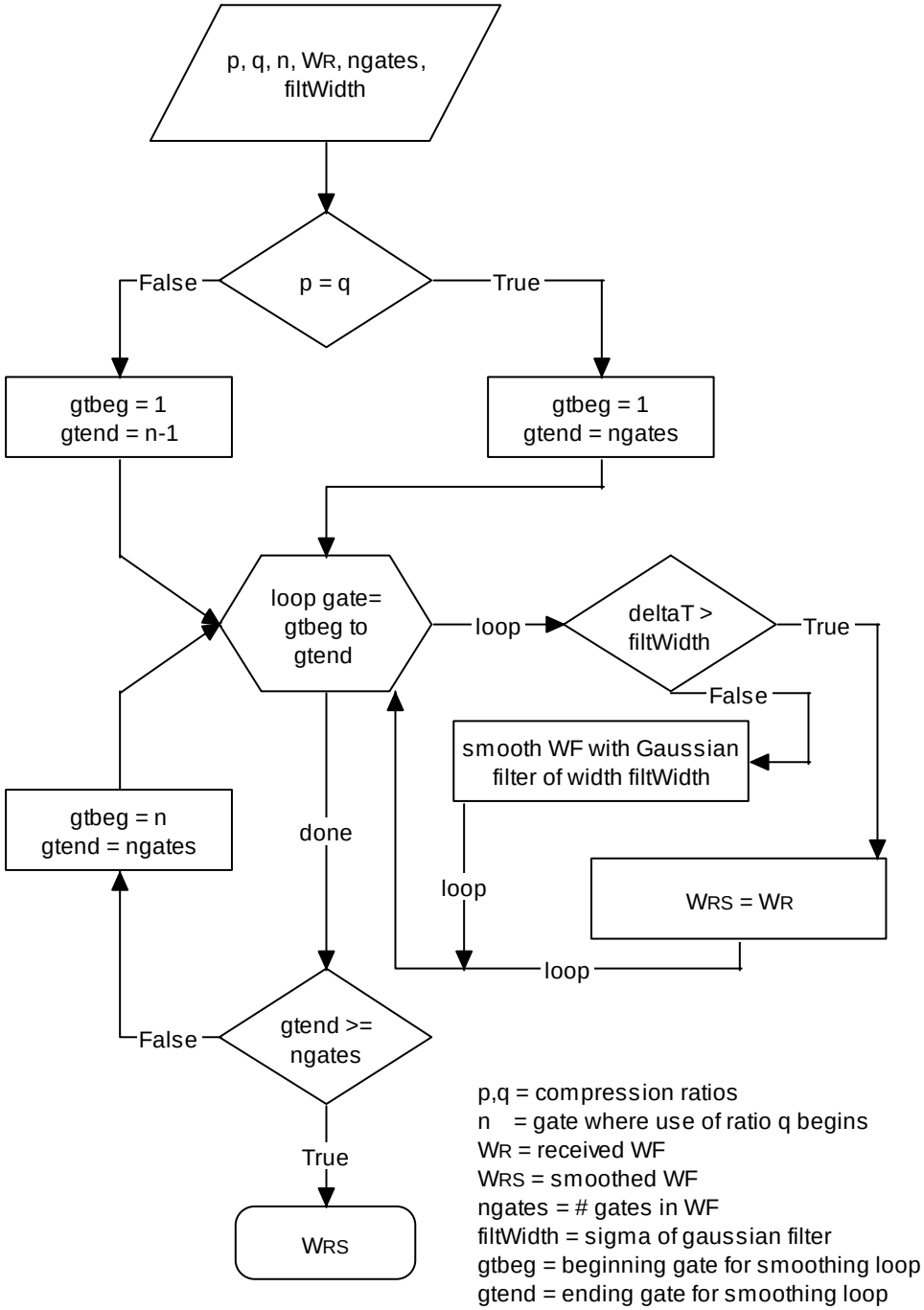

Figure 6 - Smooth WF using Gaussian filter of width filtWidth

4.1.3.11. Select Region Within The Waveform With Which To Continue Further Processing

IF slctregn is set THEN

Time_beg = beginning time of selected region = MAX [sig_beg - offsetb, t(1)]

Time_end = end time of selected region = MIN [sig_end + offsete, t(Ngates)]

These values will default to t(1) and t(ngates) respectively if slctregn is not set.

4.1.3.12. Fit The Waveform To A Function

4.1.3.12.1. Make An Initial Estimate For The Unknown Model Parameters

Calculate the second derivative of the smoothed waveform, WFsm(t), using contiguous first forward differences to calculate the first derivative and then contiguous first forward differences of the first derivative results to calculate the second derivative.

Determine all locations, where the second derivatives cross zero from positive to negative, Lpos_p_n(i). Find the minimum values of the second derivatives between contiguous locations of Lpos_p_n(i). The locations at which these minima occur are possible locations of individual Gaussian peaks in the return. Two other possible locations are the minimum of the 2nd derivative between Time_beg and the first Lpos_p_n and the minimum between the last Lpos_p_n and Time_end. All these possible peak locations will be referred to as Peak_init(i). Find the amplitude(s) at the peaks from the smoothed waveform corresponding to the time(s) for Peak_init(i). These will be referred to as AMP_init(i).

will be setLoop through all occurrences of the possible locations of the individual Gaussian peaks editing out those for which the amplitude is smaller than an input criteria:

AMP_init(i) < N_peak_min*σ_noise

Combine peaks if the interval between them is too small:

Peak_init(I)-Peak_init(I-1) < Interval_min

To combine peaks, use a weighted average of the positions, widths, and amplitudes.

The remaining peak positions and amplitude will be used to set the initial values for these parameters in the least squares fit. The initial σm values σ_m_init(i), will be set using the mathematical relationship between the amplitude, σ, and 2nd derivative of a Gaussian such that

σ_m_init(i) = √ (AMP_init(i)/2ndDeriv(i))

The maximum number of peaks that will be fit will be six. If more than six peaks are found in this process then the peaks will be ranked as explained in section 4.1.3.13 and the lowest ranked will be combined with the closest peaks until only 6 remain.

4.1.3.12.2. Perform The Nonlinear Least-Squares Fit

Use the methodology described in section 3.2.2. All calculations are to be performed in double precision arithmetic. Based on the input parameter maxfit, the fit may be performed twice.

After the first fit, if maxfit=2, then check to see if the Gaussians found in the first fit meet the criteria discussed in the previous paragraph. If not, edit and merge the peaks using the same criteria as before. If

no Gaussians are edited or merged do not perform another fit. If any Gaussians are edited and/or merged then perform a 2nd fit using the edited and merged data for the initial values.

IF the fitting procedure stops because it took too many iterations to converge, THEN set flag_fit_maxiter=1.

IF the fitting procedure stops because the normal matrix becomes singular, THEN set flag_fit_nogo=1.

4.1.3.12.3. Output Parameters From The Fitting Procedure:

1. Npeak_init: the number of peaks found in the initialization procedure. This can be greater than 6.
2. Npeak_soln: the number of peaks solved for.
3. The amplitude, σ, and position of each Gaussian in the fit
4. The noise value, signal_noise
5. The χ^2 of the fit
6. Flag_fit_nogo: a flag indicating if the fit was unsuccessful (numerical instabilities occurred).
7. Flag_fit_maxiter : a flag indicating the fit ended without meeting convergence criteria.

4.1.3.13. For Multiple-Gaussian Fits, Rank The Peaks Found

The number of peaks found by the Gaussian fitting may exceed the available space for storing the fit parameters in the final data structure, which is limited to a total of 6 Gaussian peaks. This may in particular occur for complex land returns. Peaks will be ranked based on the area of each Gaussian fit. Calculate General Waveform Assessment Parameters

The waveform assessment parameters are based on the portion of the waveform above noise level. This step therefore begins by calculating

wf(t)_signal = wf(t) - signal_noise

wf(t)_sm_signal = wf(t)_sm - signal_noise

From these, compute

maxamp	Maximum amplitude of wf(t)_signal from time_beg to time_end
centroid	Centroid of wf(t)_signal from time_beg to time_end
Total area under received pulse signal	Total Area under wf(t)_signal from sig_beg to sig_end
skewness	Skewness of wf(t)_signal from time_beg to time_end
kurtosis	Kurtosis of wf(t)_signal from time_beg to time_end
Maxamp_sm	Maximum amplitude of wf(t)_sm_signal from time_beg to time_end

4.1.3.14. Calculate a threshold retracker correction

Calculate the value, the time in ns from the beginning of the waveform to the location on the waveform where it first crosses a threshold power value based on the threshold level defined on the input parameter file, thresh_lvl. This thresh_lvl is given as a percentage of the maximum amplitude of the smoothed waveform. Find the index i within the array t(n), where wf(i) is > thresh_lvl*maxamp_sm. Then linearly interpolate between wf(i) and wf(i-1) to obtain the exact value of t that corresponds to wf(t)=thresh_lvl*maxamp_sm, (t_{TH_RET}). Calculate the threshold retracker correction to the ref range as range_th_cor=Range - ref(t_{ngates} - t_{TH_RET}).

4.1.4. Output Parameters

This table lists the output parameters from the waveform characterization process.

Table 4-3 *Output parameters from the waveform characterization process*

Range_pre_cor	range correction to be added to reference range based on location on the waveform defined as the preliminary correction location (ns)
Lat_pre_uncor	geodetic latitude associated with the preliminary range uncorrected for atmospheric delays, no tides applied (deg N)
Long_pre_uncor	geodetic longitude associated with the preliminary range uncorrected for atmospheric delays, no tides applied (deg E)
Elev_pre_uncor	surface elevation relative to the reference ellipsoid uncorrected for atmospheric delays, no tides applied (mm)
lland	1= Laser footprint is on possible land surface as indicated by regional ID grid
locean	1=Laser footprint is on possible ocean surface as indicated by regional ID grid
licesheet	1=Laser footprint is on possible ice sheet surface as indicated by regional ID grid
lseaice	1=Laser footprint is on possible sea ice surface as indicated by regional ID grid
Noise, σ_noise	Noise level and corresponding standard deviation of the waveform either calculated or set from instrument (counts)
Flag_signal	0-signal found 1-no signal found in waveform
Flag_sat	0-no saturation found in signal 1-saturation found but not considered significant 2-significant saturation found signal not processed 3-significant saturation found, signal specially processed
Sig_beg	t(n) of beginning signal in waveform in ns from gate 1 – closest gate to the spacecraft
Sig_end	t(n) of end of signal in waveform in ns from gate 1 – closest gate to the spacecraft
Time_beg, Time_end	Beginning and end time within which to process signal in ns from gate 1 – closest gate to the spacecraft
Npeak_init	Number of peaks found in waveform during initialization procedure

Npeak_soln	Number of peaks solved for during final functional fit
Amp, σ, and location	Parameters of each Gaussian fit to in the functional fit
Covariance Diagonals	Standard deviation of each parameter solved for in the functional fit
Centroid	Centroid of wf(t) from time_beg to time_end in ns from gate 1
Total_area	Total area under wf(t) from time_beg to time_end
Flag_fit_maxiter	1=Fitting procedure ended because number of iterations exceeded maxiter
Flag_fit_nogo	1=Fitting procedure was unsuccessful, i.e. normal matrix turned singular, etc.
Maxamp	Maximum amplitude of wf(t) from time_beg to time_end (counts)
Range_th_cor	Range correction to br added to the reference range to give the range based on the threshold retracker in ns

4.2. Variance Or Uncertainty Of Estimates

The estimation procedure will give quantitative values for the uncertainties in the parameters being estimated. However there are many surface, instrument, and atmospheric characteristics that will affect the shape of the return waveform. Our algorithms are based on several assumptions. This section examines the uncertainties in the physical quantities being calculated when these assumptions do not hold, and their effect on the ice sheet, sea ice, land, and ocean products.

The anticipated ranging error of single laser pulses comprises the time of flight measurement error and the clock frequency estimation error. Gardner (1992) developed analytic expressions to compute the variance of the centroid time and the received laser pulse width for the simple terrain surface pictured in Figure 2. Gardner (1992) and Harding et al., (1994) used these expressions to determine the RMS range and pulse width errors to evaluate the expected performance of different satellite laser altimeter designs.

The analytic expression (adapted from Harding et al., 1994) separates the sources of the received pulse centroid time variance into five components (impulse response, surface roughness, beam curvature, nadir angle and slope, and pointing uncertainty):

$$
\begin{aligned}
&\mathrm{var}(T_p) = F\ \mathrm{var}(s_l)/N_r + (FN_B + N_D)T^3/(N_s^2 \cdot 12 \cdot \Delta t) + \Delta t^2/12 + \\
&+ (F/N_r + 1/K_s)\frac{4\,\mathrm{var}(\Delta\xi)\cos(S_x)}{c^2\cos^2(f+S_x)} + \\
&+ (F/N_r + 1/(2\cdot K_s))\frac{4z^2\tan^4 q_T}{c^2\cos^2 f} + \\
&+ (F/N_r + 1/(2\cdot K_s))\frac{4z^2\tan^2 q_T}{c^2\cos^2 f}\cdot\left[\tan^2(f+S_x) + \frac{\tan^2(S_y)\cos^2(S_x)}{\cos^2(f+S_x)}\right] + \\
&+ \frac{4z^2(1+\tan^2 q_T)^2}{c^2\cos^2 f}\left[\tan^2(f+S_x)\,\mathrm{var}(\Delta f_x) + \frac{\tan^2(S_y)\cos^2(S_x)\cos^2 f}{\cos^2(f+S_x)}\,\mathrm{var}(\Delta f_y)\right]
\end{aligned}
\qquad [34]
$$

where T_P is the propagation delay measured by the pulse centroid time as it is introduced in 3.1.2.1.,

F is the avalanche photodiode excess noise factor,

$\mathrm{var}(s_l)$ is the variance of transmitted laser pulse width,

N_r is the mean signal photoelectrons,

N_B is the mean solar background photoelectrons,

N_D is the mean detector dark counts,

T is the detector integration time,

Δt is the time-interval-unit resolution,

K_s is the speckle signal-to-noise ratio $= \pi A_r [2 \cdot \tan(q_T / \lambda)]^2$, A_r is the receiver area, and λ is the laser wavelength,

$\mathrm{var}(\Delta\xi)$ is the variance of the surface roughness,

c is the effective velocity of light,

f is the off-nadir pointing angle of laser beam,

S_x is the surface slope in (xz) plane, S_y is the surface slope in (yz) plane,

z is the altimeter height above the terrain,

q_T is the halfwidth divergence angle of the laser beam measured at the $1/\sqrt{e}$ point,

Δf_x is the pointing error parallel to the pointing direction, and Δf_y is the pointing error perpendicular to the pointing direction.

The first four components in (34), that is the impulse response, the surface roughness, the beam curvature, and the geometric component dependent on the off-nadir angle of the laser beam and the slope of the surface, account for effects that cause pulse spreading in time of the received pulse. Note, however, that equation (34) does not include the effects of pulse spreading by forward scattering of the laser pulse by thin clouds and aerosols. With increased spreading of the pulse, range errors are increased because the centroid of the broad pulse is less accurately determined than that of a narrow pulse, given the same total energy, due to a lower peak signal to noise ratio.

These pulse spreading components are dominated by the photon noise. The photon noise contributions are inversely proportional to the mean signal photoelectrons (N_r), which is the number of photoelectrons detected per laser pulse:

$$N_r = \left(\frac{E_r \eta}{h\nu}\right)\left(\frac{A_r}{z^2}\right)\tau_{sys}\tau_{sys}^2\left(\frac{r_{surf}}{\Omega_{surf}}\right) \qquad [35]$$

where E_r is the transmitted laser energy,

η is the quantum efficiency of the detector,

$h\nu$ is the photon energy

A_r is the telescope area,

z is the range from the spacecraft to the Earth surface,

τ_{atm} is the atmospheric transmission,

τ_{sys} is the system transmission,

Ω_{surf} is the surface scattering angle, and

r_{surf} is the surface diffuse reflectivity.

For GLAS values the average number of photoelectrons received is expected to be typically 5,000-40,000. Link margin calculations indicate high SNR for the GLAS system. For example, in the case of moderately sloping ice/snow terrain (slope=3^o, reflectivity=0.6), the estimated link margin is 14.5 dB at night and 13 dB in the daytime. This SNR is high enough to obtain reliable range and surface roughness measurements even in case of large changes in surface albedo and roughness, and atmospheric transmission variability due to aerosol and cirrus cloud scattering process (Bufton, 1989).

The pulse spreading components also include the speckle noise contributions. The speckle noise effects are inversely proportional to K_s, which is the ratio of the receiver aperture area to the speckle correlation area. According to Bufton (1982), speckle noise is negligible for the GLAS system because of the large number of spatial and temporal speckle cells averaged during each individual range measurement.

The final component in (34) is sensitive to laser pointing angle uncertainties. For small pointing uncertainties Bufton (1982) approximated the range error due to this component by

$$\Delta Z = Z \Delta f \tan(S + f)$$

For the GLAS system both the pointing uncertainty (1.5 arcsec) and the normal off-nadir pointing angles (< 1 deg) are small and therefore the ranging error due to the pointing uncertainty will be dominated by the effect of surface slope.

Gardner (1992) also derived an analytical expression similar to (34) for estimating the variance of the received pulse width.

To evaluate the performance of the waveform algorithms the analytical expressions and laser altimetry simulations will be used to compute the RMS range error and RMS pulse width errors of the GLAS system. These errors will be estimated over different types of ice sheet, sea ice, ocean and land topography and they will be analyzed in a similar fashion as it was reported in Gardner 1992, and Harding et al., 1994.

The algorithm described in the theory section and the analytical expression presented in this section are valid in cases of horizontal, linear sloping, isotropic, and stationary rough surfaces, uniform Lambertian reflectivity, and Gaussian laser beam far field pattern and atmospheric effects are neglected. Further research should be undertaken to analyze the errors introduced by the deviations from this ideal case or by distortions caused by the atmosphere.

4.3. Numerical Computation Considerations

The mathematical procedures described in the previous sections were tested on SLA-2 and the large footprint aircraft laser configuration (Bigfoot) waveforms. The results are discussed in section 4.3.2. These procedures appear to work with real data, but there are other techniques that may be computationally faster and further research is needed to determine the best method. This section describes the problem in more detail and suggests references to check for prototyping different numerical methods for solving the non-linear estimation problem.

The problem is to fit an equation of the form

$$y = a + \Sigma b_i G_I \qquad [36]$$

where the G_i are functions which also contain parameters, subject to the constraints

1. $a > 0$
2. $b_i > 0$
3. For each G_i, bounds on the location of the peak and the width of the function.

In addition, there is information available on the uncertainties in the estimates of the parameters. The code used at GSFC for analysis of radar altimetry data incorporates this information by doing Bayesian least squares analysis (Zwally et al, 1990). Without the Bayesian constraints, the calculation frequently did not converge.

The Shuttle Laser Altimeter group is using a Levenberg-Marquardt (LM) algorithm (Press et al, 1986) with constraints, coded in IDL (Interactive Data Language) (Harding et al, 1998). The constraints are handled as follows: at the end of an iteration, if any parameters are outside the acceptable region, do the following before continuing with the next iteration:

1. determine the minimum linear interpolation step that takes any one parameter from its value at the start of the iteration to its limiting value. Assume this is the step size rather than the step size used and scale all changes in the parameters to this value.
2. compute the derivatives of all parameters that are at their limits. If the derivative tends to move the parameter out of the acceptable region, set it to zero. In optimization terminology, this has the effect of removing the variable from the "active set."

This same algorithm could be used to fit the GLAS waveforms, possibly with the addition of Bayesian constraints on the parameters in the LM algorithm. The GLAS code should be written in Fortran or C for efficiency, and the derivatives should be computed using the known form of the fitting function for both efficiency and accuracy (SLA code uses a numerical derivative).

Initial estimates

A high-quality initial estimate of the parameters is important to reduce the time it takes the nonlinear least squares procedure to converge.

4.3.1. Programmer/Procedural Considerations

Though we have data from several aircraft and SLA data sets with which to test our algorithms, we do not currently have test waveforms that emmulate all the expected performance characteristics of the GLAS instrument. Test data will be available prior to the ICESat launch from the Vegetation Canopy Lidar (VCL) mission, scheduled for launch in 2000. VCL utilizes a similar waveform acquisition approach and will telemeter full waveforms to the ground for processing. Test data will also likely be available from the VCL airborne simulator (LVIS) for testing of GLAS processing algorithms. Prior to the availability of these test data, the GLAS similator is being used to exercise processing algorithms. However, it must be recognized that the GLAS instrument is different from any previously flown, and therefore the algorithms need to be programmed so that changes can be incorporated easily. To allow for this the following should be taken into consideration.

- The parameter estimation procedure must be written in distinct modules so that it can accept a change in the fitting function or the technique used to solve for the function parameters with minimal code changes.

- The algorithms must be run off of a parameter file which can contain different values for the same parameter based on region. This is with the expectation that the land parameters will be different from those used for the other three surface types.

- The program must be able to process data from all four surface types or to select and process only ice sheet and sea ice data.

NOTE: all calculations are to be done in double precision arithmetic.

4.3.2. Calibration And Validation

4.3.2.1. Ice Sheet Validation With Existing Data

The waveform assessment algorithms and fitting procedure described in section 4.1 has been tested with over 800,000 Bigfoot aircraft laser waveforms over Greenland, 159,800 SLA-2 waveforms from observation 3 (an assigned ID from the mission) over land and water, and around 70 GLAS simulated forward scattering waveforms, and 270 2D simulated waveforms. The fitting process converged more than 99% of the time for reasonably good waveforms. Bigfoot data were acquired by NASA's airborne laser altimeter over Greenland in 1993 using the instrument in a configuration that produced a GLAS size footprint. Most of the waveforms are single peaked pulses. A single Gaussian function fits these waveform very well as shown in Figure 7.

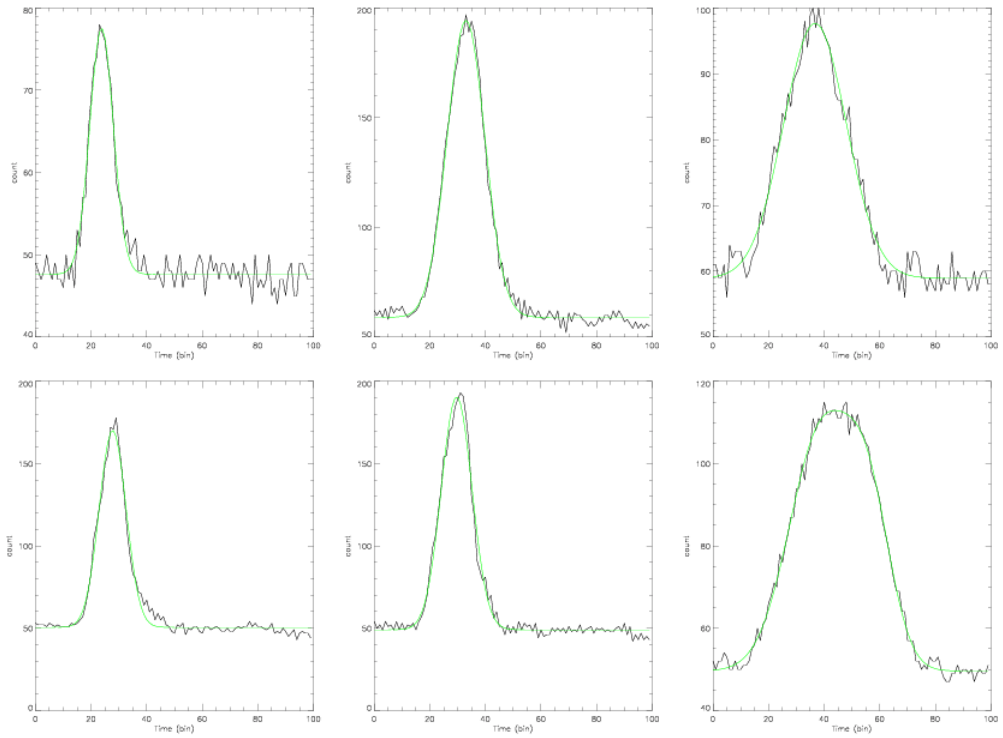

Figure 7 - Bigfoot waveforms over Greenland Fit with a Gaussian Function

SLA02 data cover both land and ocean. Most of the waveforms are single peaked and can be fit by a single Gaussian function. Sometimes the waveforms over land are multi-peaked and need to be fit by multi-Gaussian-functions as shown in Figure 8. This may be caused by multiple elevation levels within the laser footprint caused by buildings, vegetation or terrain. The ringing in the SLA02 data after the peak is caused by the instrument and is not expected in the GLAS data.

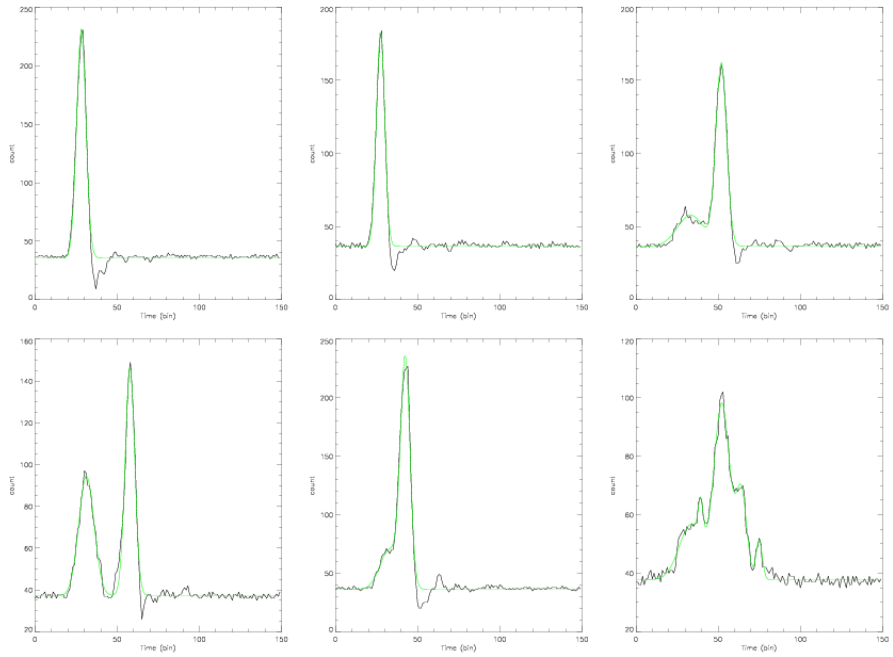

Figure 8 - SLA02 data fit with a Gaussian function

Atmosphere forward scattering changes the shape of the return waveforms. Over flat surfaces this portrays itself as a rise in the tail over the leading edge. David Duda and Jim Spinhirne (personal communications 1998) provided simulated waveforms for various cloud conditions that are expected to cause forward scattering. For these non-symmetrical returns, calculating the range to the centroid of the fitted Gaussian gives better agreement with the actual surface than using the centroid of the received waveform. Figure 9 shows the forward scattering waveform, its non-forward scattering component, its forward scattering component, and a Gaussian fit to the forward scattering waveform. The centroid of the non-scattering component at 14.95 ns is the known surface position. The centroid of the forward scattering waveform is at 16.88 ns, which gives a bias of 1.93 ns (equals to 28.95 cm in elevation) compare to the known surface. The centroid of the fitted Gaussian (±3σ edited Gaussian fit) is at 15.41ns, which gives a bias of 0.46 ns (equals to 6.9 cm in elevation) compare to the known surface. This result shows that the difference between the centroid of the fitted Gaussian pulse and the forward scattering waveform is 1.5 ns (equals to 22.5 cm in elevation) which is a significant decrease in elevation bias introduced by forward scattering.

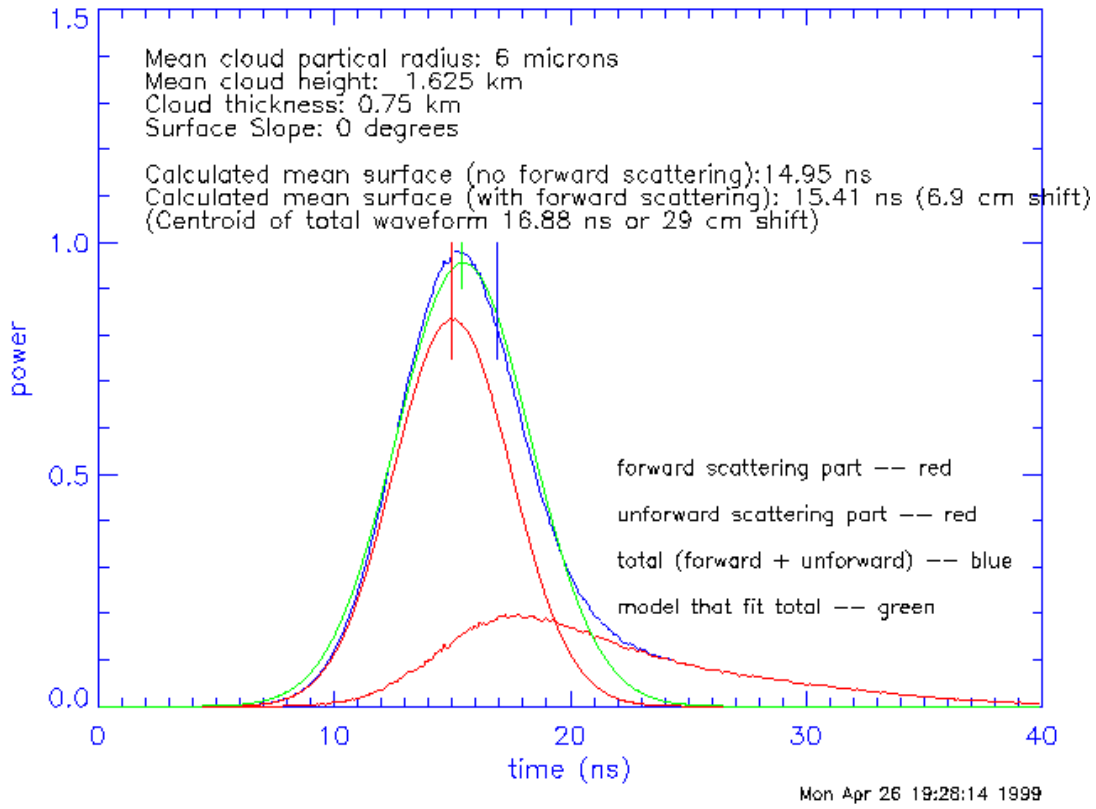

Figure 9 - Forward Scattering Effect on the Laser Return Waveform

Figure 10 shows the biases incurred in the calculation of the surface elevation from the return when the centroid of the Gaussian fit and the centroid of the received return are used as the position on the return which pertains to the mean surface for various cloud heights, particle size and cloud thickness. Using the centroid of the Gaussian fit always decreases the effect of forward scattering on the calculated elevation. Significant decreases are shown for low clouds where the forward scattering bias is high. Using the centroid of the Gaussian fit can reduce the forward scattering bias, but cannot eliminate it. The GLAS science team will study this problem further.

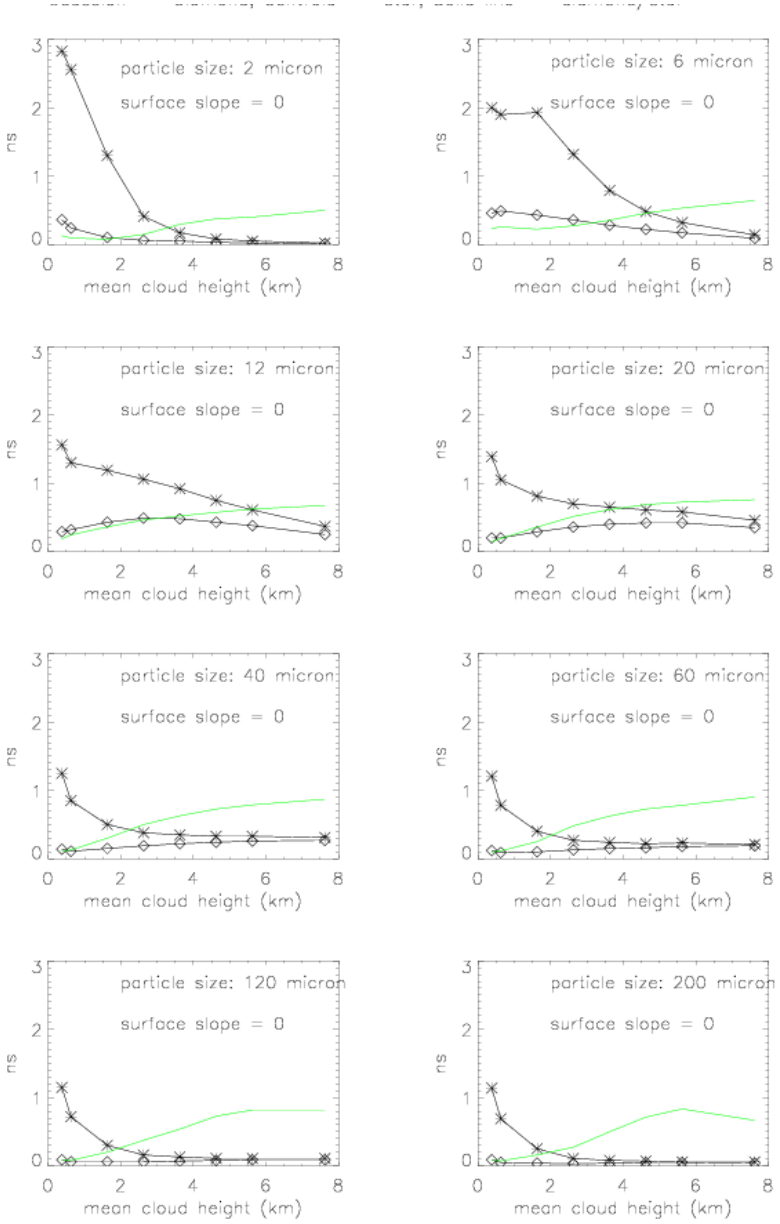

Figure 10 - Bias in ns from surface elevation; star - centroid of the return, diamond - centroid of the Gaussian fit

As a test of the algorithm, a simulation was carried out by using a real surface elevation profile over Greenland. The data were collected on the Jakobshavns glacier by the NASA ATM system. The profile is about 50 km along with 10 cm spacing between data. The surface profile was put into a 2D simulator to generate waveforms. The generated waveforms were analyzed by the retracking algorithm. The calculated surface elevation agrees with the known surface elevation very well. For the 270 simulated waveforms, the error is 5 cm without three points in a very rough zone (Figure 11). The calculated surface slope and surface roughness were compared with known surface roughness and surface slope (Figure 12). Figure 13 and Figure 14 are two examples that show surface elevations within the footprint and their waveforms. The waveform in these figures shows the simulated return. The elevation profiles show the elevation over the footprint with the x denoting the mean elevation calculated from the surface and the rectangle

denoting the mean elevation calculated from using the algorithms described in section 4. In figure 13, the return is a single peak Gaussian and the mean elevation from the algorithms agrees with the actual value. In figure 14, the return is a sum of two Gaussians due to the different elevations in the footprint and the calculated value (which corresponds to the centroid of the last Gaussian) is lower than the actual mean elevation because it represents the mean from the lower surface.

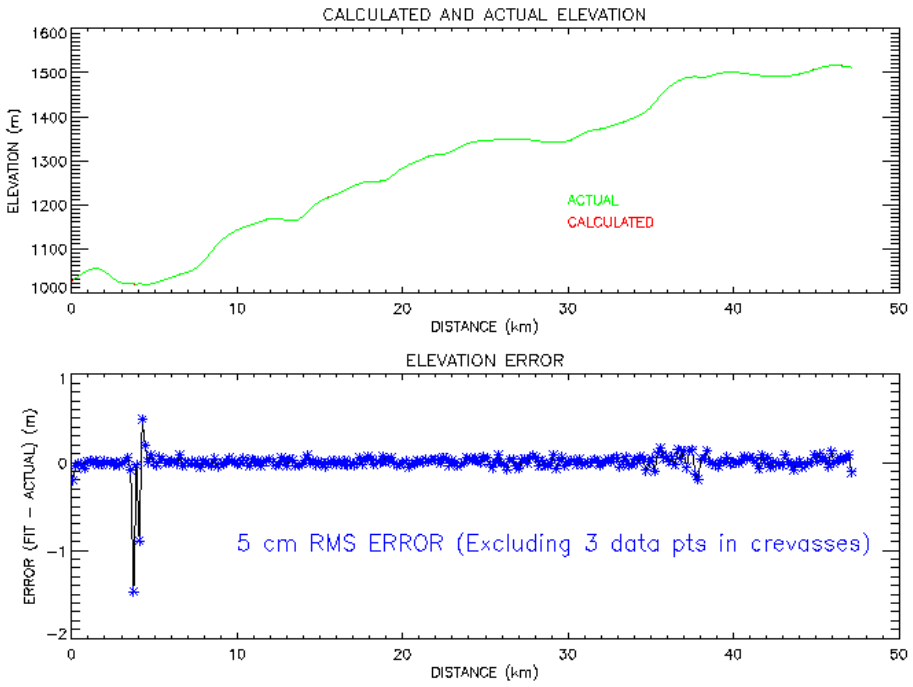

Figure 11 - Comparizon of simulated and actual surface and resultant GLAS elevation algorithm error

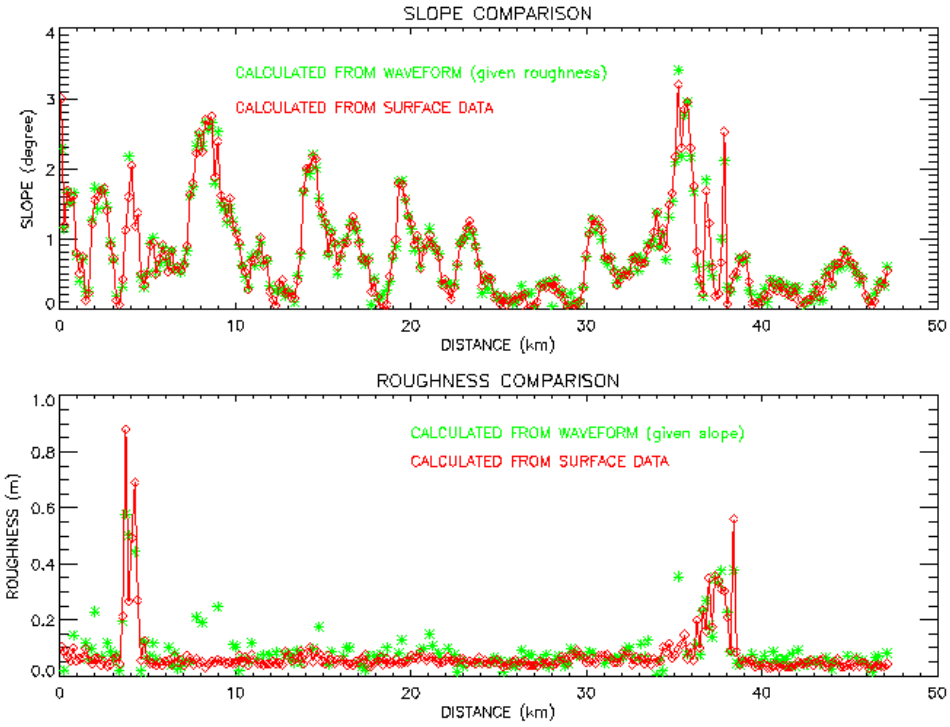

Figure 12 - Comparison of actual vs calculated surface roughness and slope.

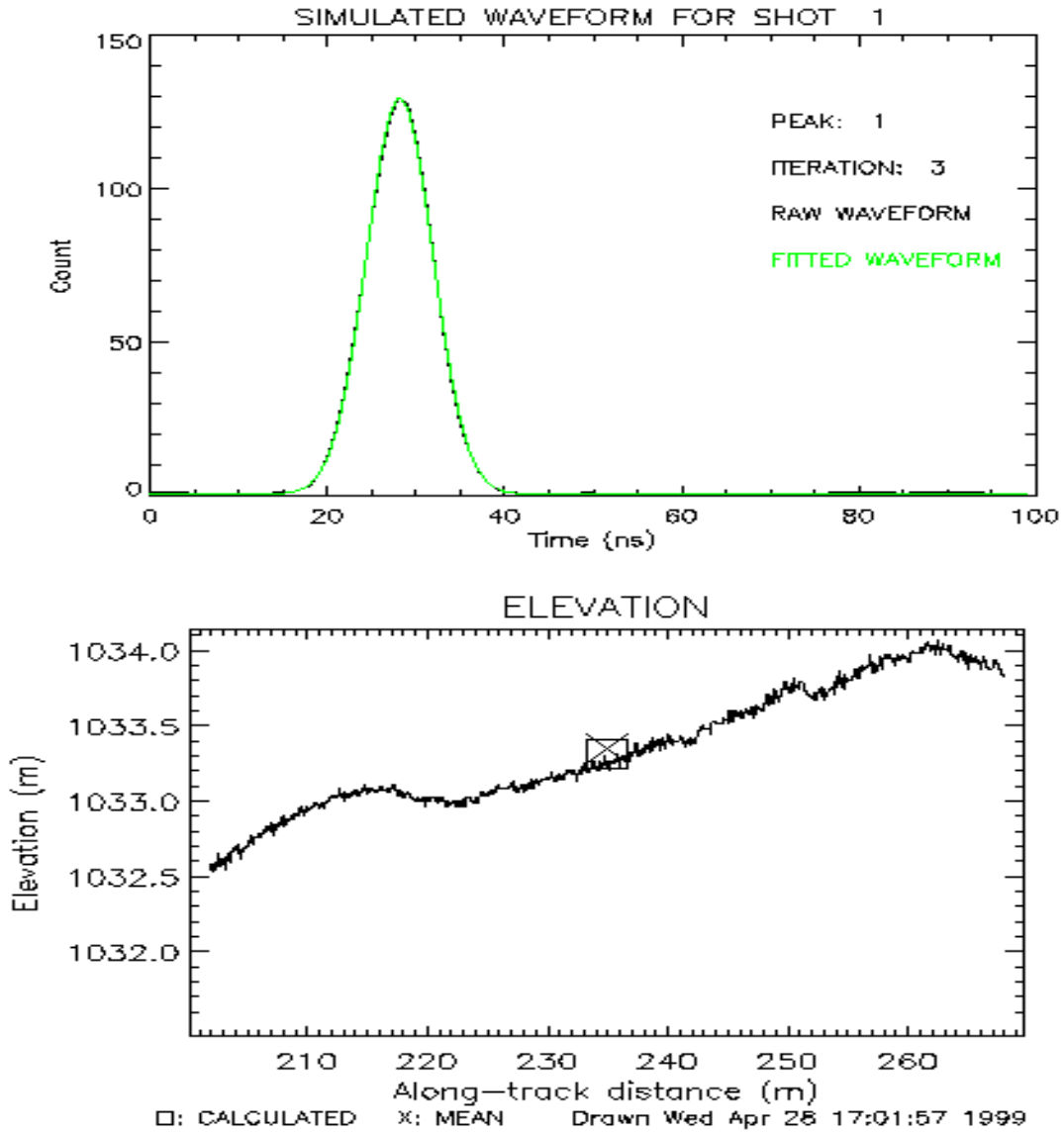

Figure 13- Simulated elevation and corresponding waveform using real ice sheet profile

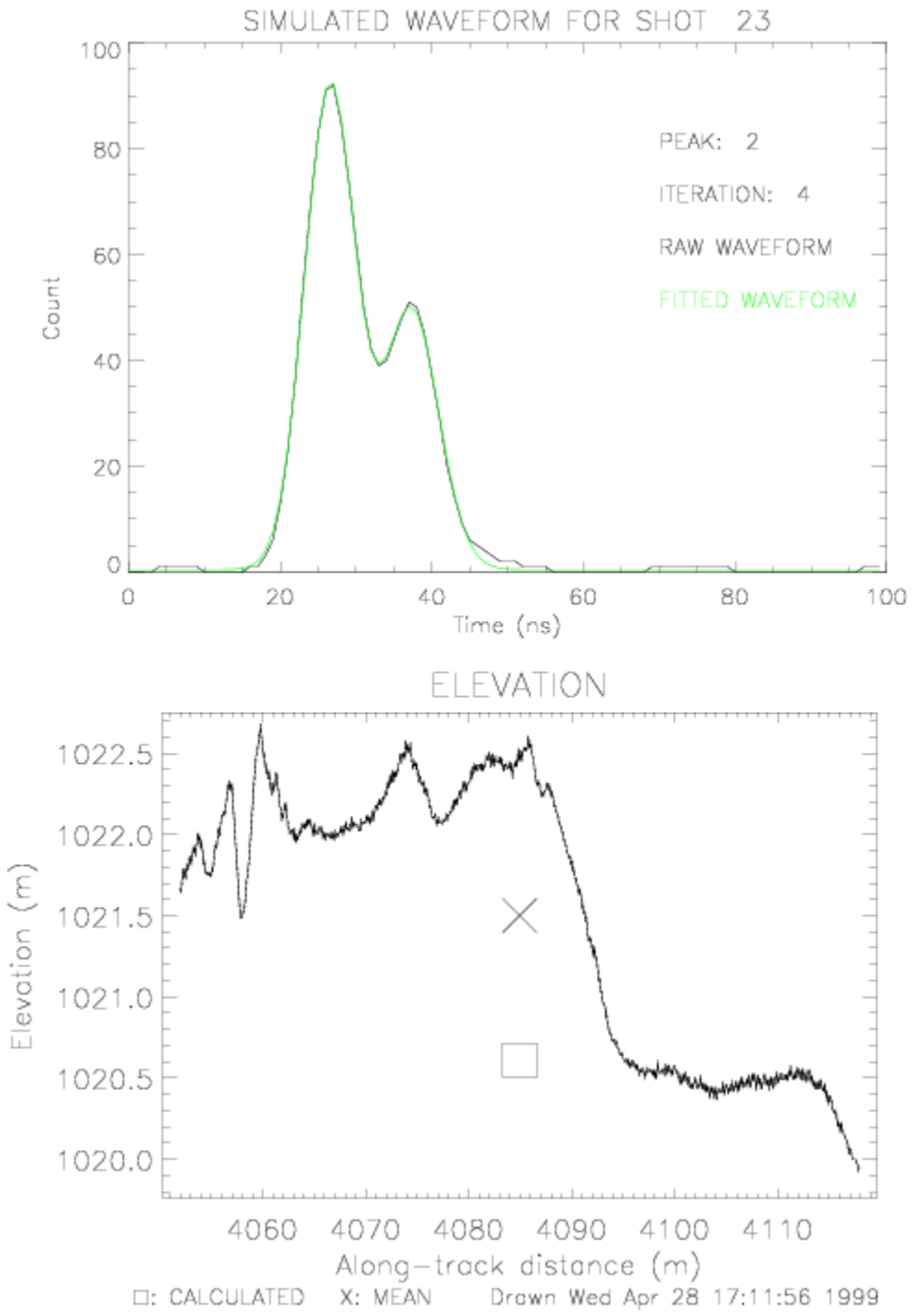

Figure 14 - Simulated elevation and corresponding waveform using real ice sheet profile

4.3.2.2. Validation of Sea Ice Algorithm

The algorithm has been tested by computing laser waveforms for various sea ice models using the Goddard Laser Altimeter Simulator (Version 3.8). The simulator program derives altimeter return-pulse waveforms in a simplified two-dimensional (height versus along-track distance) measurement geometry. The waveform is computed as it propagates to the terrain surface and back to the altimeter receiver. The simulator's receiver includes a telescope, an optical bandpass filter, either a photomultiplier or an avalanche photodiode optical detector (Si APD), a low pass filter, a timing discriminator, a time interval unit and a waveform digitizer. Simulation does not model the effects of atmospheric refraction or scattering. The terrain surface is assumed to be a Lambertian reflector, and its reflectivity and height can be specified for every centimeter of along-track distance. For details on the operation of the simulator see Abshire et al, 1994. Examples of computed waveforms are presented in Figure 15 and in Csathó and Thomas (1995).

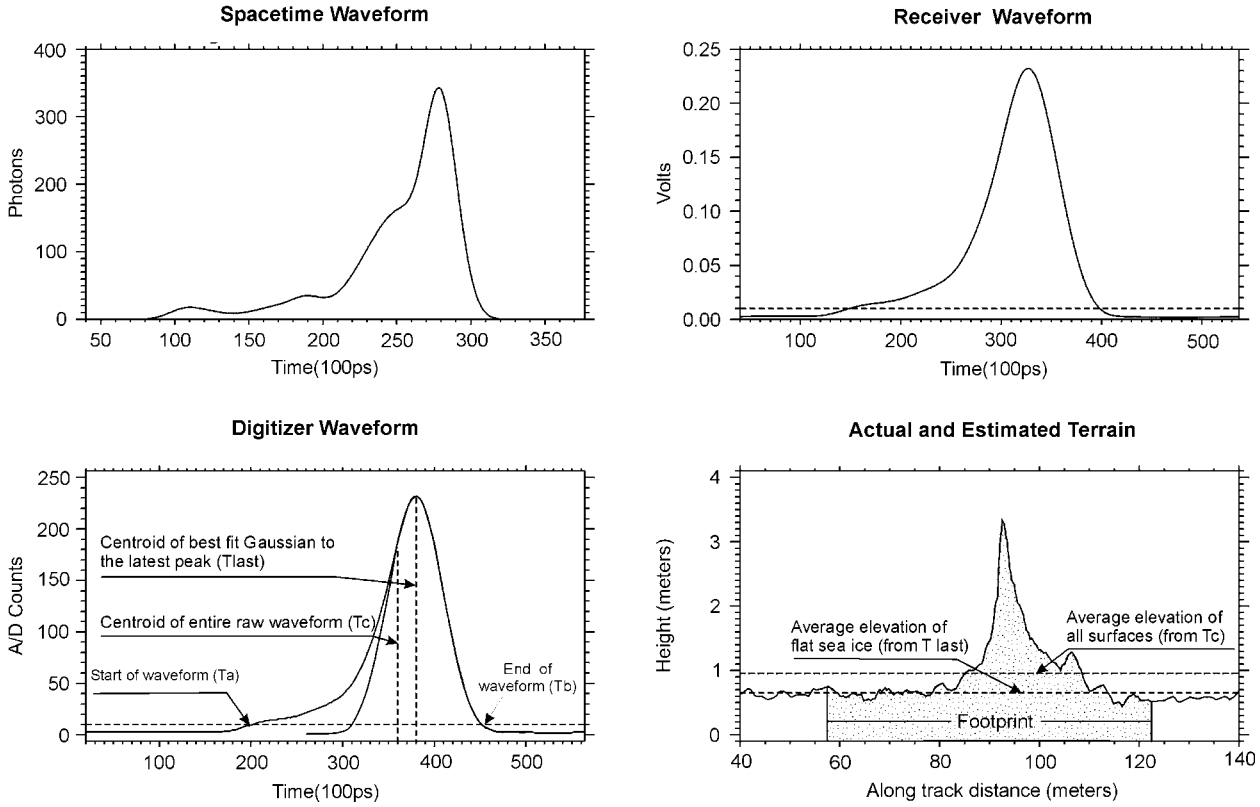

Figure 15 - Simulated laser altimetry waveforms

For evaluating the surface roughness algorithm we used the icex.dat sea-ice data set distributed with the GLAS simulator software (Abshire et al, 1994). The surface elevations were measured by an airborne laser altimeter every 1 m along a 110-km profile on May 20, 1987, north of Greenland. Surface roughness was computed from surface elevations and from simulated GLAS waveforms for several different flight segments to evaluate the performance of the estimator. The different stages of the simulation are illustrated in Figure 15. The spacetime waveform (Figure 15, upper left) shows the laser pulse shape after it is reflected back from the terrain to the receiver. The largest peak is caused by the photons reflected from the nearly horizontal sea ice comprising most of the footprint (Figure 15, lower right). The small peaks and 'shoulders' on its left are associated with the photons reflected back from the ridges. The spacetime waveform is further processed by the simulator to model the influence of the receiver and the background noise. The smooth electrical waveform (upper right) emerging from the

receiver has an asymmetric shape and a single peak associated with the flat sea ice. The digitized waveform (Figure 15, lower left) was used as input for the range and surface roughness computation. The average surface elevation was estimated from the centroid time delay, while the centroid of the last Gaussian shaped peak provides a very precise measure of the elevation of the flat sea ice (Figure 15, lower right).

The surface roughness computed from the laser-altimeter waveforms compares well with the surface roughness derived directly from the elevation (Figure 16). However, it generally underestimates the roughness of highly ridged areas, where surface is not "stationary". This is because most of the ridges on this profile are located in the outer part of simulated footprints, and pulse spreading is determined by the within-footprint elevation profile weighted by the normalized cross section of the laser beam (Gardner, 1982). Ridges located away from the footprint center have smaller weight and therefore produce less pulse spreading.

Soon after the ICESat launch, we plan aircraft measurements of sea-ice topography at very high spatial resolution (using the conical-scanning Airborne Topographic Mapper (ATM)), which will provide a detailed description of the sea-ice surface within many GLAS footprints. Data products derived by the GLAS sea-ice algorithm will be compared with equivalent products derived from the detailed mapping. These flights will probably be conducted out of Thule Air Force Base in northern Greenland in conjunction with underflights to validate GLAS performance over the ice sheet.

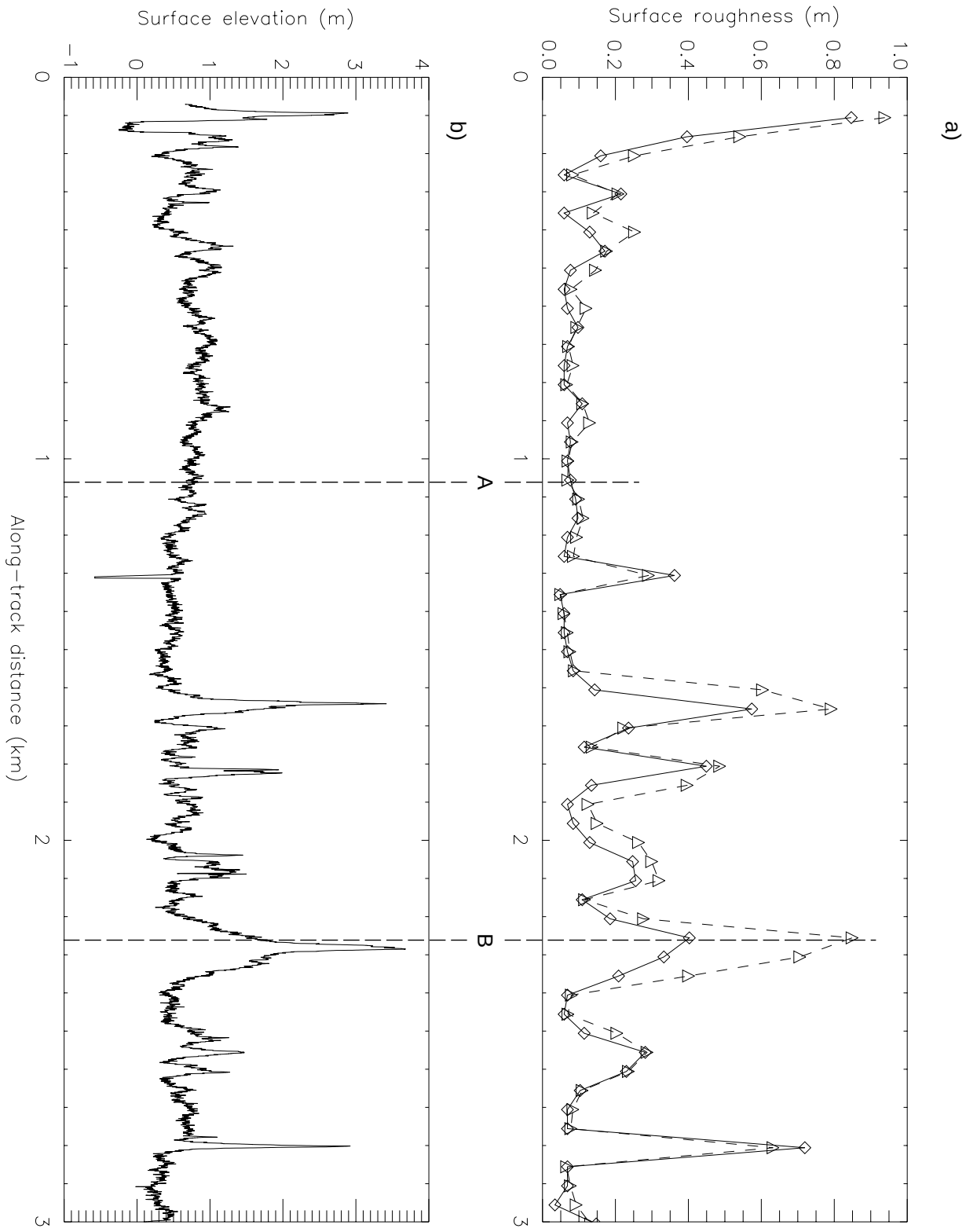

Figure 16 - a)Comparison of surface roughness computed from laser-altimeter waveforms (solid line with diamonds) and from surface elevation (dashed line with triangles), b)Surface elevation profile from airborne laser-altimeter data (reflectivity = 0.8)

4.3.2.3. Land Validation with Existing Data

The validity of the GLAS waveform processing algorithms for determination of land topography parameters (elevation, slope and roughness, vegetation height) is being evaluated using airborne emulation data. ICESat emulation data with 70 m diameter footprints are being compared to higher resolution data (contiguous, 12 m diameter footprints in a narrow swath). Both data sets were acquired by the airborne SLICER instrument along a common transect in the southern part of Gifford Pinchot National Forest in south eastern Washington state. The transect crosses a diverse landscape with a variety of slope and vegetation cover conditions. The smaller footprint data permit accurate separation of lidar backscatter returns from canopy layers and the underlying ground, and thus characterization of canopy structure and ground elevation and slope. The large diameter footprints are being compared as a function of slope to coincident aggregates of the higher resolution footprints in order to establish the amount of mixing between canopy and ground returns at the scale of ICESat footprints. Initial comparisons show that the large-diameter backscatter returns from sites with low slope are typically bimodal with separate canopy and ground returns but, as expected, increasing slope causes increased mixing and resulting ambiguity in establishing canopy structure and underlying ground elevations. These effects will be quantified by applying the GLAS waveform processing algorithms.

4.3.2.4. Validation Of Ocean Algorithm

The ocean algorithm is being tested, using the same approach as described in Section 4.3.3.2, by using waveforms simulated from airborne laser-altimeter measurements of ocean topography. First the surface elevation and surface roughness are estimated from each individual waveforms. Then the average surface elevation and the significant wave height are computed from the "composite" waveforms (Section 3.1.2.2.5).

After launch, GLAS ocean products will be validated against equivalent products derived from satellite radar-altimeter data at locations where the orbits cross at approximately the same time.

4.3.2.5. Validation During The 90 Day Cal/Val Period

The first 90 days of the ICESat mission have been designated as a validation period. This will be the first time the algorithms presented in section 4.1 will be tested on real GLAS data. There are several assumptions upon which the algorithms depend, the validity of which can be tested using real data. The first of these is the assumption that the transmitted pulse is Gaussian in shape. 32 gates defining the transmitted pulse will be telemetered each measurement. Plots of the transmitted pulse, the Gaussian fit, and the difference between the two will be interrogated to determine any significant non-Gaussian features.

The return pulse over flat surfaces should look like an impulse response. The validation period orbit will take the satellite over salt flats and desert regions that can be used to determine the nature of this response. Interrogating the return pulse, the Gaussian fit to it and the difference between the two will show any fundamental problems that would force us to drop the assumptions that we can fit to a Gaussian.

During this period we will also keep statistics as described in section 4.3.3 to determine how well the algorithm performs with real data. The fitting procedure will be fine-tuned to minimize failures (where the waveform fit will not converge) and optimize the accuracy of the surface elevation measurement. One of the biggest unknowns is how the atmosphere will affect the return and how much forward scattering will cause errors in the calculated elevation. The satellite will be in an 8-day repeat cycle during this period and we will try to compare data over known terrain in different atmospheric conditions to get a better handle on the actual effect. For ice sheet validation, we hope to underfly the satellite with an aircraft laser altimeter that will be able to verify the surface elevation and roughness characteristics. These will be compared with those calculated from the GLAS data and, given the correct conditions, we may be able to tune the algorithm to minimize the effect of the forward scattering.

Validation of the roughness algorithm for the ice sheet will be provided by underflights of the GLAS track in a suitable location in Greenland by Airborne Topographic Mapper. We are investigating the possibilities of underflights with an airborne laser altimeter in Antarctica as well. The algorithm for slope will be tested by off-nadir pointing (by several degrees) onto one or more of the flat, smooth test areas (White Sands, Bonneville Salt Flats) discussed in the GLAS validation plan.

4.3.3. Quality Control And Diagnostics

As part of the production process, we need to calculate statistics that will allow us to determine the overall data quality and the quality of the physical properties calculated from the data.

4.3.3.1. Quality Control And Diagnostics For Ice Sheet Products

The following information will be provided to allow the scientist to assess the quality of the data and related products.

- The percent of ice sheet measurements for which no signal was found
- For the subset of measurements for which a signal was found the following will be tabulated
  - The percentage of measurements for which the fitting procedure did not converge
  - The percentage of measurements for which no cloud layers were found
  - The percent of measurements that could not be processed due to saturation
- When a signal is found and the fitting procedure is successful, the following statistics are to be tabulated in such a manner that a histogram showing the distribution of these values can be generated. Except for the number of peaks, where the histogram bins will be integers from 1 to 6, the number of histogram bins should be 100. There is to be one set of histograms created for each granule of data.
  - The differences between the centroid of the received waveform and the centroid of the Gaussian fit to the last peak.
  - The number of peaks found in each smoothed waveforms.
  - The standard deviation of the fit to the received waveform
  - The skewness of each single peak return.
  - The kurtosis of each single peak return.
  - The percent of saturated signal compared to real signal within the signal region (from sig_beg to sig_end)
- For the subset of measurements for which a signal was found and successfully processed the mean and standard deviation of the following quantities will be calculated for each 100km strip (adjustable) along the ground track and color coded plots overlayed on maps showing these results will be generated for Greenland and Antarctica.
  - The number of peaks in the smoothed waveform
  - The number of peaks in the gaussian fit
  - The standard deviation of the fit to the received waveform for each measurement.
  - The skewness of each single pulse return
  - The differences between the centroid of the received waveform and the centroid of the Gaussian fit to the last peak
  - The maximum smoothed amplitude
  - The reflectance
  - A forward-scattering parameter TBD

- The ice sheet roughness (assuming a flat surface)
- The surface slope (assuming a smooth surface)
- The surface elevation
- The percent of clear sky (no cloud layers found)

For the same 100km strips (adjustable), the number of problem flags will be calculated and displayed, and the map will be marked if the surface ID (land, ocean, ice sheet, sea ice) has changed.

4.3.3.2. Quality Control And Diagnostics For Sea-Ice Products

For each sea-ice footprint not obscured by cloud, the following information will be provided on each data record to allow the user to assess data quality: RMS wave height

T_{last} = the time delay of the center of the peak from the Gaussian fit to the last peak

T_c = time delay of the centroid of the received waveform from sig_beg to sig_end

T_a = the time delay to sig_beg

T_b = the time delay to sig_end

Goodness of fit of the Gaussian approximating the latest peak;

From this information the following can be calculated.

- Number of peaks, and (T_{last} - T_c), indicating complexity of topography in the footprint;
- (T_{last} - T_a), and (T_b-T_{last}), expressed as distances, indicating the symmetry of the waveform and the possibility of forward scattering;

Browse products will be separate for Arctic and Antarctic, and will refer to all data from within the sea-ice mask.

The following will be provided per granule:

- percent bad data, or instrument off
- percent cloud cover
- histogram of roughness
- histogram of freeboard (GLAS sea-ice elevation - tide-corrected local geoid elevation)

Weekly (adjustable) statistics should be compiled during data processing of "successful" sea-ice data acquisitions (i.e. acquired elevations) expressed as percentages of possible sea-ice footprints within the sea-ice masks for each 30 degrees of longitude.

Per several granules (adjustable - approximately one week), maps of the Arctic and of the Antarctic, showing along each orbit:

1. cloud cover in gray
2. average roughness over approximately 1 km (adjustable)
3. average freeboard over approximately 1 km (adjustable)

Items 2 and 3 should be presented in colors with five classes (adjustable) between 0 and the maximum value. As the mission progresses the maximum value will be replaced by the upper-limit maximum value.

Before averaging, reject values of roughness or freeboard more than N times standard deviation. Take averages for any M km of data containing 90% (adjustable) coverage, to take account of spotty cloud cover.

4.3.3.3. Quality Control And Diagnostics For Ocean Products

For each ocean footprint not obscured by cloud, the following information will be provided to allow the user to assess data quality:

- $(T_c - T_a)$, and $(T_b - T_c)$, expressed as distances, indicating the symmetry of the waveform and the possibility of forward scattering;
- Goodness of fit of the Gaussian fit to the waveform.

In addition, (GLAS ocean elevation - tide-corrected local geoid elevation) should be provided as a "reasonableness" check.

Weekly statistics should be compiled during data processing of "successful" ocean data acquisitions (i.e. acquired elevations) expressed as percentages of possible ocean footprints for each 30 degrees longitude X 30 degrees latitude.

4.3.3.4. Quality Control And Diagnostics For Land Products

Quality control and diagnostic products for the land will utilize the same methods as for ice sheets.

5.0 WAVEFORM, WAVEFORM ANALYSIS AND ELEVATION OUTPUT PRODUCTS

GLAS standard output products, GLA05, 6, and 12-15 will be generated based on this ATBD. The actual waveform will be present on GLA01, a level 1A product, that will also have a predicted orbit at the accuracy of 0.1 deg. GLA05 is a level 1B waveform parameter product. This product will contain the parameters calculated from the waveforms, but the waveforms will not be repeated here. GLA06 is a level 1b global elevation product and will be similar to the existing geodetic data records from the radar altimetry satellites

There will be one level 2 product for each region; ice sheet, sea ice, land, and ocean, GLA12-15. Conforming to NASA's definition of level 2 products these will have the full rate data in a form usable by the science community. For GLAS this means that there will be a defined region-specific surface elevation with all required parameters necessary for it to be useable by a scientist. There will be masks provided that will define which data go on each product by location on the earth. These masks can overlap so that one measurement may be contained on multiple level 2 products. All GLAS output products will be archived at the NSIDC (National Snow and Ice Data Center) DAAC, which is also responsible for their distribution. After the initial calibration period of 90 days, the operational mission data products will be sent regularly to the NSIDC where they will be distributed upon request.

In addition to being able to correlate the products using time, there will be a unique index assigned to each 1 sec frame of data as it is processed from the level 0 products. That index will remain with that frame of data on every product for which information on that frame of data exists. Therefore, if one wants to find a specific waveform frame that corresponds to a level 2 elevation frame, one needs only to line up these indices. This is done to circumvent the confusion that occurs in trying to align products using time when a time correction has been applied to the higher level products but not the lower level ones. In accordance with the EOSDIS design, each product will be distributed by granules. The final definition of the granule sizes will be in a later ICESat data management publication. GLA01, 05, and 06 granule sizes are defined to be ¼ revolution of data where the granules are split at 50 deg latitude, both North and South. This keeps the polar regions on separate granules and should simplify distribution of the lower level data. The level 2 elevation product granules will each contain data from 14 revolutions of the spacecraft. The science team will deliver all GLAS standard products to the NSIDC within a few

weeks of real time and is working with the NSIDC to assure that all level products will be easily distributed.

The following sections describe parameters that are to go on each of these GLAS products covered by this ATBD.

5.1. Level 1b Waveform Parameter Product –GLA05

The waveform parameter product will have all of the parameters from the waveform characterization procedure and other parameters required to calculate physical properties of the surface. These are to include all parameters listed in table 5-1. Section 4.1 gives all algorithms for calculating these parameters.

Table 5-1 Parameters required to calculate physical properties of the surface for level 1b waveform product

#	Parameter	Precision
1	UTC time of laser pulse corrected for system delay, transit delay using the preliminary range, and timing bias from Jan 0 2000.	μsec
2	Range from the peak position of the transmit pulse to the telemetered gate farthest from the spacecraft (reference range).	.01 ns
3	Time increment from the reference range to the location on the waveform corresponding to the threshold retracker, t_{TH}	.01 ns
4	Maximum amplitude of the smoothed waveform	0.01 counts
5	Satellite position from the best available POD as a vector in ITRF at the ground bounce time of the measurement	mm
6	Off-nadir pointing direction (unit vector) in ITRF from the Precision attitude calculation	1.5 arc sec
7	Geodetic latitude and longitude calculated using the preliminary range with no atmospheric corrections.	μdeg
8	Surface elevation calculated using the preliminary range with no atmospheric corrections or tides applied.	mm
9	Surface identifier flags from regional ID grid –All 4, locean.lice,lseaice,lland.	N/A
10	Noise level from telemetry.	.01 counts
11	Received pulse Gain value.	N/A
12	Received Energy.	N/A
13	Transmitted Energy.	N/A
14	Percent of signal saturated from sig_beg to sig_end.	N/A
15	Transmitted gain value.	N/A
	There needs to be two sets of items 16-31 one for land and one for other surfaces for each received waveform.	
16	Kurtosis of the received waveform from signal begin to signal end	
17	Skewness of the received waveform from signal begin to signal end	

18	Initial number of peaks	N/A
19	Noise level from the functional fit	.01 counts
22	Amplitude of each Gaussian peak from the functional fit	.01 counts
21	Sigma of each Gaussian from the functional fit	.01 ns
22	Centroid position of each Gaussian from the functional fit as offset from last telemetered gate	.01 ns
23	Standard deviation from the covariance matrix for each fit parameter to the same accuracy as the parameter	
24	Flags indicating 1) successful functional fit, 2) fit convergence criteria met	N/A
25	X^2 of the functional fit	
26	Ranks of each peak in the solution	N/A
27	Area under the received waveform from signal begin to signal end	.01 counts^2 x ns
28	Time increment from reference range to Centroid of the received signal using only the portion of the return between sig_beg and sig_end	.01 ns
29	Time increment from reference range to sig_beg	.01 ns
30	Time increment from reference range to sig_end (used to calculate preliminary range)	.01 ns
31	Saturation flag	N/A
	The following 32-38 are from the transmitted waveform	
32	Amplitude of the Gaussian fit	.01 counts^2 x ns
33	Sigma of Gaussian fit	.01 ns
34	Centroid position of Gaussian fit as offset from gate 1 of transmitted waveform	.01 ns
35	Skewness of transmitted pulse	
36	Centroid of transmitted pulse	.01 ns
37	Area under the transmitted pulse	.01 Counts^2
38	Maximum amplitude of the signal	counts

5.2. Level 1b Global Elevation Product-GLA06

The global elevation product will contain information to calculate surface elevations and associated parameters and geodetic corrections required to calculate physical quantities associated with the surface. This product is intended as a research product and a stepping stone from which the region-specific level 2 elevation products are generated. Since this is a level 1 product, the corrections need to be available on the product with enough corresponding information to calculate a new surface elevation if users want to supply their own correction(s). For this same reason all elevations are given relative to a reference ellipsoid and a geoid elevation is provided for users to reference the elevations to sea level. Information is also given here to calculate basic region-specific elevations based on the results of the waveform

assessment. The geoid, and tides are quantities that vary at long wavelengths and only need to be calculated once per second (approximately 7 km along the ground). Users can linearly interpolate between the one second values for the value associated with the individual measurement. Table 5-2 lists parameters that are to be output for every measurement. Table 5-3 lists parameters that are to be output every second.

5.2.1. Region Specific Range Increments

Based on current knowledge, the region-specific range increments are defined to the position on the waveform corresponding to the centroid of the peak closest to the ground. This centroid is calculated from the functional fit. For the land range correction the land parameters are used in the fitting procedure. For the ocean, sea ice, and ice sheet range correction the ice sheet parameters are used in the fitting procedure. More research needs to be done with data that more closely resemble GLAS output. We hope to achieve this with special aircraft instrumentation flights over the next two years. These tests may show that a different location on the waveform should be used for some regions. To accommodate any changes, this global output product should have distinct parameters for four different region-specific range corrections. Whereas on the waveform parameter product all range values are given in ns, on the elevation products the range values will be given in mm. The values given in ns are a two-way travel time. To convert Range_ref, which is the two-way time in ns, to a one way range in mm use the following

$Range\_ref_{mm} = Range\_ref_{ns} * c/2$, where c is the speed of light in mm/ns

All other ranges are on the data record as increments to $Range\_ref_{mm}$. These increments are calculated using the following

$Range\_inc = (t(inc) - t_{ngates}) * c/2$, where t(inc) is the time (in ns from gate 1) associated with the location on the waveform to which the range increment corresponds.

5.2.2. Calculation Of Surface Elevation

Calculating an accurate surface elevation from the altimetry measurement involves accounting for not only the waveform range corrections which are discussed in section 4.1 but also correcting the range for atmospheric delay and applying appropriate tidal elevations to remove the time-varying tidal effect. After these corrections are applied to the range, the geolocation then needs to be recalculated because of the non-nadir pointing direction. The algorithms for calculating the atmospheric corrections and the tides and how to apply these to calculate the correct geolocation and surface elevation are presented in other

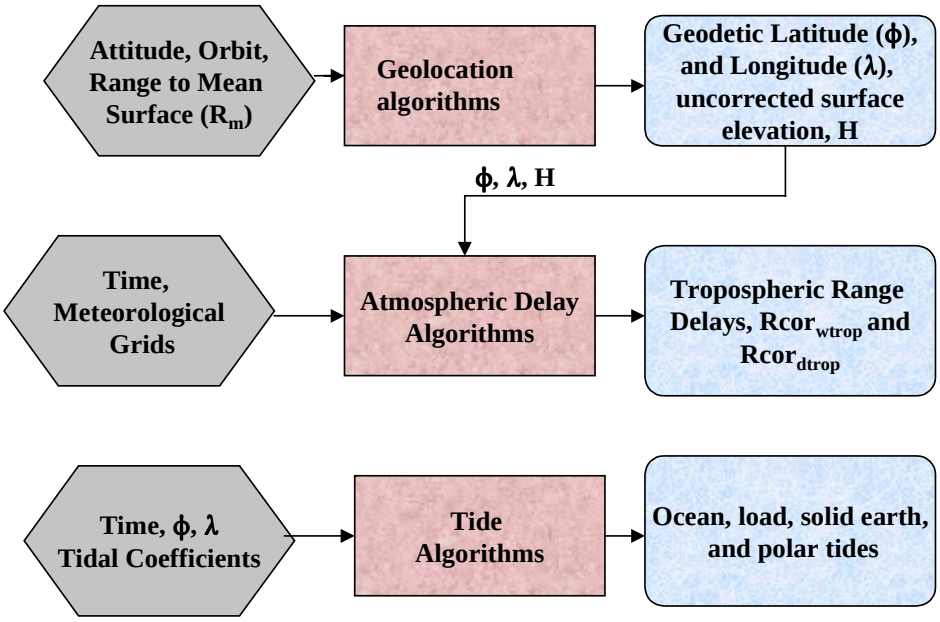

Figure 17 – Calculate Range Corrections

ATBDs in the GLAS document series. The mean range calculated from the centroid position of the last peak using the ice sheet, ocean, and sea ice functional fit results will be used to calculate the geolocation for GLA05. Block diagrams showing the order in which the parameters will be calculated are given in Figures 17 and 18.

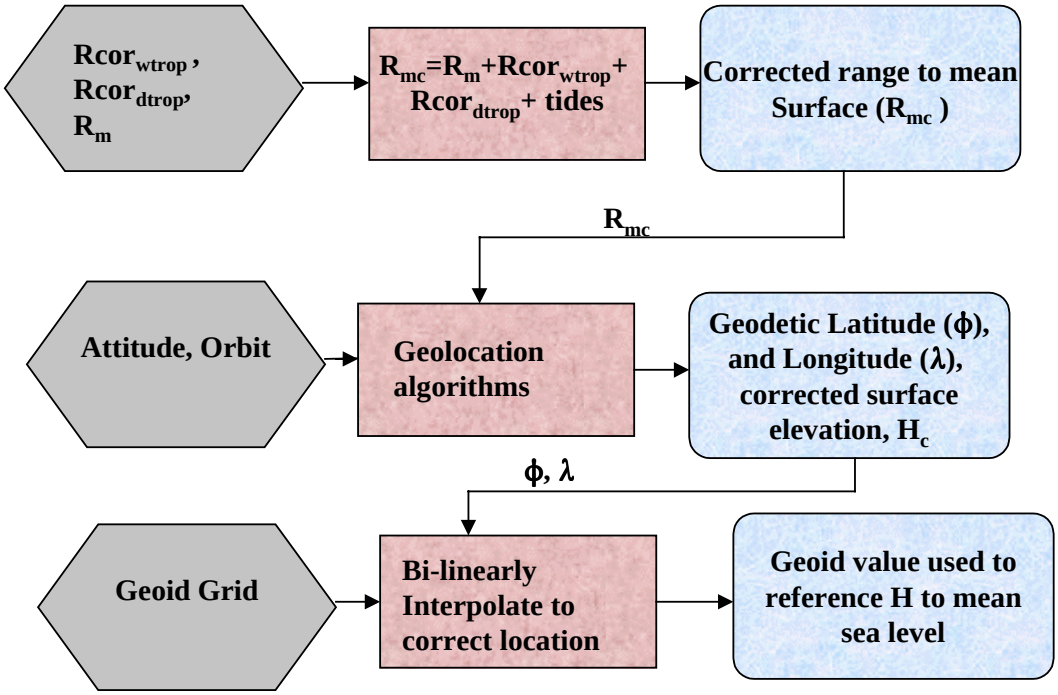

Figure 18 – Correct Range and Calculate Precise Geolocation and Elevation

First, as shown in Figure 17, the mean range, PAD, and POD are used to calculate a more precise geolocation. This geolocation along with time and meteorological data is input to the atmospheric delay algorithms to calculate the range corrections due to the signal interaction with the troposphere. The geolocation and time are then input to the tidal algorithms to calculate the ocean, load, and solid earth tides. The polar tide correction is included in the PAD. Figure 18 then shoes how these corrections are used to correct the range from which a more accurate geolocation and surface elevation are calculated. The value of the geoid is then interpolated to allow the user to reference the elevation to mean sea level.

5.2.3. Calculate of Reflectance

The reflectance is calculated as the ratio of the received energy after it has been scaled for range and the transmitted energy. The unscaled received energy is calculated as the area under the received waveform from sig_beg to sig_end after the noise has been subtracted scaled by the receiver gain and the optical to detector volt efficiency for the receiver pulse The transmitted energy is calculated as the area under the transmitted waveform scaled by the transmitted gain and the optical to detector volt efficiency for the transmitted pulse

The equation for the surface reflectivity is:

$$\rho_{surf} = \frac{\pi \; E_{rec} \; R^2}{E_{trans} \; A_{telescope} \; \tau_{opt} \; \tau_{RTatm}} \qquad [37]$$

$$\tau_{RTatm} = e^{-2(\tau_c+\tau_a+\tau_m)} \qquad [38]$$

where ρ_{surf} is the surface reflectivity, E_{rec} is the received energy, R is the range in meters, E_{trans} is the transmitted energy, $A_{telescope}$ is the telescope area (0.709 m^2), τ_{opt} is the optics transmission (55.5%), τ_{RTatm} is the roundtrip atmosphere transmission, τ_c is the cloud (column) integrated optical depth (one per second), τ_a is the aerosol (column) integrated optical depth (once per four seconds), and τ_m is the molecular optical depth.

The received and transmitted energy are determined by the following procedure:

- Identify the location of the pulse (position of maximum amplitude between signal begin and end).
- Compute the threshold amplitude from the pulse amplitude and the threshold percentage (*thrPcnt* TBD).

  $$threshold\_amp_{rec} = thrPcnt * (pulse\_amp_{rec} - mean\_noise_{rec}) + mean\_noise_{rec} \quad [39]$$

  The mean noise for the transmitted pulse is expected to be zero, so:

  $$threshold\_amp_{trans} = thrPcnt * pulse\_amp_{trans} \quad [40]$$

- From the pulse location, find the locations where the waveform amplitude falls below threshold_amp.
- Calculate the sum of the waveform data (A_{pulse} area under waveform above mean noise).
- Calculate the pulse energy as the product of the above sum and a calibration coefficient.

  $$E_{pulse} = A_{pulse} * Gain_{pulse} * calib\_coef_{pulse} \quad [41]$$

  $Gain_{trans}$ will be held constant (over a period of months), and $Gain_{rec}$ will be adjusted every second depending on the maximum received amplitude.

5.2.4. Calculation of The Footprint Orientation

There will be an LCD image of the laser beam for each measurement from which the footprint orientation and shape can be derived. To facilitate further research we request that the shape and orientation of this footprint, calculated as part of the attitude determination process, explained in the GLAS PAD ATBD, be written on the output product for each measurement. Ellipsoid parameters defining the footprint shape and the orientation of the major axis relative to true north are to be saved for this product.

5.2.5. Ancillary Information

The science team will provide the 1 km resolution land DEM from the Global 30 Arc-Second Elevation Data Set (GTOPO30) and geoid grids from TBD source for reference on the elevation products. These products will be provided on a latitude and longitude grid and bi-linear interpolation to the location of the footprint is to be used to calculate the specific value associated with each measurement. The LIDAR will provide some information concerning cloud coverage as explained in the GLAS atmospheric ATBDs. Several flags will be set based on this information:

- Flag indicating no cloud layers found
- Flag indicating no aerosol layers found
- Flag indicating that the LIDAR data give evidence of good conditions for forward scattering to occur. This will be based on the lowest cloud layer boundary falling within TBD km of the surface as indicated by the DEM and the optical depth associated with the cloud layer being within TBD bounds. Research is ongoing to try to determine how to set this flag.

5.2.6. Quality Information

- To aid in using this as a research product, there needs to be some indication of whether there was a problem in calculating any of the parameters on the product. For the following parameters this indication is to be a flag set to 0 if there was no problem and set to 1 if any problem occurred in the calculation. Quantities calculated and flags set once per second:
- Solid earth tides
- Ocean tides
- Load tides
- Geoid interpolation

Quantities calculated and flags set once per measurement:

- DEM interpolation
- Wet troposphere correction
- Dry troposphere correction
- Off-nadir pointing direction
- Satellite position
- Range increments based on the waveform for ice sheet
- Range increments based on the waveform for sea ice
- Range increments based on the waveform for land
- Range increments based on the waveform for ocean

Table 5-2 Parameters to be output every measurement –level 1b elevation product

Parameter Description	Precision
UTC time of laser pulse corrected for system and transit delay from Jan 0 2000	μsec
Altimeter range to the telemetered gate farthest from the spacecraft - reference range = Range_ref (ns) * c/2	mm
Satellite position from the best available POD as a vector in ITRF at the ground bounce time of the measurement	mm
Off-nadir pointing direction (unit vector) in ITRF from the Precision attitude calculation	1.5 arc sec
Geodetic Latitude and longitude calculated using range increment to centroid of last peak with all atmospheric corrections and tides applied	μdeg
Surface Elevation calculated using range increment to centroid of last peak with all atmospheric corrections and tides applied	mm
Surface Identifier flags from regional ID grid – All 4, locean.lice,lseaice,lland	N/A

Range increment from reference range to threshold retracker range	mm
Range increment from reference range to signal begin	mm
Range increment from reference range to signal end	mm
Range increment from reference range to ice sheet specific range.	mm
Range increment from reference range to sea ice specific range	mm
Range increment from reference range to land specific range	mm
Range increment from reference range to ocean specific range	mm
Number of peaks from smoothed waveform	N/A
Peak Amplitude from smoothed waveform	counts
Range increment from reference range to centroid of received waveform from signal begin to signal end	mm
Solar incidence angle	.01 deg
Reflectance * round trip atmospheric transmission	
Surface Roughness from Ice sheet algorithms	mm
Surface slope from ice sheet algorithms	.01 deg
A set of flags indicating problems with any of the parameters to include: surface elevation from DEM, waveform-based range corrections, orbit, attitude, and atmospheric delay corrections	N/A
Surface elevation from DEM	cm
Orientation of the laser footprint measured clockwise from true north from attitude determination system	.01 deg
Wet troposphere atmospheric delay correction	mm
Dry troposphere atmospheric delay correction	mm
Length of the major axis of the laser footprint from attitude determination system	cm
Length of the minor axis of the laser footprint from attitude determination system	cm

Table 5-3 Parameters to be output once per second level 1b elevation product

Parameter Description	Precision
Cloud coverage flag from LIDAR products	
Solid earth tide elevation	mm
Ocean tide elevation	mm
Load tide elevation	mm
A set of flags indicating problems with any of the parameters to include: geoid, load tides, solid tides, and ocean tides	N/A

include: geoid, load tides, solid tides, and ocean tides	
For the atmospheric corrections a flag indicating what source was used.	N/A
Flag indicating aerosol layer (s) were detected in LIDAR data	N/A
Flag indicating conditions for forward scattering to occur were detected in LIDAR data	N/A
Flag indicating cloud layer (s) were detected in LIDAR data	N/A
Geoid	mm

5.3. Ice Sheet Product – GLA12

The level 2 ice sheet product is generated for the ice sheet community with the intent that it be usable by glaciologists as a source of ice sheet elevation and surface characteristics within the limitations of the GLAS system. To this extent, the surface elevation will be calculated using a pre-determined "best" algorithm for ice sheets applying all pertinent corrections and accounting for the time-varying tidal effects. Since this is a level 2 product, the corrections need to be available on the product with enough corresponding information to calculate a new surface elevation if users want to supply their own correction(s). For this same reason all elevations are given relative to a reference ellipsoid and a geoid elevation is provided for users to reference it to sea level. As with the level 1b elevation product, the corrections and tides that vary at a long wavelength need to be calculated every second and can be linearly interpolated for the correct value to correspond to the 40/sec measurement.

Over most of the ice sheets the return waveform will resemble a simple Gaussian with one peak. There will be exceptions over crevasses and near cliffs and other features where the return will have multiple peaks. Multiple peaks can also occur due to low clouds or ice fog. The main requirement of ICESat is to measure elevation changes. This requires that a mean elevation be associated with each ice sheet measurement. Therefore when there are multiple peaks, the range will be calculated based on the position of the centroid of the last peak. The increment in range between the last and first peaks needs to be tabulated also so users can recalculate the surface elevation based on the first peak if conditions warrant it. The number of peaks needs to be indicated so the user can tell how complicated the surface was. This product should also contain P^2 of the received waveform to the functional fit as an indication of surface or transmit pulse irregularities that the user may want to research further using the lower level products. The range to the centroid of the received waveform and the ranges to the beginning and end of signal, and the skewness and kurtosis of the received waveform need also be supplied so the user can use these to look for surface characteristics specific to their research.

All flags present in the level 1b elevation product that affect the ice sheet surface elevations need also be provided along with the ancillary information discussed in 5.2. Table 5-4 lists the parameters to be supplied every measurement. The parameters to be output every second are the same as those listed in Table 5.3.

Table 5-4 Parameters to be output every measurement-level 2 ice sheet product

Parameter Description	Precision
UTC time of laser pulse corrected for system and transit delay from Jan 0 2000	μsec

Altimeter range to telemetered gate farthest from the spacecraft - reference range	mm
Range increment from reference range to threshold retracker range	mm
Satellite position from the best available POD as a vector in ITRF at the ground bounce time of the measurement	mm
Off-nadir pointing direction (unit vector) in ITRF from the Precision attitude calculation	1.5 arc sec
Geodetic Latitude and longitude calculated using ice sheet-specific range with all atmospheric corrections and tides applied	μdeg
Surface Elevation calculated using the ice sheet-specific range with all atmospheric corrections and tides applied	mm
Surface Identifier flags from regional ID grid – All 4, locean.lice,lseaice,lland	N/A
Range increment from reference range to signal begin	mm
Range increment from reference range to signal end	mm
Range increment from reference range to produce ice sheet specific range based on the last peak in the return	mm
Range increment from reference range to produce ice sheet specific range based on the first peak in the return	mm
Standard deviation of received waveform to fit using ice sheet parameters	.01 counts
Solar Incidence Angle	.01 deg
Number of peaks from Gaussian fit	N/A
Peak Amplitude from smoothed waveform	counts
Kurtosis of the received waveform from signal begin to signal end	
Skewness of the received waveform from signal begin to signal end	
Range increment from reference range to centroid of received waveform	mm
Reflectance * round trip atmospheric transmission	
Surface Roughness from Ice sheet algorithms	mm
Surface slope from ice sheet algorithms	.01 deg
A set of flags indicating problems with any of the parameters to include: DEM, waveform-based range corrections, orbit, and attitude	N/A
DEM	cm
Orientation of the laser footprint measured clockwise from true north from attitude determination system	.01 deg

Length of the major axis of the laser footprint from attitude determination system	cm
Length of the minor axis of the laser footprint from attitude determination system	cm

5.4. Level 2 Sea Ice Product – GLA13

The sea-ice algorithm is designed to provide estimates of:

a. Average range to the surface of smooth or randomly rough ice or of open water within the footprint will be inferred from the time delay of the centroid of the best-fit Gaussian associated with the latest peak in the return pulse. For sea ice, this elevation will be slightly above the local sea surface, and time series of such data might provide an indication of the temporal variability of sea-ice freeboard during the period of the mission if we also have information on temporal variability of sea-surface elevation in the same regions. For orbit tracks crossing open-water leads and polynas, is should be possible to estimate the freeboard of surrounding sea ice, giving an indication of sea-ice thickness (Wadhams et al, 1992), as proposed by Peacock et al, (1998) using satellite radar-altimeter data.

b. Average range to all surfaces in the footprint will be inferred from the time delay of the centroid of return waveform above noise threshold. For smooth and randomly rough sea ice and for open water, this should be almost identical to (a). The difference between (a) and (b) gives an indication of whether a significant fraction of the footprint is occupied by a large ice ridge or an iceberg, causing an asymmetric, non-Gaussian return waveform.

c. Sea-ice surface roughness estimates will be obtained from the RMS width of the whole return pulse as well as from the RMS width of best-fit Gaussian associated with its latest peak. The first is a measure of the total surface elevation variation, and the latter a measure of the roughness of the smooth ice of or open ocean surface within the footprint.

d. Range to the highest surface in the footprint will be inferred from the time delay of the centroid of the best-fit Gaussian associated with the first peak in the return waveform. This indicates the highest large roughness element, or surface of iceberg, floating glacier tongue, or land within the footprint.

e. Average reflectivity within the footprint will be obtained from the total energy in the return pulse, taking account of the transmitted energy, height of spacecraft, receiver characteristics etc.

Table 5-5 Level 2 sea-ice parameters to be output every measurement

Parameter Description	Precision
UTC time of laser pulse corrected for system and transit delay from Jan 0 2000	μsec
Altimeter range to telemetered gate farthest from the spacecraft - reference range	mm
Range increment from reference range to threshold retracker range	mm
Satellite position from the best available POD as a vector in ITRF at the ground bounce time of the measurement	mm

Off-nadir pointing direction (unit vector) in ITRF from the Precision attitude calculation	1.5 arc sec
Geodetic latitude and longitude calculated using sea ice-specific range with all atmospheric corrections and tides applied	μdeg
Sea-ice surface elevation calculated using the last peak of the waveform, with all atmospheric corrections and tides applied	mm
For waveforms with more than one peak, 'iceberg' elevation calculated using the first peak in the waveform, with all atmospheric corrections and tides applied	mm
Average elevation of all surfaces in the footprint from the centroid of the received waveform, with all atmospheric corrections and tides applied	mm
Surface Identifier flags from regional ID grid – All 4, locean.lice,lseaice,lland	N/A
Range increment from reference range to signal begin	mm
Range increment from reference range to signal end	mm
Range increment from reference range to produce sea ice specific range based on the last peak in the return	mm
Range increment from reference range to produce sea ice specific range based on the first peak in the return	mm
Standard deviation of received waveform to fit using sea ice parameters	.01 counts
Solar incidence angle	.01 deg
Number of peaks from smoothed waveform	N/A
Peak amplitude from smoothed waveform	counts
Skewness of the received waveform from signal begin to signal end	
Range increment from reference range to centroid of received waveform between signal begin and signal end	mm
Reflectance * round trip atmospheric transmission	
Surface roughness of 'flat' sea ice or ocean within the footprint from the RMS width of the best fit Gaussian to the last peak	mm
Average surface roughness of the entire footprint from the RMS width of the entire waveform	mm
A set of flags indicating problems with any of the parameters to include: DEM, waveform-based range corrections, orbit, and attitude	N/A
DEM	cm
Orientation of the laser footprint measured clockwise from true north from attitude determination system	.01 deg

Length of the major axis of the laser footprint from attitude determination system	cm
Length of the minor axis of the laser footprint from attitude determination system	cm

5.4.1. Ancillary Information

In addition to the information needed to correct measured ranges for atmospheric effects, and to locate the footprint, these sets of information will be required:

a. Sea-ice mask, defined from the GSFC SMMR-SSM/I ice concentration data

b. Land mask, to include most recent estimates of the seaward margins of icebergs and glaciers. For Greenland and Antarctica, this could probably best be obtained from available SAR imagery. For other land masses, the best-available sources should be used. Sea-ice products should be produced for all ocean and lake areas included within a mask bounded by the lowest latitude of sea-ice extent plus 50 km, and excluding land areas.

Users may find it useful if the following parameters are archived with each GLAS sea-ice product:

Mean sea surface and geoid for high latitudes, with best estimates of sea-surface height variability. For much of the Arctic, this can probably be obtained from work done by S. Laxon and his group at Mullard Space Science Laboratory (Personal communication from S. Laxon, November, 1998).

5.5. Level 2 Land Product – GLA14

Because of the potential complexities of land returns, the level 2 land product is intended to describe the waveform in a way that, in combination with independent knowledge of, or assumptions about, local relief and land cover interpretations can be made regarding elevation, slope, roughness, and vegetation and/or cultural feature height. To this end, a land-specific range is defined which is the centroid of the received waveform signal between the defined signal start and signal end. This land-specific range is used for computation of the final Geolocated Latitude and Longitude and Footprint Elevation. Absent independent information this is the best, most representative elevation for the land. Range offsets from this land-specific range to the start and end of signal are to be provided that, in combination with the provided laser pointing vector, can be used to compute the elevation of the highest and lowest detected features within the footprint. For the most common orientation (nadir pointing) the range offsets are equivalent to elevation offsets. Similarly range offsets from the land-specific range to the centroid for each of the Gaussian distributions fit to the waveform peaks is to be provided. This includes up to 6 Gaussian fits. Where more than 6 peaks were fit to the waveform (anticipated to be rare), the fit to the last (lowest) peak and the 5 other most significant fits (based on the area of the Gaussian distributions) are to be used. The one sigma width of each Gaussian fit, converted to units of range, and the amplitude and area of each of the Gaussian fits is also to be provided. From these data the Gaussian fit approximation of the waveform can be recreated along the laser pointing vector positioned with respect to the geolocated land-specific range. Inferences can then be made, in conjunction with independent knowledge or assumptions, about how, and if, the return signal is separated into surface, vegetation and cultural feature components. With these inferences, measures of surface elevation and relief and vegetation and/or building height can be derived. In order for the user to know how robust the Gaussian fits conformed to the waveform, Chi^2 and standard deviation measures of the fit to the waveform should be provided using all the Gaussian fits as well as using the 6 stored fits. For cases of 6 or fewer fits these measures will be equivalent. In order to provide model measures of slope and roughness, the ice sheet algorithms

assuming no-roughness and no-slope end-members will also be applied. These algorithms will be applied to the Gaussian fit to the last (lowest) peak. Last peak model results are provided for those cases where it is inferred that the last peak corresponds to the surface beneath vegetation and/or cultural features. Full peak model results are also provided for those cases where it is decided that no vegetation and/or cultural features are present, or where it is decided that multiple components in the footprint have not been reliably separated in the waveform. Additional parameters are provided analogous to those provided for the ice sheet product.

Table 5-6 Lists the Level 2 land parameters to be output for every measurement. In addition, the same parameters as found in Table 5-3 for ice sheets need to be output once per second

Table 5-6 Parameters to be output every measurement for level 2 land product

Parameter Description	Precision
UTC time of laser pulse corrected for system and transit delay from Jan 0 2000	μsec
Altimeter range to farthest telemetered gate from the spacecraft-reference range	mm
Range increment from reference range to threshold retracker range	mm
Satellite position from the best available POD as a vector in ITRF at the ground bounce time of the measurement	mm
Off-nadir pointing direction (unit vector) in ITRF from the Precision attitude calculation	1.5 arc sec
Geodetic Latitude and longitude calculated using land-specific range with all atmospheric corrections and tides applied	μdeg
Surface Elevation calculated using the land-specific range with all atmospheric corrections and tides applied	mm
Surface Identifier flags from regional ID grid – All 4, locean.lice,lseaice,lland	N/A
Range increment from reference range to signal begin	mm
Range increment from reference range to signal end	mm
Range increment from reference range to land- specific range	mm
Range increment from reference range to centroid of Gaussian fits (6 elements)	mm
One-sigma width of Gaussian fits (6 elements)	mm
Amplitude of Gaussian fits (6 elements)	counts
Area of Gaussian fits (6 elements)	counts
Standard deviation of received waveform using all fits	.01 counts
Standard deviation of received waveform using stored fits	.01 counts
Solar Incidence Angle	.01 deg
Number of peaks from smoothed waveform	N/A

Peak Amplitude from smoothed waveform	counts
Skewness of the received waveform from signal begin to signal end	
Reflectance * round trip atmospheric transmission	
Surface Roughness from Ice sheet algorithms using last (lowest) fit	mm
Surface slope from ice sheet algorithms using last (lowest) fit	.01 deg
A set of flags indicating problems with any of the parameters to include: DEM, waveform-based range corrections, orbit, and attitude	N/A
DEM	cm
Orientation of the laser footprint measured clockwise from true north from attitude determination system	.01 deg
Length of the major axis of the laser footprint from attitude determination system	cm
Length of the minor axis of the laser footprint from attitude determination system	cm

5.6. Level 2 Ocean Product – GLA15

The ocean algorithm is designed to provide estimates of:

a. Average elevation of each footprint.

b. Highest and lowest elevations within each footprint.

c. The product of reflectance and the roundtrip atmospheric transmission of each footprint.

d. Mean elevation over 1 sec segment.

e. RMS roughness within this 1 sec segment .

'Ocean' data will be as determined from the global DEM, to include all regions larger than, say 1000 sq km that are at sea level. Thus, 'ocean' tracking will be implemented over large lakes and over sea ice, in addition to the special tracking appropriate to these areas.

Table 5-7 lists the ocean parameters to be provided every measurement; parameters listed in Table 5-3 will be provided every second.

Table 5-7 Level 2 ocean parameters to be output every measurement

Parameter Description	Precision
UTC time of laser pulse corrected for system and transit delay from Jan 0 2000	μsec
Altimeter range to farthest telemetered gate from the spacecraft-reference range	mm
Range increment from reference range to threshold retracker range	mm

Satellite position from the best available POD as a vector in ITRF at the ground bounce time of the measurement	mm
Off-nadir pointing direction (unit vector) in ITRF from the Precision attitude calculation	1.5 arc sec
Geodetic latitude and longitude calculated using ocean-specific range with all atmospheric corrections and tides applied	μdeg
Ocean surface elevation calculated using the centroid of the waveform, with all atmospheric corrections and tides applied	mm
Highest elevation in the footprint, with all atmospheric corrections and tides applied (corresponds to signal begin)	mm
Lowest elevation in the footprint, with all atmospheric corrections and tides applied (corresponds to signal end)	mm
Elevation associated with the threshold retracker	mm
1-sec Elevation calculated using a linear filter to the full rate (40/sec) ocean elevations with all atmospheric corrections and tides applied	mm
RMS of the full rate elevations that went into calculation of the 1-sec elevation	mm
Surface Identifier flags from regional ID grid – All 4, locean.lice,lseaice,lland	N/A
Range increment from reference range to signal begin	mm
Range increment from reference range to signal end	mm
Range increment from reference range to produce ocean specific range based on the last peak in the return	mm
Range increment from reference range to produce ocean specific range based on the first peak in the return	mm
Standard deviation of received waveform to fit using ocean parameters	.01 counts
Solar incidence angle	.01 deg
Number of peaks from smoothed waveform	N/A
Peak amplitude from smoothed waveform	counts
Skewness of the received waveform between signal begin and signal end	
Range increment from reference range to centroid of the received waveform between signal begin and signal end	mm
Reflectance	
A set of flags indicating problems with any of the parameters to include: DEM, waveform-based range corrections, orbit, and attitude	N/A
DEM	cm
Orientation of the laser footprint measured clockwise from true north from attitude determination system	.01 deg

Length of the major axis of the laser footprint from attitude determination system	cm
Length of the minor axis of the laser footprint from attitude determination system	cm

5.6.1. Ancillary Information

In addition to the information needed to correct measured ranges for atmospheric effects, and to locate the footprint, these sets of information will be required:

a. Ocean mask, including sea-ice covered areas

b. Geoid elevation, with a tidal model to permit correction of geoid elevation to a sea-surface elevation appropriate to the time of GLAugust 10, 2000March 31, 1999AS footprints

6.0 CONSTRAINTS, LIMITATIONS, AND ASSUMPTIONS

This section speaks to the effect on the derived physical surface properties and elevation of the constraints, limitations, and assumptions that have been used to develop the algorithms presented in this document. Also discussed are research studies that need to be carried out to better understand the effect of these assumptions on the products.

6.1. Surface Characteristics

All the algorithms presented assume a Gaussian distribution of the surface undulations. Over the ice sheets the slope algorithm assumes a linear slope within the footprint and over sea ice the roughness algorithm assumes no slope. Actual ice sheet, sea ice and land surfaces do not behave as assumed though to first order these assumptions are valid over the ice sheets and sea ice. In addition to non-Gaussian uniform undulations there are many sudden irregularities in the surface all of which contribute to errors in the slope, roughness, and surface elevation calculated using our algorithms.

6.1.1. Effect On Slope Calculations

The algorithm for calculating the slope within the laser footprint is based on the assumption that the slope is linear at the 70m level and therefore the maximum and minimum surface heights lie on opposite edges of the footprint. The error in the slope calculated using this algorithm could be as great as 100% if, for example, a uniform mound is centered in the footprint. We rely here on an assertion that the spectrum of surface irregularities has a minimum at wavelengths of a few hundred meters. For ice sheets, this theoretically appears to be valid, since these wavelengths are too long for wind-caused features and too short to reflect subglacial topography. We need to study the existing aircraft laser data over Greenland for information on the spectrum of surface irregularities that exist over the ice sheets and use the results in the GLAS simulator to obtain realistic error envelopes for this calculation.

6.1.2. Effect On Roughness Calculations

The algorithm used to calculate the roughness over the sea ice and ice sheet surfaces assumes a pure Gaussian distribution. The actual surface has roughness characteristics that presumably lie somewhere between a Gaussian distribution of irregularities and a uniform distribution of linear wave-like features with a single amplitude. As mentioned previously surface roughness and slope cannot be empirically solved for from the information provided in one measurement. As the mission progresses, if the density of the elevation measurements will allow us to calculate slopes without using the waveform shape on a small enough scale then we can use this slope to calculate the roughness more accurately. This will allow us to remove the effect of slope from the waveform shape and then study the remaining roughness effect.

Over ice sheets, crevasses introduce a disturbance of the surface that can effect the roughness calculation. In most crevassed regions most of the illuminated spots on the surface will fall between individual crevasses and will therefore not be affected at all. Where the spot overlaps the edge of an open crevasse there will probably be multiple returns from different levels of a discontinuous surface. In cases where crevasses, ridges, vegetation or buildings (as could occur over land) cause multiple peaks in the return, no meaningful value for roughness can be calculated. However, it should be possible to devise an algorithm to filter out such returns. The existence of multiple peaks and or large discrepancies between the functional fit and the waveform, both of which are carried on the level 1 and 2 elevation products, can be used to filter out regions where these surface irregularities are present. This can also be used by glaciologists to point them to crevasse regions where the waveforms and other products from GLAS may be used to better understand the crevasse distribution.

The roughness calculation over sea ice assumes a horizontal surface. This is not always locally the case, causing similar problems to those encountered over grounded ice: pulse broadening caused by roughness and that caused by the slope of the surface cannot be separated without additional information. However, large slopes are rare, and a sloping sea-ice surface within the footprint will be caused by some larger-scale undulation that can reasonably be included as a roughness feature.

Real surfaces exhibit anisotropy and non-stationarity. Our algorithms assume isotropy and stationarity. Isotropy means that the statistics of the surface is independent of the direction along the surface. Stationarity means translational invariance, so that the statistics of one section of the surface will be the same as the statistics determined from a different section of the same surface. As the laser beam has a Gaussian or near-Gaussian far field pattern, the central part of the footprint receives more energy. Pulse spreading is determined by weighting the elevations with the normalized intensity cross section of the laser beam as described by Gardner (1982). Thus, surface roughness computed from the waveform is most representative of conditions near the middle of the footprint. This should not have any significant impact on roughness statistics derived from many footprints.

A non-uniform reflectivity distribution could affect sea ice roughness calculations. Sea ice reflectivity may vary greatly inside the laser footprint, especially during the summer melting season. Initial results (Csathó and Thomas, 1995) suggest that although the reflectivity distribution has a profound influence on the shape of the waveform, its RMS width is the same for models with different reflectivity distribution but the same topography.

The effect of other factors, such as non-Lambertian reflectivity, non-Gaussian far field pattern etc. requires further study, but is not expected to be large.

Penetration of the beam will also affect the roughness calculation. Although the light signal does not penetrate the ice-sheet signal nearly as deeply as the signal from a radar altimeter, there nevertheless may be penetration that must be evaluated. Experiments in Greenland show that there is still measurable 1064-nm energy from sunlight at a depth of 50 mm below the surface in Greenland (A. Nolin, personal communication, 1996). This effect has not yet been evaluated quantitatively, but at a first guess we can estimate that volume scattering from within the upper 0.1 m of the firn will broaden the return pulse by an amount comparable to that produced by a 0.1 m roughness. This is another error source that the GLAS Team will be evaluating further.

6.1.3. Effect On Surface Elevation

Small amplitude roughness and slopes will cause a broadening of the return pulse. Multiple surface elevations within the footprint will cause the return waveform to be a sum of the Gaussian-type distribution from each surface elevation present within the footprint. Most of the ice sheet surface returns will contain a single pulse. No matter what the shape of the return, if we ignore forward scattering, which is discussed in Section 6.3, the mean surface within the footprint is calculated using the centroid of the return waveform. However, the main mission requirement is to calculate elevation changes over the ice sheets. Therefore we need to take into account how the calculation of the elevation for each measurement affects our ability to calculate elevation change.

Measuring elevation changes requires comparing multiple elevation measurements over the same location at different times. The ICESat ground track passes over the same location for two types of circumstances; 1) when an ascending pass crosses a descending pass, referred to as crossovers and 2) when the orbit repeats itself (for GLAS the main mission will consist of six repeat cycles of 183 days each). Due to instrument characteristics and laser pointing accuracy and knowledge, even when the ICESat ground track overpasses a previous ground track, the portion of the surface illuminated will be different.

For repeat passes, the project is considering dynamic pointing control to maintain the footprint as close as possible to footprints from corresponding repeats. The precision of the pointing control is 30 arc sec or 87 m on the ground with post-processing expecting to improve the knowledge of the pointing to 1.5 arc sec or 4.4 m. The footprint is expected to look like an irregularly shaped ellipse with a major axis of 70m. The irregularities and the orientation of the major axis of the ellipse are expected to change slowly with time. Therefore for repeat passes, the footprints may overlap some, but still will not be illuminating the exact same portion of the surface.

At crossover locations, it will be necessary to interpolate between measurements that are approximately 175 m apart and have an error in location of 4.4m due to the accuracy of the pointing knowledge. In addition, crossovers on the same tracks from different repeats will be calculated from footprints that are offset from each other.

The main challenge in calculating elevation changes from GLAS is to find a method to calculate the surface elevation from the measurement that is as insensitive as possible to small scale topography at the shot spacing level. Several different methodologies can be used to decide to where to calculate the range. These include 1) for multiple peaks taking the average of the centroid positions of the multiple Gaussian fit, 2) for single peaks taking the centroid of the Gaussian fit, 3) taking the centroid of the peak closest to the ground, and 4) taking the centroid of the received or smooth return. More research needs to be carried out to test what method will give the most repeatable results for repeat groundtracks and crossovers.

6.2. Instrument Effects

The biggest effect the instrument will have on the algorithms is in the shape of the transmitted pulse. The engineers (J. Abshire and X. Sun personal communication 1999) have told us that after it comes through the detector for all practical purposes it will be Gaussian. If this pulse is not circularly symmetric, the returned pulse-shape will contain a bias toward the part of the footprint illuminated by an excess of energy. This bias would cause an error in the surface elevation calculated using our centroid algorithm over sloping surfaces. J. Abshire (personal communication, 1995) has calculated as an extreme case that a side lobe containing 10% of the outgoing energy on one edge of the beam would cause an error in a centroid detector of surface height of 18 cm on a surface with a 3deg slope. This is about 5% of the height difference across the footprint.

For a flat surface of uniform roughness the error in the roughness calculation would be extremely small, because the entire footprint is illuminated at essentially the same instant.

6.3. Atmospheric Effects

When there are thin clouds or aerosols in the atmosphere such that there is atmospheric interference with the light beam, yet a significant fraction of the signal is transmitted through the atmosphere so that a return is received at the GLAS telescope, there may be a broadening of the return pulse due to forward scattering of the light. Forward scattering produces ray paths that are slightly longer than the straight-line path and thus produces a delayed arrival of some energy. This has the effect of broadening the pulse and causing the tail to be longer and higher than the leading edge.

Our surface-slope/roughness algorithm is based on pulse broadening, so forward scattering, if not recognized, will lead to overestimates of the roughness and/or slope. Preliminary calculations by J. Spinhirne (personal communication, 1996) suggest that the broadening could be on the order of 1 ns. An error of this magnitude would lead to an overestimate of the roughness by 0.15 m, a figure that is comparable to the expected real values. The error in the slope from a 1-ns broadening would be about 0.1, again a significant factor in the central parts of the ice sheets where the actual slopes are of the same order.

The elevation calculation can also be significantly affected. As presented in the section 4.3.2 , this effect can be minimized by using the centroid of the Gaussian fit to calculate the range.

Forward scattering will have to be dealt with, either by correcting for its effects or deleting data that are affected. The GLAS Science Team is supporting research in the area. Results to date show that there will be insufficient atmospheric information from the LIDAR with which to model the forward scattering effect. However, we can tell from the LIDAR when conditions are present that could cause forward scattering and a flag is placed on the level 1 and 2 elevation products indicating this.

REFERENCES

Abshire, J.B., J.F. McGarry, L. K. Pacini, J.B. Blair, and G.C. Elman (1994) Laser Altimetry Simulator, Version 3.0 User's Guide. NASA Technical Memorandum 104588, NASA/GSFC, Greenbelt, MD, 70 p

Abshire, J. and X. Sun (1999) Personal communication

Abshire, J.B. (1995) Personal communication

Aldred, A., and G. Bonner (1985) Application of Airborne Lasers to Forest Surveys, Canadian Forestry Service, Petawawa National Forestry Centre, Information Report PI-X-51, 62 pp

Bamber, J.L., and J.P. Muller (1998) Derivation of a global land elevation data set from satellite radar altimeter data for topographic mapping. J. Geophys. Res.-Atmos., Vol. 103, No. D24, 32159-32168

Bamber, J.L. (1994) Ice sheet altimeter processing scheme. Int. J. Remote Sensing, Vol. 15, No. 4, 925-938

Bamber, J.L., and P. Huybrechts (in press) Geometric boundary conditions for modeling the velocity field of the Antarctic ice sheet. Annals of Glaciology, 23

Bevington, P.R. and D.K. Robinson (1992) Data Reduction and Error Analysis for the Physical Sciences, second edition. McGraw-Hill, NY

Blair, J.B., D.B. Coyle, J.L. Bufton, and D.J. Harding (1994) Optimization of an airborne laser altimeter for remote sensing of vegetation and tree canopies. Proc. IGARSS'94, 939-941

Brenner, A.C., H.V. Frey, and H.J. Zwally (1990) Comparisons between GEOSAT and SEASAT tracking over nonocean surfaces. Geophys. Res. Lett., Vol. 17, No. 10, 1537-1540

Brenner, A.C., R. Bindschadler, R.H. Thomas, and H.J. Zwally (1983) Slope-induced errors in radar altimetry over continental ice sheets. J. Geophys. Res. Vol. 88, 1617-1623

Brooks, R.L., W.J. Campbell, R.O. Ramseier, H.R. Stanley and H.J. Zwally (1978) Ice sheet topography by satellite altimetry. Nature, 274, 539-543

Brown, G.S. (1977) The average impulse response of a rough surface and its applications. IEEE Transactions on Antennas and Propagation, Vol. Ap-25, No. 1, 67-74

Budd, W.F. (1970) Ice flow over bedrock perturbations. J. Glaciology, Vol. 9, No. 55, 29-48

Budd, W.F., and D.B. Carter (1971) An analysis of the relation between the surface and bedrock profiles of ice caps. J. Glaciology, Vol. 10, No. 59, 197-209

Bufton, J.L., J.B. Garvin, J.F. Cavanaugh, L. Ramosizquierdo, T.D. Clem, and W.B. Krabill (1991) Airborne lidar for profiling of surface topography. Opt. Eng., Vol. 30, No. 1, 72-78

Bufton, J.L., J.E. Robinson, M.D. Femiano, and F.S. Flatow (1982) Satellite laser altimeter for measurement of ice sheet topography. IEEE Transactions on Geoscience and Remote Sensing, GE-20 (4), 544-549

Bufton, J.L. (1989) Laser altimetry measurements from aircraft and spacecraft. Proceedings of the IEEE, 77(3), 463-477

Carsey, F.D., ed. (1992) Microwave remote sensing of sea ice. American Geophysical Union, 462 pages

Comiso, J.C. (1995) Satellite remote sensing of the Arctic Ocean and adjacent seas. Arctic Oceanography: Marginal ice zones and continental shelves, Coastal and estuarines studies, 49, 1-50

Csathó, B.M. and R.H. Thomas (1995) Determination of sea ice surface roughness from laser altimetry waveform. BPRC Technical Report No. 95-03, Byrd Polar Research Center, The Ohio State University, Columbus, Ohio, 45 pages

Davis, C.H., and H.J. Zwally (1993) Geographic and seasonal variations in the surface properties of the ice sheets by satellite-radar altimetry. J. Glaciology, Vol. 39, No. 133, 687-697

Davis, C.H., C.A Kluever, and B.J. Haines (1998) Elevation Change of the Southern Greenland Ice Sheet. Science, Vol. 279, pp. 2086-2088

Doumani, G.A., 1967. Surface structures in snow. H. Oura, ed., Physics of Snow and Ice: Sapporo Conference, 1966, Inst. of Low Temp. Science, U. Hokkaido, 1119-1136.

Duda, D. and J. Spinhirne, Personal Communication

Drewry, D.J., N.F. McIntyre, and P. Cooper (1985) The Antarctic ice sheet: a surface model for satellite altimeter studies. Woldenberg, H. J., ed. Models in Geomorphology. Allen and Unwin, Boston, 1-23

Endo, Y., and K. Fujiwara (1973) Characteristics of the snow cover in East Antarctica along the route of the JARE South Pole traverse and factors controlling such characteristics. Japanese Antarctic Research Expedition Scientific Reports, C, 4-11

Fifield, R. (1987) International Research in the Antarctic. Oxford University Press, New York, 146 p

Frey, H. and A.C. Brenner (1990) Australian topography from SEASAT overland altimetry. Geophys. Res. Lett., Vol. 17, No. 10, 1533-1536

Furukawa, T., O. Watanabe, K. Seko, and Y. Fujii (1992) Distribution of surface conditions of ice sheet in Enderby Land and East Queen Maud Land, East Antarctica. Proceeding of NIPR Symposium on Polar Meteorology and Glaciology, Vol. 5, 140-144

Gardner, C. S. (1982) Target signatures for laser altimeters: An analysis. Applied Optics, 21(3), 448-453

Gardner, C. S. (1992) Ranging performance of satellite laser altimeters. IEEE Transactions on Geoscience and Remote Sensing, 30(5), 1061-1072

Garvin, J., J. Bufton, J. Blair, D. Harding, S. Luthcke, J. Frawley, and D. Rowlands (1998) Observations of the Earth's topography from the Shuttle Laser Altimeter(SLA): laser-pulse echo-recovery measurements of terrestrial surfaces. Phys. Chem. Earth, Vol. 23, No. 9-10, 1053-1068

Grenfell, T.C., and D.K. Perovich (1984) Spectral albedos of sea ice and incident solar irradiance in the southern Beaufort Sea. J. Geophys. Res., 89(C3), 3,573-3,580

Harding, D.J., J.L. Bufton, and J.J. Frawley (1994) Satellite laser altimetry of terrestrial topography: vertical accuracy as a function of surface slope, roughness, and cloud cover. IEEE Transactions on Geoscience and Remote Sensing, 32(2), 329-339

Harding, D., C. Carabajal, and W. Fong (1998) Suggested ICESat Waveform Processing Procedures Based on SLA Methodologies. Input to Waveform ATBD Working Group

Harding, D.J., J.B. Blair, J.B. Garvin, and W.T. Lawrence (1994) Laser altimetry waveform measurement of vegetation canopy structure. Proc. IGARSS'94, 1251-1253

Harding, D.J., (1998) Airborne lidar observations of canopy structure at the BOREAS tower flux sites. Proc. IGARSS '98, 1550-1552

Herzfeld, U. (1996) Personal communication

Hofton, M.A., J.B. Blair, J.B. Minster, J.R. Ridgway, N.P. Williams, J.L. Bufton, D.L. Rabine (in press) An airborne scanning laser altimetry survey of Long Valley, California. Int. J. Rem. Sens.

Hofton, M.A., J.B. Minster, J.R. Ridgway, N.P. Williams, J.B. Blair, D.L. Rabine, J.L. Bufton (in press) Using Airborne

Laser Altimetry to Detect Topographic Change at Long Valley Caldera, California. Remote

Sensing of Active Volcanism, ed. P. Mouginis Mark, AGU Monograph Series

Hutter, K., F. Legerer, and U. Spring (1981) First-order stresses and deformations in glaciers and ice sheets. J. Glaciology, Vol. 27, No. 96, 227-270

Koblinsky, C.J., R.T. Clarke, A.C. Brenner, and H. Frey, (1993) Measurement of rive level variations with satellite altimetry. Water Resour. Res., Vol. 29, No. 6, 1839-1848

Kotlyakov, V.M. (1966) The snow cover of the Antarctic and its role in the present-day glaciation of the continent. Israel Program for Scientific Translation, Jerusalem, 256 p

Krabill, W., R. Thomas, C. Martin, R. Swift, and E. Frederick (1995) Accuracy of airborne laser altimetry over the Greenland ice sheet, Int. J. Remote Sensing, 16, 1211-1222.

Krabill, W., W. Abdalati, E. Frederick, S. Manizade, C. Martin, J. Sonntag, R. Swift, R. Thomas, W. Wright, and J. Yungel (2000) Greenland ice sheet: high-elevation balance and peripheral thinning, Science, 289, 428-429.

Laxon, S (1998) Personal communication

Ledroit, M., F. Rémy, and J.F. Minster (1992) Observation of the Antarctic ice sheet by Seasat scatterometer: relation to katabatic wind intensity and direction. J. Glaciology, Vol. 39, No. 132, 385-396

Lefsky, M.J. (1997) Application of Lidar Remote Sensing to the Estimation of Forest Canopy Structure. Univ. of Virginia, Ph.D. Dissertation, 185 pp

Lefsky, M.A, D.J. Harding, W.B. Cohen, G.G. Parker, and H.H. Shugart (1999) Surface lidar remote sensing of basal area and biomass in deciduous forests of Eastern Maryland, USA. Rem. Sens. Environ,, Vol. 67, 83-98

Lefsky, A., W.B. Cohen, S.A. Acker, T.A. Spies, G.G. Parker, and D.J. Harding (1998) Lidar remote sensing of forest canopy structure and related biophysical parameters at the H.J. Andrews experimental forest, Oregon, USA. Proc. IGARSS'98, 1252-1254

Martin, T.V., A.C. Brenner, H.J. Zwally, and R.A. Bindschadler (1983) Analysis and retracking of continental ice sheet radar altimeter waveforms. J. Geophys. Res., Vol. 88, 1608-1616

McGarry, J.F., J B. Abshire, X. Sun, J. Saba, A. Brenner, and D. Yi, GLAS Flight Science Data Selection Algorithms For The Altimeter (1064nm) Version 4.03, in process

McIntyre, N. F. (1986) Antarctic ice-sheet topography and surface-bedrock relationships. Annals of Glaciology, Vol. 8, 124-128

Means, J.E., S.A. Acker, D.J. Harding, J.B. Blair, M.A. Lefsky, W.B. Cohen, M.E. Harmon, and W.A. McKee, W.A. (in press) Use of a large-footprint scanning airborne lidar to estimate forest stand characteristics in the western Cascades of Oregon. Rem. Sens. Environ. Vol. 67, 298-308

Menke W. (1989) Geophysical Data Analysis: Discrete Inverse Theory, revised edition. International Geophysical Series, Vol. 45, Academic Press, NY

Nilsson, M. (1996) Estimation of tree heights and stand volume using an airborne lidar system. Remote Sens. Environ, Vol. 56, 1-7

Nolin, A. (1996) Personal communication

Ogilvy, J. A. (1991) Theory of Wave Scattering from Random Rough Surfaces. Adam Hilger, Bristol, England, 277 p

Partington, K. C., J. K. Ridley, C. G. Rapley, and H. J. Zwally (1989) Observations of the surface properties of the ice sheets by satellite radar altimetry. J. Glaciology, Vol. 35, No. 120, 267-275

Paterson, W. S. B. (1994) The Physics of Glaciers. Permagon, Tarrytown, New York, 480 p

Peacock, N. R., S. W. Laxon, W. Maslowski, D. P. Winebrenner, and R. J. Arthern (1998) Geophysical signatures from precise altimetric height measurements in the Arctic Ocean

Perovich, D. K. (1996) The optical properties of sea ice. CRREL Monograph 96-1, U.S. Army Corps of Engineers CRREL, Hanover, NH, 24 p

Press, W.H., B.P. Flannery, S.A. Teuloksky, and W.T. Vettering (1986) Numerical Recipes. Cambridge U Press

Reeh, N., S. J. Johnsen, and D. Dahl-Jensen (1985) Dating of the Dye 3 deep ice core by flow model calculations. C. C. Langway, Jr., H. Oeschger, and W. Dangaard, eds. Greenland ice core, geophysics, geochemistry, and the environment, Am. Geophys. Union Geophys. Monograph 33, 57-65

Rémy, F., P. Mazzega, S Houry, C. Brossier, and J. F. Minster (1989) Mapping of the topography of continental ice by inversion of satellite-altimeter data. J. Glaciology, Vol. 35, 38-97

Rémy, F., C. Brossier, and J. F. Minster (1990) Intensity of satellite radar-altimeter return power over continental ice: a potential measurement of katabatic wind intensity. J. Glaciology, Vol. 36, No. 123, 133-142

Rémy, F., and J.F. Minster (1991) A comparison between active and passive microwave measurements of the Antarctic ice sheet and their association with the surface katabatic winds. J. Glaciology, Vol. 37, No. 125, 3-10

Rémy, F., M. Ledroit, and J.F. Minster (1992) Katabatic wind intensity and direction over Antarctica derived from scatterometer data. Geophys. Res. Letters, Vol. 19, 1021-1024

Robin, G. de Q. (1967) Surface topography of ice sheets. Nature, Vol. 189, 1029-1032

Seko, K., T. Furukawa, and O. Watanabe (1991) The surface condition on the Antarctic ice sheet. G. Weller, ed., International Conference on the Pole of the Polar Regions in Global Change, Vol. 1, U. Alaska - Fairbanks, 238-242

Spinhirne, J (1996) Personal Communication

Stremler, F. G. (1990) Introduction to Communication Systems. Addison-Wesley Publishing Company, Reading, Massachusetts, 757p. East Antarctic ice sheet. Annals of Glaciology, 20, 137-142

Sun X. (1996) unpublished, presented at GLAS Science Team Meeting

Thomas, R.H., W. Krabill, S. Manizade, R. Swift, and A. Brenner (1994) Comparison of Radar Altimetry Data over Greenland with Surface Topography Derived from Airborne Laser Altimetry. Proceedings Second ERS-1 Symposium, 11-14 Oct 1993, ESA SP-361

Tsai, B. M., and C. S. Gardner (1982) Remote sensing of sea state using laser altimeters. Applied Optics, 21(21), 3932-3940

Tucker, W. B., D. K. Perovich, A. J. Gow, W. F. Weeks, and M. R. Drinkwater (1992) Physical properties of sea ice relevant to remote sensing. F. D. Carsey, ed. Microwave remote sensing of sea ice, American Geophysical Union, 9-27

Wadhams, P., W. B. Tucker III, W. B. Krabill, R. N. Swift, J.C. Comiso, and N. R. Davis (1992) Relationship between sea-ice freeboard and draft in the Arctic basin, and implications for ice-sheet monitoring. J. Geophys. Res, 97(C12), 20,325-20,334

Watanabe, O. (1978) Distribution of surface features of snow cover in Mizuho Plateau. Memoirs of National Institute of Polar Research (Japan), Special Issue #7, 44-62

Whillans, I. M., and S. J. Johnsen (1983) Longitudinal variations in glacial flow: theory and test using data from the Byrd Station strain network. J. Glaciology, Vol. 29, No 101, 78-97

Wingham, D.J., A.J. Ridout, R. Scharroo, R.J. Arthern, and C.K. Shum (1998) Antarctic Elevation Change from 1992-1996. Science, Vol 282 456-458

Yi, D., and C. R. Bentley, (1994). Analysis of satellite radar-altimeter return wave forms over the East Antarctic ice sheet. Annals of Glaciology, 20, 137-142

Zuber, M.T., D.E. Smith, S.C. Solomon, J.B. Abshire, R.S. Afzal, O. Aharonson, K. Fishbaugh, P.G. Ford, H.V. Frey, J.B, Garvin, J.W. Head, A.B. Ivanov, C.L. Johnson, D.O. Muhleman, G.A. Neumann, G.H. Pettengill, R.J. Phillips. X. Sun, H.J. Zwally, W.B. Banerdt, T.C. Duxbury (1998) Observations of

the North Polar Region of Mars from the Mars Orbiter Laser Altimeter. Science, Vol. 282, pp. 2053-2060

Zuber, M.T., D.E. Smith, S.C. Solomon, D.O. Muhlemen, J.W. Head, J.B. Garvin, J.B. Abshire, J.L. Bufton (1992) The Mars Observer laser altimeter investigation. J. Geophys. Res., Vol 97, No. E5, 7781-7797

Zwally, H. J., R.A. Bindschadler, A.C. Brenner, T.V. Martin, and R.H. Thomas (1983) Surface elevation contours of Greenland and Antarctic Ice sheets. J Geophysics, Res., Feb 28

Zwally, H.J., A.C. Brenner, J.A. Major, R.A. Bindschadler, and J.G. Marsh (1989) Growth of Greenland Ice Sheet: Measurement. Science, Vol. 246, pp/1587-1589

Zwally, H.J., A.C. Brenner, J.A. Major, T.V. Martin, and R.A. Bindschadler (1990) Satellite Radar Altimetry Over Ice. Volume 1, NASA Ref Pub 1233, Vol 1

Zwally, H.J., A.C. Brenner, J.P. DiMarzio, and T. Seiss (1994) Ice Sheet Topography from Retracked ERS-1 Altimetry. Proceedings Second ERS-1 Symposium, 11-14 Oct 1993, ESA SP-361